SHARE

SEVENTH FRAMEWORK PROGRAMME

Grant Agreement no. 226967

Seismic Hazard Harmonization in Europe

Project Acronym: SHARE

SP 1-Cooperation

Collaborative project: Small or medium-scale focused research project

THEME 6: Enviroment

Call: ENV.2008.1.3.1.1 Development of a common methodology and tools to evaluate earthquake hazard in Europe

D4.2 – Regionally adjusted Ground Motion Prediction Equations (GMPE) for Europe

Due date of deliverable: 30.11.2010
Actual submission date: 26.11.2010

Start date of project: 2009-06-01 Duration: 36

Laboratoire de Geophysique Interne et Tectonophysique, Universite Joseph Fourier (LGIT-UJF)
Stéphane Drouet, Fabrice Cotton, Céline Beauval

Middle East Technical University (METU)
Sinan Akkar

Revision: 1

Dissemination Level		
PU	Public	x
PP	Restricted to other programme participants (including the Commission Services)	
RE	Restricted to a group specified by the consortium (including the Commission Services)	
CO	Confidential, only for members of the consortium (including the Commission Services)	

Deliverable 4.2: Regionally adjusted Ground Motion Prediction Equations (GMPE) for Europe

Stéphane Drouet, Fabrice Cotton, Céline Beauval

LGIT, CNRS, Université Joseph Fourier
BP 53, 38041 Grenoble Cedex 9
France

November 15, 2010

Contents

List of Figures

List of Tables

1 Introduction

This report describes the procedures of selection and adjustment of Ground-Motion Prediction Equations (GMPEs) for use within the Share program.

The selection procedure is based on objective criteria as first defined in Cotton et al. [2006] and updated in Bommer et al. [2010] within the Share project. The application of those criteria in order to select ground-motion prediction equations (GMPEs) for use in the Euro-Mediterranean regions is presented in Douglas [2009].

The selected GMPEs are using different horizontal component definitions and some of the models do not use style-of-faulting as a predictor variable. Consequently, one needs to correct for those differences to homogeneously estimate ground-motions. The component and style-of-faulting adjustment strategies have been presented in a previous report [Drouet et al., 2010a]. The final effect of those adjustments will also be presented in the current report.

A third kind of adjustment is needed because models for stable continental regions are developed for very hard rock sites and we are aiming at predicting ground-motion for a "standard rock site" characterized by v_{S30}=800 m/s. Preliminary work has been done on the estimation of the high-frequency attenuation characteristics of rock sites [Drouet et al., 2010b,c]. The resulting rock site adjustment strategy is presented in the current report.

2 Selected GMPEs

Due to the very large number of available GMPEs, some clear and objective criteria must be adopted to select a subset of the existing GMPEs in order to predict ground-motion in the region of interest. There are three main families of GMPEs:

- Models for active crustal regions
- Models for stable continental regions
- Models for subduction zones

The three seismotectonics contexts can be found in the Euro-Mediterranean region considered in Share plus three specific contexts where specific GMPEs should be used: volcanic regions, deep-focus non-subduction events regions, and coastal regions where seismic waves travel mostly through the oceanic crust.

For each of these contexts, the pre-selection criteria defined by Cotton et al. [2006] and updated by Bommer et al. [2010] have been applied to the existing GMPEs by Douglas [2009]. The pre-selected models are given in Tables 1 to 4.

All the preselected models have been plotted for different magnitudes, distances and periods in Drouet et al. [2010a]. From this visual check and taking into account some problems with predictive variable definitions Drouet et al. [2010a] suggested that some of the models might be removed from the selection. Those are highlighted with red color in Tables 1 to 4. They are still indicated here because in the ranking

procedure an expert judgment on the models is needed and they might choose to keep those models with a very low weight.

During the Share meeting in Roma, June 15-16, 2010, the existence of new models or model updates that could be helpful for Share has been highlighted:

- Cauzzi & Faccioli update for PGV
- Toro update for Toro et al. [1997] GMPE, there are two options in this update: Shall we use both?
- Abrahamson new model for subduction
- Chiou & Youngs new model extension of their NGA models to a broader range of magnitudes

Those models will be implemented before the end of the project.

Table 1: Description of the ground-motion prediction equations for Stable Continental Regions.

Reference	Area	M range	D range (km)	T range (s)	Site classification v_{S30}	sof or pN, pR	H definition
Atkinson [2008]	ENA	M_w=4.3-7.6	R_{JB}=10-1000	0.1-5.0, PGA, PGV	760 m/s	N, R, S, U	GMRotI50
Atkinson and Boore [2006]	ENA	M_w=3.5-8.0	R_{rup}=1-1000	0.025-5.0, PGA, PGV	2000 m/s and 760 m/s	0.01, 0.81	GM
Campbell [2003]	ENA	M_w=5.0-8.2	R_{rup}=0-1000	0.02-4.0, PGA	2800 m/s	0.01, 0.81	GM
Douglas et al. [2006]	Southern Norway	M_w=4.5-7.5	R_{JB}=1-1000	0.02-2.0	2800 m/s	N, R, S	GM
Tavakoli and Pezeshk [2005]	ENA	M_w=5.0-8.2	R_{rup}=0-1000	0.05-4.0, PGA	2900 m/s	0.01, 0.81	GM
Toro et al. [1997]	ENA	M_w=5.0-8.0	R_{JB}=1-1000	0.03-2.0, PGA	2800 m/s	0.01, 0.81	GM

The red color indicates models that might be removed depending on the experts judgement

Table 2: Description of the ground-motion prediction equations for subduction areas.

Reference	Area	M range	D range (km)	Depth range (km) (a)	T range (s)	Site classification v_{S30}	sof (a)	H definition
Atkinson and Boore [2003]	Worldwide	M_w=5.5-8.3	R_{rup}=11-550	F:0-50, B:0-120	0.04-3.0, PGA	x≤180, 180<x≤360, 360<x≤760, x>760 m/s	F, B	Random
Atkinson and Macias [2009]	Cascadia	M_w=7.5-9.0	R_{rup}=30-400	6-60	0.05-10.0, PGA	x=760 m/s	F	GM
Garcia et al. [2005]	Central Mexico	M_w=5.2-7.4	R_{rup}=4.0-400 (R_{hyp} for M_w <6.5)	35-138	0.04-5.0, PGA	760≤x≤1500 m/s (NEHRP B only)	B, normal events	GM
Kanno et al. [2006]	Japan + some foreign	M_w=5.5-8.0 (M_{JMA})	R_{rup}=30-450	F:0-30, B:30-185	0.05-5.0, PGA	Continuous function of vS30	F, B	VC
Lin and Lee [2008]	Northern Taiwan + some foreign	M_w=4.1-8.1 (ML converted)	R_{hypo}=15-630	F:5.54-30, B:39.9-161	0.01-5.0, PGA	x≤360, x>360 m/s	F, B	GM
McVerry et al. [2006]	New Zealand	M_w=5.08-7.09	R_{rup}=6-400	F:10-25, B:25-150	0.075-3.0, PGA	x≤180, 180<x≤360, x>360 m/s	F, B	GM
Youngs et al. [1997]	Worldwide	M_w=5.0-8.2 (MS and mb converted)	R_{rup}=8.5-550.9	F:10-50, B:13-229	0.075-3.0, PGA	x≤750, x>750 m/s	F, B	GM
Zhao et al. [2006]	Japan	M_w=5.0-8.3	R_{rup}=0-300	F:10-50, B:20-122	0.05-5.0, PGA	x≤200, 200<x≤300 , 300<x≤600, 600<x≤1100, x>1100 m/s	F, B	GM

(a) "B" refers to inslab earthquakes and "F" to interface earthquakes
The red color indicates models that might be removed depending on the experts judgement

Table 3: Description of the ground-motion prediction equations for active crustal Regions.

Reference	Area	M range	D range (km)	T range (s)	Site classification v_{S30}	sof or pN, pR	H definition
Abrahamson and Silva [2008]	California + Taiwan + other regions	M_w=5.0-8.5	R_{rup}=0-200	0.01-10.0, PGA, PGV	Continuous function of v_{S30}	N,R/T, S	GMRotI50
Ambraseys et al. [2005]	Europe and Middle East	M_w=5.0-7.6	R_{JB}=0-100	0.05-2.5, PGA	x<360 , 360≤x<750, x≥750 m/s	N, R/T, S, O	LE
Akkar and Bommer [2010]	Europe and Middle East	M_w=5.0-7.6	R_{JB}=0-99 (R_{epi} for small events)	0.05-3.0, PGA, PGV	x<360, 360≤x<750, x≥750 m/s	N, R/T, S	GM
Boore and Atkinson [2008]	California + Taiwan + other regions	M_w=4.27-7.9	R_{JB}=0-280	0.02-10.0, PGA, PGV	Continuous function of v_{S30}	N, R, S, U	GMRotI50
Campbell and Bozorgnia [2008]	California + Taiwan + other regions	M_w=4.27-7.9	R_{rup}=0.07-199.27	0.02-10.0, PGA, PGV	Continuous function of v_{S30}	N, R, S	GMRotI50
Cauzzi and Faccioli [2008]	worldwide	M_w=5.0-7.2	R_{hypo}=15-150	0.05-20, PGA	x<180, 180≤x<360, 360≤x<800, x≥800 m/s	N, R/T, S	GM
Chiou and Youngs [2008]	California + Taiwan + other regions	M_w=4.27-7.9	R_{rup}=0.2-70	0.02-10.0, PGA, PGV	Continuous function of v_{S30}	N, R, S	GMRotI50
Cotton et al. [2008]	Japan	M_w=4.0-7.3	R_{rup}=5-100	0.01-3.0	x≤180, 180<x≤360, 360<x≤800, x>800 m/s	0.0525, 0.3150	GM
Idriss [2008]	California + Taiwan + other regions	M_w=5.0-8.0 (SS) or 8.5 (R)	R_{rup}=0-200	0.02-10, PGA	450<x≤900, x>900 m/s	N, R/T, S	GMRotI50
Kanno et al. [2006]	Japan + some foreign	M_w=5.0-8.2 (M_{JMA})	R_{rup}=1-450	0.05-5.0, PGA	Continuous function of v_{S30}	*No information*	VC
McVerry et al. [2006]	New Zealand	M_w=5.08-7.09	R_{rup}=6-400	0.075-3.0, PGA	x≤180, 180<x≤360, x>360 m/s	N, R/T, S	GM
Pankow and Pechmann [2004]	Extensional regime	M_w=5.0-7.0	R_{JB}=0-100	0.1-2.0, PGA	x≤750, x>750 m/s	0.45, 0.00	GM
Zhao et al. [2006]	Japan	M_w=5.0-8.3	R_{rup}=0.0-300.0	0.05-5.0, PGA	x≤200, 200<x≤300 , 300<x≤600, 600<x≤1100, x>1100 m/s	N, R, S	GM

The red color indicates models that might be removed depending on the experts judgement

Table 4: Description of the region-specific ground-motion prediction equations for active crustal regions.

Reference	Area	M range	D range (km)	T range (s)	Site classification v_{S30}	sof or pN, pR	H definition
Bindi et al. [2009]	Italy	M_w=4.0-6.9	R_{JB}=2.8-100	0.03-2.0, PGA, PGV	x≤800 (2 classes depending on sediment thickness), x>800 m/s	0.47, 0.16	LE
Danciu and Tselentis [2007]	Greece	M_w=4.5-6.9	R_{epi}=0-136	0.1-4.0, PGA, PGV	x≤360, 360<x≤800, x>800 m/s	N, R/T, S	AM
Douglas et al. [2006]	Southern Spain	M_w=4.5-7.5	R_{JB}=1-1000	0.02-2.0	1870 m/s	0.1875, 0.1875	GM
Kalkan and Gülkan [2004]	Turkey	M_w=4.0-7.4 (scale not specified)	R_{JB}=1.2-250 (R_{epi} for small events)	0.1-2.0, PGA	Continuous function of v_{S30}	0.1574, 0.0463	LE
Massa et al. [2008]	Northern Italy	M_w=4.0-6.5	R_{epi}=4-100	0.04-2.0, PGA	x≤800, x>800 m/s	0.0, 0.5	LE
Özbey et al. [2004]	Northern Western Turkey	M_w=5.0-7.4	R_{JB}=5-200	0.1-4.0, PGA	x≤180, 180<x≤360, x>360 m/s	0.0366, 0.0244	GM

The red color indicates models that might be removed depending on the experts judgement

Table 5: Description of the ground-motion prediction equations for deep focus earthquakes.

Reference	Area	M range	D range (km)	Depth range (km)	T range (s)	Site classification v_{S30}	sof or pN, pR	H definition
Sokolov et al. [2008]	Romania	M_w=5.0-8.0	R_{epi}=1-500	70-160	0.1-3.0, PGA	8 sets of coefficients to account for region-specific site amplification	pr=1.0 (reverse events only)	GM

3 Component adjustment effect

The component conversions proposed in Drouet et al. [2010a] based on the study by Beyer and Bommer [2006] show that the largest conversions factors are those from the larger envelope definition to the geometrical mean. As an illustration the effect of the conversion is shown in Figure 1 for the Massa et al. [2008] GMPE. We also show the adjustment for the Kanno et al. [2006] model which uses the time domain vectorial composition of the two horizontal components (Fig. 2). The conversion in this case is based on Bragato and Slejko [2005] study which indicate that on average this definition is 27% higher than the geometrical mean. The component conversions do not depend on magnitude, on distance or on the original model.

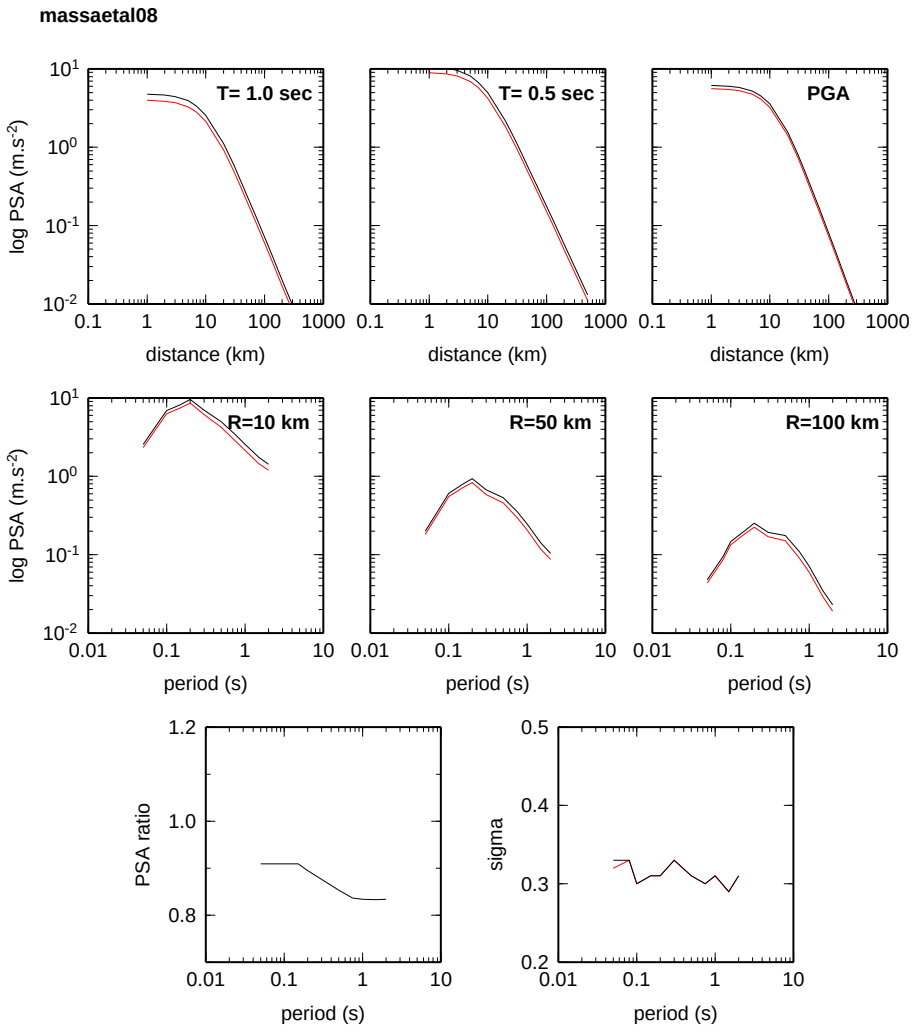

Figure 1: Original model for larger envelope (black) and component adjusted model to geometrical mean (red) models based on Massa et al. [2008] GMPE.

Figure 1 shows the original model and the adjusted one for different periods and distances for a magnitude 6 scenario (note that the adjustment only depends on period). The effect on the amplitude is ranging between 0.83 and 0.91 depending on

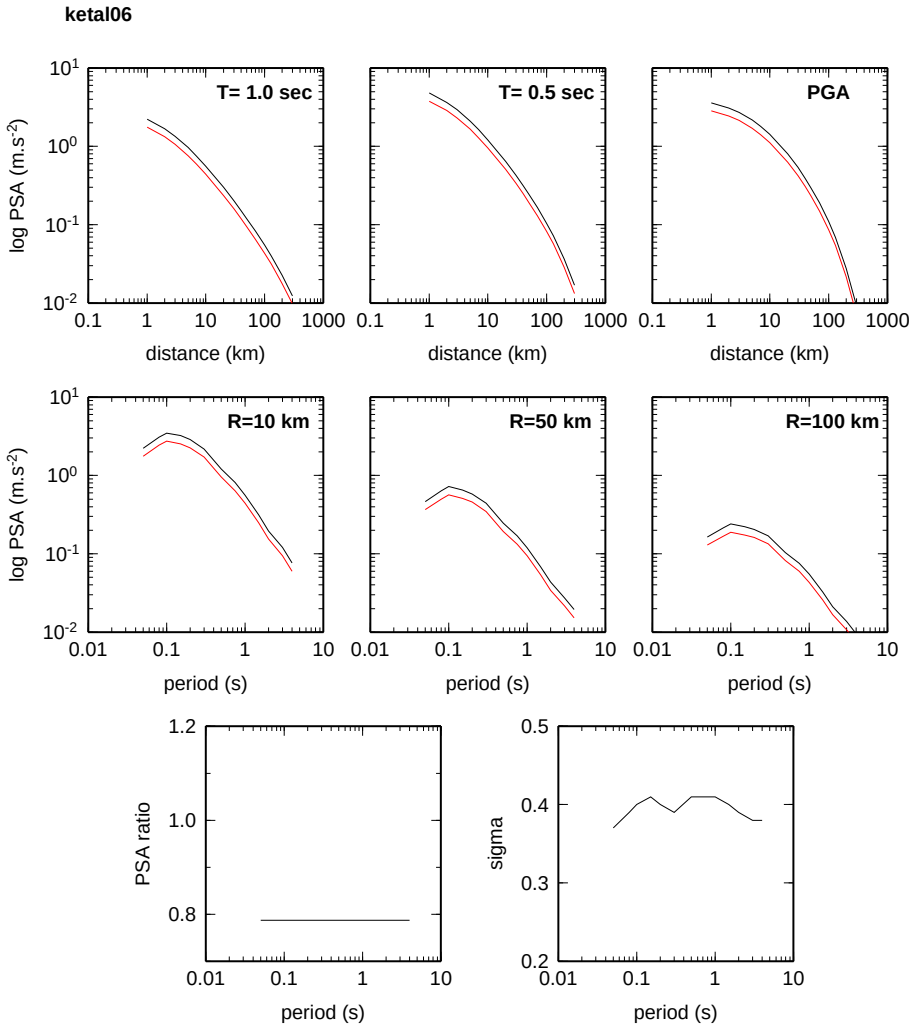

Figure 2: Original model for time domain vectorial composition of the two horizontal components (black) and component adjusted model to geometrical mean (red) models based on Kanno et al. [2006] GMPE.

the period, and the standard deviation is almost unchanged. We suggest then not to modify the standard deviations for the component conversions. Figure 2 shows that the ratio between the original model and the adjusted one is quite large (larger than the ratio between LE and GM definitions). However, we have no clue of the effect of this conversion on the standard deviation since Bragato and Slejko [2005] only give an average ratio.

We recall now how these conversions are performed technically. The response spectra are simply divided by a period dependent filter. For the conversions of rotated geometrical mean as defined by Boore et al. [2006] (GR), arithmetic mean (AM), larger envelope (LA), random horizontal (RA) and larger PGA (LP) component definitions to geometrical mean (GM), the period dependent filter is the

following:

$$adjustment = \begin{cases} c_1 \ if \ T \leq 0.15 \ s \\ c_1 + (c_2 - c_1) * \frac{ln\left(\frac{T}{0.15}\right)}{ln\left(\frac{0.8}{0.15}\right)} \ if \ 0.15 < T \leq 0.8 \ s \\ c_2 \ if \ T > 0.8 \ s \end{cases} \quad (1)$$

where T is the period, and the coefficients c_1 and c_2 depend on the original component definition (see Table 6). Note that these conversions are valid from 0.02 to 5 s. From the example shown in Figure 1, we suggest not to modify the standard deviation of the original GMPE.

Table 6: Coefficients for the component conversion.

Original component definition	GR	AM	LE	RA	LP
c_1	1.0	1.0	1.1	1.0	1.1
c_2	1.0	1.0	1.2	1.0	1.0

For the conversion of the time domain vectorial composition of the two horizontal components (VC) to geometrical mean (GM) the adjustment factor is independent of period and is equal to 1.27.

4 Style-of-faulting adjustment effect

On the contrary to the component adjustment, the style-of-faulting adjustment is model-dependent since it uses the proportions or normal and reverse events in the underlying database of each model [Bommer et al., 2003]. These values are given in Tables 1 to 4. A combination of adjustment factors for normal and reverse events weighted by the above mentioned proportions are used to define the adjustment factor [see Drouet et al., 2010a, for details]. Note that this adjustment does not depend on magnitude or distance. Figure 3 is an illustration of the effect of the style-of-faulting adjustment for the Bindi et al. [2009] GMPE. The main difference exist for reverse faulting. Figures 4 to 10 show the ratios between style-of-faulting adjusted and original models for active crustal regions.

The effect of the style-of-faulting adjustment on the response spectral amplitudes ranges between 0.85 and 1.27, and again the standard deviation is not varying very much. Thus one can keep the original standard deviation unchanged.

There are 4 other models which require such style-of-faulting adjustments but are not plotted here:

- Atkinson and Boore [2006]
- Campbell [2003]
- Tavakoli and Pezeshk [2005]

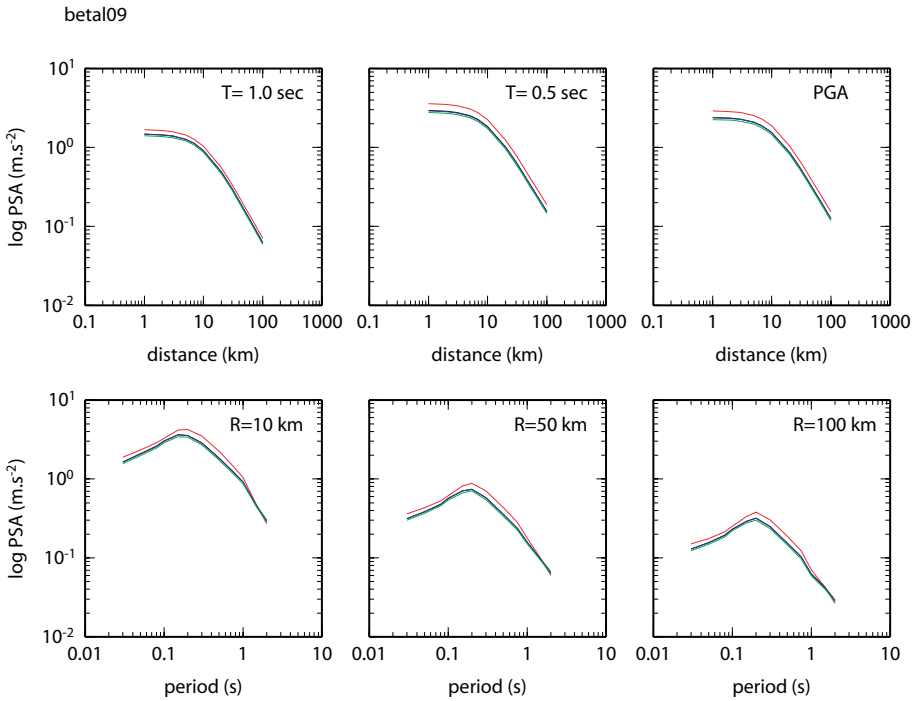

Figure 3: Original (black) and style-of-faulting adjusted (red: reverse, blue: strike-slip, green: normal) models based on Bindi et al. [2009] GMPE.

- Toro et al. [1997]

Technically the adjustment is a period dependent filter, and response spectra have to be multiplied by this filter:

$$\begin{cases} Strike-slip\ event: \ adjustment = F_{R:SS}(T)^{-p_R} \times F_{N:SS}^{-p_N} \\ Normal\ event: \ adjustment = F_{R:SS}(T)^{1-p_R} \times F_{N:SS}^{-p_N} \\ Reverse\ event: \ adjustment = F_{R:SS}(T)^{-p_R} \times F_{N:SS}^{1-p_N} \end{cases} \quad (2)$$

with p_N and p_R given in Tables 1 to 4, and $F_{R:SS}(T)$ is given in Table 7, and $F_{N:SS}(T)$=0.95.

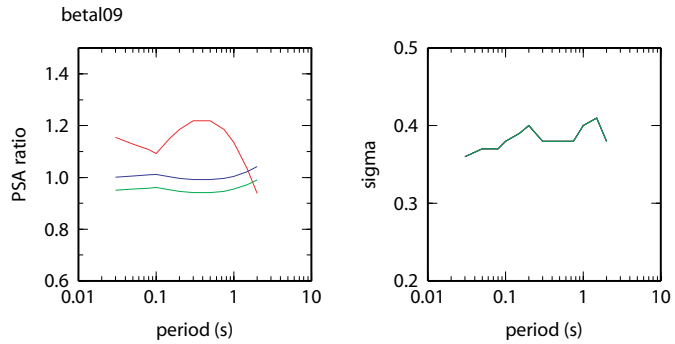

Figure 4: Ratio between style-of-faulting adjusted models (red: reverse, blue: strike-slip, green: normal) and the original model based on Bindi et al. [2009] GMPE.

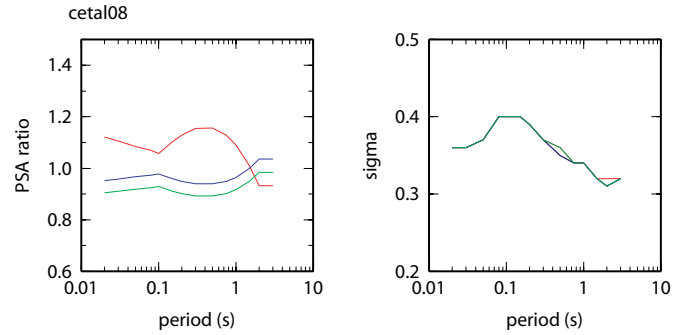

Figure 5: Ratio between style-of-faulting adjusted models (red: reverse, blue: strike-slip, green: normal) and the original model based on Cotton et al. [2008] GMPE.

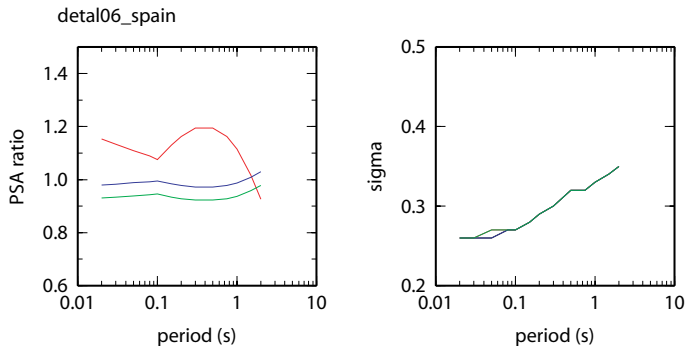

Figure 6: Ratio between style-of-faulting adjusted models (red: reverse, blue: strike-slip, green: normal) and the original model based on Douglas et al. [2006] GMPE.

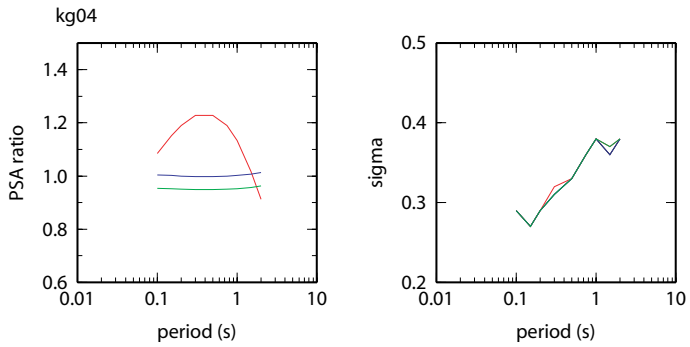

Figure 7: Ratio between style-of-faulting adjusted models (red: reverse, blue: strike-slip, green: normal) and the original model based on Kalkan and Gülkan [2004] GMPE.

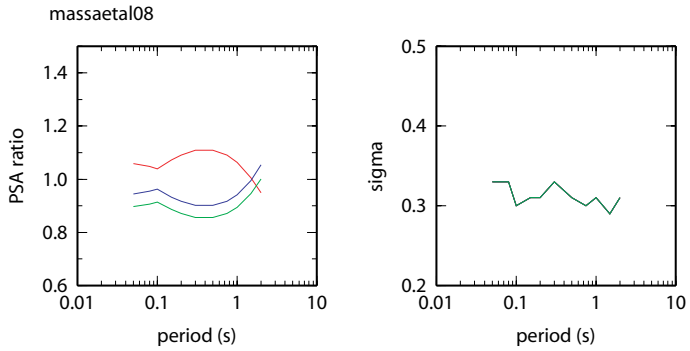

Figure 8: Ratio between style-of-faulting adjusted models (red: reverse, blue: strike-slip, green: normal) and the original model based on Massa et al. [2008] GMPE.

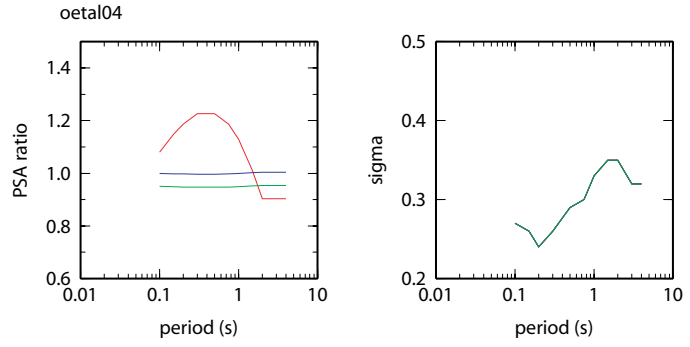

Figure 9: Ratio between style-of-faulting adjusted models (red: reverse, blue: strike-slip, green: normal) and the original model based on Özbey et al. [2004] GMPE.

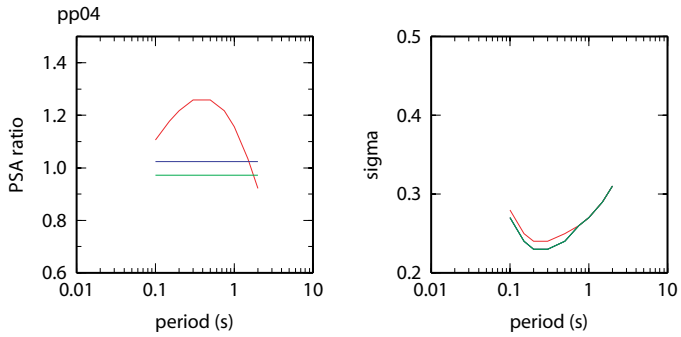

Figure 10: Ratio between style-of-faulting adjusted models (red: reverse, blue: strike-slip, green: normal) and the original model based on Pankow and Pechmann [2004] GMPE.

Table 7: Coefficients for the style-of-faulting conversion.

T (s)	$F_{R:SS}(T)$
0.00 (PGA)	1.22
0.10	1.08
0.11	1.10
0.12	1.11
0.13	1.13
0.14	1.13
0.15	1.15
0.16	1.16
0.17	1.16
0.18	1.17
0.19	1.18
0.20	1.19
0.22	1.20
0.24	1.20
0.26	1.21
0.28	1.22
0.30	1.23
0.32	1.23
0.34	1.23
0.36	1.23
0.38	1.23
0.40	1.23
0.42	1.24
0.44	1.23
0.46	1.24
0.48	1.23
0.50	1.23
0.55	1.23
0.60	1.22
0.65	1.21
0.70	1.20
1.60	1.19
1.70	1.18
1.80	1.17
1.90	1.16
2.00	1.14

5 Very hard to hard rock adjustment

One of the aim of Share WP4 is to provide GMPEs for rock conditions defined by v_{S30}=800 m/s. Most of the models are able to predict ground motion for such v_{S30} or rock site category. However, the GMPEs for stable continental regions are usually derived for very hard rock sites with v_{S30} ranging between 2000 and 2900 m/s with the exception of Atkinson [2008] and Atkinson and Boore [2006] who provide GMPEs for v_{S30}=760 m/s.

Additionally to the change in response spectral amplitude linked with lower v_{S30} values, one has to take into account the high-frequency decay effect [Anderson, 1986] which is very different for the two types of rock. A first effort was made to determine both v_{S30} and κ (the high-frequency decay parameter), and their correlation using the French weak-motion database [Drouet et al., 2010b]. It was followed by the analysis of NGA and KIKNET data with measured v_{S30} values in order to determine κ [Drouet et al., 2010c]. These new results and some others from the literature [Silva et al., 1998, Chandler et al., 2006, Douglas et al., 2010, Edwards (2009) personal communication] were used to analyse the relationship between v_{S30} and κ [Drouet et al., 2010c]. Drouet et al. [2010c] results are reproduced in Figure 11. There is a large scatter in the v_{S30}-κ correlation, however, very hard rock sites (v_{S30}=2000 m/s) seem to be characterised by a κ of the order of 0.01 sec or below while "standard" rock site (v_{S30}=800 m/s) have a κ around 0.03 sec.

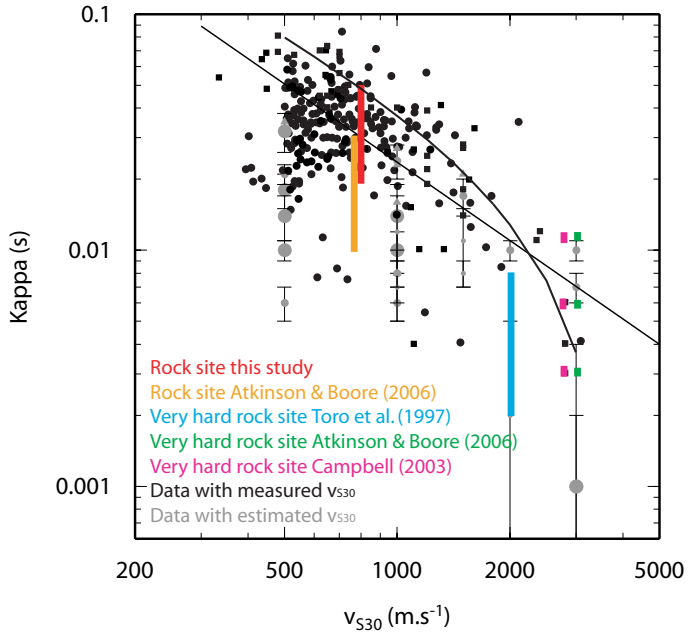

Figure 11: Correlation between v_{S30} and κ from Drouet et al. [2010c]. The linear fit is from Silva et al. [1998] and the non-linear fit from Chandler et al. [2006]. The colored areas indicate the κ-values for rock sites and very hard rock sites used in the present study, in Toro et al. [1997], in Campbell [2003], and in Atkinson and Boore [2006].

The reference rock site has been defined within Share WP4 by v_{S30}=800 m/s (Ankara meeting, November 2009). From Figure 11 we can propose a range of κ values from 0.02 to 0.05 s corresponding to v_{S30}=800 m/s. The standard rock definition given by Atkinson and Boore [2006] corresponds to v_{S30}=760 m/s associated with κ values ranging from 0.01 to 0.03 s. Those κ values are low compared to the results from Figure 11.

Very hard rock sites are defined in three ways in Toro et al. [1997], Campbell [2003], and Atkinson and Boore [2006]. Toro et al. [1997] use v_{S30}=2800 m/s and three equally weighted κs (0.003, 0.006, 0.012 s). Campbell [2003] also use v_{S30}=2800 m/s and the same κ values but with higher probability for κ=0.006 s than for the other two values. Finally, Atkinson and Boore [2006] use v_{S30}=2000 m/s and a uniform distribution for κ between 0.002 and 0.008 s.

Figure 11 indicates the "rock site" and "very hard rock site" domains as defined above.

In order to perform the adjustment of both v_{S30} and κ, we used Campbell [2003] host-to-target adjustment methodology. The basic idea is that having a GMPE for a host region and a set of seismological stochastic parameters which allows the simulation of ground-motions [i.e. using SMSIM Boore, 2003] for both the host and the target regions, the original GMPE can be adjusted using the ratio between the simulations for the target and the host regions. The requirement is then a set of seismological stochastic parameters which can reproduce the ground-motions predicted by the "host" GMPE. Such sets of parameters have been determined by Scherbaum et al. [2006] for various popular GMPEs and more specifically for the Toro et al. [1997] GMPE (Table 8) which is part of those considered in Share WP4. For the Campbell [2003] GMPE, the set of parameters is given in Table 2 of the original paper (Table 8). The site amplification relative to the target v_{S30} have been computed from the Boore and Joyner [1997] generic rock velocity profiles [Cotton et al., 2006].

Table 8: Host stochastic parameters for Toro et al. [1997] GMPE (equivalent stochastic parameters as determined in Scherbaum et al. [2006]) and for Campbell [2003] GMPE (as given in Campbell [2003]: ENA model).

GMPE	Stress drop (bar)	κ (sec)	Geometrical spreading exponent	Quality factor	v_{S30} (m/s)	Duration parameter
Toro et al. [1997]	198	0.01	-0.826 if 1≥R<29.3 -0.998 if 29.3≥R<97.3 -0.5 if R≥97.3	$225 \times f^{0.613}$	3000	0.067
Campbell [2003]	150	0.006	-1.000 if 1≥R<70.0 0.000 if 70.0≥R<130.0 -0.5 if R≥130.0	$680 \times f^{0.36}$	2800	0.04

Using a Fortran program written by J. Douglas and used in Douglas et al. [2006], we computed the host-to-target adjustments for the Toro et al. [1997] and the Campbell [2003] GMPE. The adjustment in this study takes into account only the site effect terms: v_{S30} and κ. Spectral accelerations are computed for a set of periods,

magnitudes and distances. For the same set of periods, magnitudes and distances stochastic amplitudes (Fourier spectra) are computed using SMSIM for the host model (see parameters in Table 8) and for the target model (same parameters except v_{S30} and κ). The spectral accelerations are then multiplied by the ratios of the stochastic amplitudes to create a new data set of adjusted spectral accelerations. Finally, those new data are regressed using the same functional form as in the original model.

We first started by the adjustment of the original GMPEs (i.e. Toro et al. [1997] and Campbell [2003]) to alternative very hard rock site definitions (v_{S30}=2000, 2600, 2800 m/s and κ=0.002, 0.005, 0.01 s for Toro et al. [1997] and v_{S30}=2000, 2600, 2800 m/s and κ=0.002, 0.006, 0.01 s for Campbell [2003]). The coefficients of the new models are given in annex. The adjusted models and the original ones, for a specific magnitude-distance scenario (M=6, R=20 km), are shown in Figure 12. One can first check that the adjustment (correction of original spectral amplification by the ratios of target and host Fourier amplitudes plus new regression) with the original very hard rock site definition gives a model equivalent to the original GMPE which valids the methodology. However, we observed that the adjustment of the Toro et al. [1997] GMPE performs poorly for distances greater than 100 km, which is not the case for the Campbell [2003] GMPE. This is due to the set of parameters used. Indeed the equivalent stochastic parameters determined by Scherbaum et al. [2006] are valid up to distances of 100 to 200 km. In the following we then will not use the adjusted Toro et al. [1997] GMPEs for distances greater than 100 km.

We then made the adjustment from the original very hard rock definition to rock site definition (v_{S30}=800 m/s and four values of κ: 0.01, 0.02, 0.03 and 0.05 sec). The coefficients of the new models are given in annex. The results for a specific magnitude-distance scenario (M=6, R=20 km) are shown in figure 13. The effect of a lower v_{S30} value is to increase the spectral amplitudes at all periods, but this effect is counter-balanced by a drastic diminution of the amplitudes due to higher κ values especially for periods lower than 0.5 s.

In order to evaluate the variability of the predictions for different very hard rock conditions, we have computed the ratios between the models shown in Figure 12 over the original one for both the Toro et al. [1997] GMPE and the Campbell [2003] GMPE. The ratios are computed for a number distances and magnitudes (R=1, 2, 3, 5, 10, 20, 30, 50, 100, 200, 300, 500 km; M=5, 6, 7). Distances greater than 100 km are not used in the case of the Toro et al. [1997] GMPE as explained above. The results are shown in Figure 14, and the average ratio can be seen as the ratio between the Toro et al. [1997] or Campbell [2003] models and a generic very hard rock model.

Similar ratios between the Toro et al. [1997] or Campbell [2003] models and a generic rock site (v_{S30}=800 m/s and κ=0.02 to 0.05 s) are shown in Figure 15 using the results from Figure 13. Since Atkinson and Boore [2006] give two sets of coefficients for very hard and hard rock sites, we computed the same ratios between very hard rock and rock predictions. Those are also plotted in Figure 15. Their definitions of very hard and hard rock sites are as follows: v_{S30}=2000 m/s, κ=0.002-0.008 sec, and v_{S30}=760 m/s, κ=0.01-0.03 sec (respectively). The low κ for rock sites

chosen by Atkinson and Boore [2006] are leading to low amplitude ratios compared to the ratios we computed using the Toro et al. [1997] and the Campbell [2003] GMPEs.

The scatter seen in the ratios using Toro et al. [1997] or Campbell [2003] GMPEs does not depend on the host v_{S30}-κ couple which is fixed (see Table 8). The same is true for the ratios in both Figure 14 and Figure 15. In the case of Atkinson and Boore [2006], it includes the effect of the uncertainty on the host κ since these authors used uniform distributions for κ from 0.002 to 0.008 sec.

Our aim is to take into account the uncertainty associated with the very hard rock definition for both v_{S30} and κ, and with the κ which has to be assigned to a rock site defined by v_{S30}=800 m/s in order to compute ratios to convert motions from very hard rock sites to motion for rock sites. This is finally done by computing the ratios between the average ratios of Figures 14 and 15 (which we note $ratio_{Very\ hard\ rock}$ and $ratio_{Rock}$, respetively).

$$\begin{aligned} Final\ ratio &= \frac{ratio_{Very\ hard\ rock}}{ratio_{Rock}} \\ \sigma_{Final\ ratio} &= \sqrt{\left(\frac{\sigma_{Very\ hard\ rock}}{ratio_{Rock}}\right)^2 + \left(\frac{\sigma_{Rock} \times ratio_{Very\ hard\ rock}}{ratio_{Rock}^2}\right)^2} \end{aligned} \tag{3}$$

In this case we end up with the ratios between a generic rock site (with v_{S30}=800 m/s and κ ranging between 0.02 and 0.05 s) and a generic very hard rock site (with v_{S30} ranging between 2000 and 2800 m/s and κ ranging between 0.002 and 0.01 s). These final ratios are obtained for both Toro et al. [1997] and Campbell [2003] models and are shown in Figure 16 together with the average ratios from Atkinson and Boore [2006]. Again the rock site κ used by Atkinson and Boore [2006] is rather low compared to the results of Figure 11 which explains the slightly higher amplitude ratios in this case.

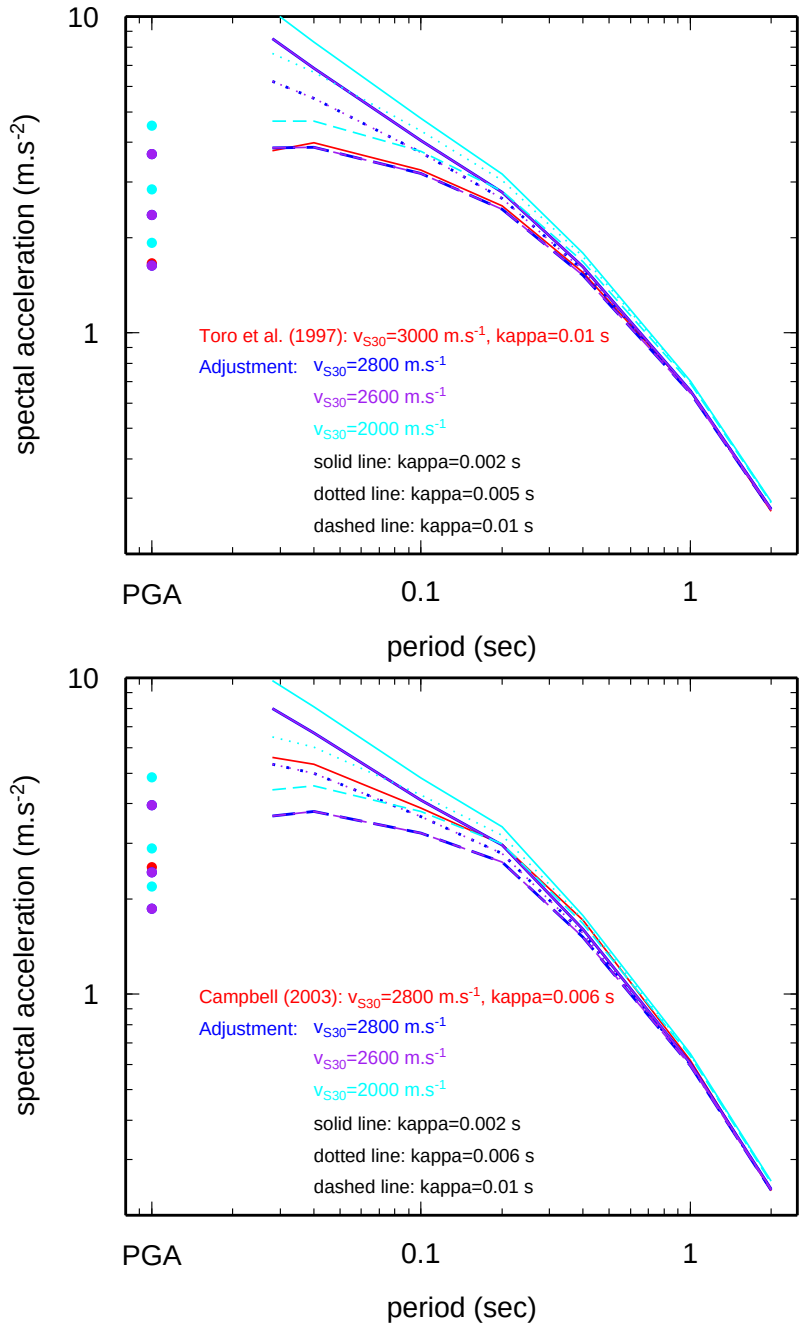

Figure 12: Top: Ground-motion predictions for a M=6, R=20 km scenario using the original Toro et al. [1997] GMPE and the "very hard rock-site" adjusted Toro et al. [1997] GMPE (v_{S30}=2000, 2600 and 2800 m/s; κ=0.002, 0.005, 0.01 sec). Bottom: Same plot using Campbell [2003] GMPE (v_{S30}=2000, 2600 and 2800 m/s; κ=0.002, 0.006, 0.01 sec).

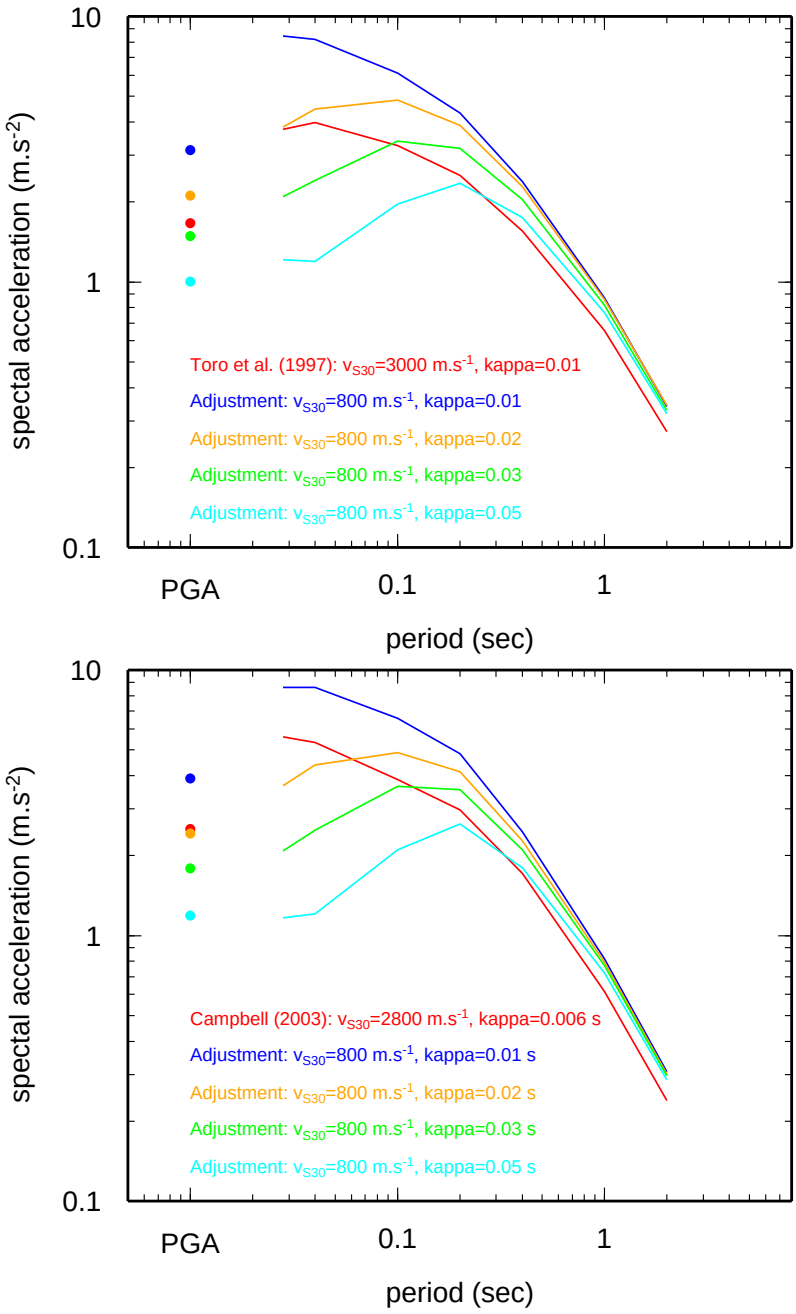

Figure 13: Top: Ground-motion predictions for a M=6, R=20 km scenario using the original Toro et al. [1997] GMPE and the "rock-site" adjusted Toro et al. [1997] GMPE (v_{S30}=800 m/s; κ=0.01, 0.02, 0.03 and 0.05 sec). Bottom: Same plot using Campbell [2003] GMPE.

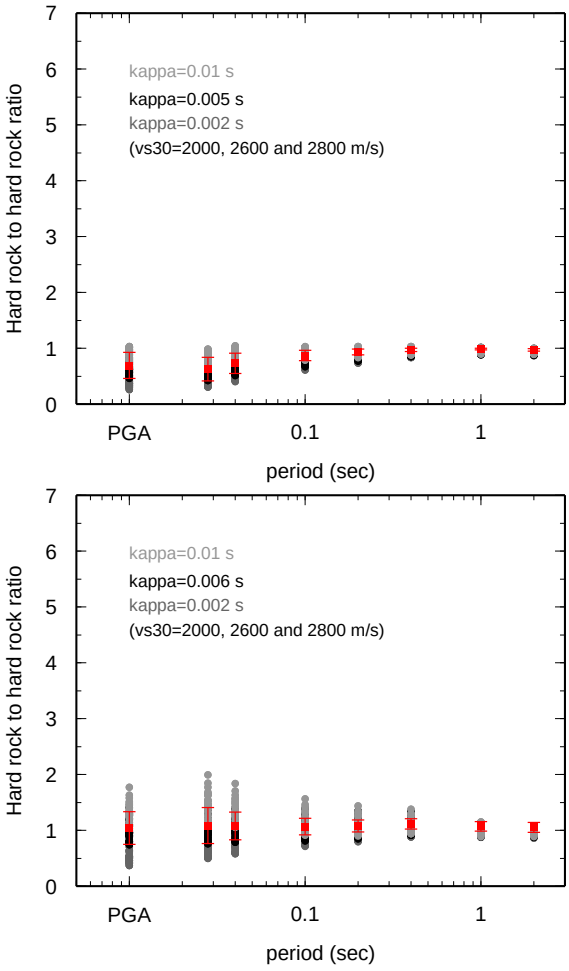

Figure 14: Ratios between the original model (top: Toro et al. [1997]; bottom: Campbell [2003]) and the adjusted ones to several very hard rock definitions (v_{S30}=2000 to 2800 m/s and κ=0.002 to 0.01 s). The ratios are computed for several magnitudes and distances (see text). Average ratios and error bars are plotted in red.

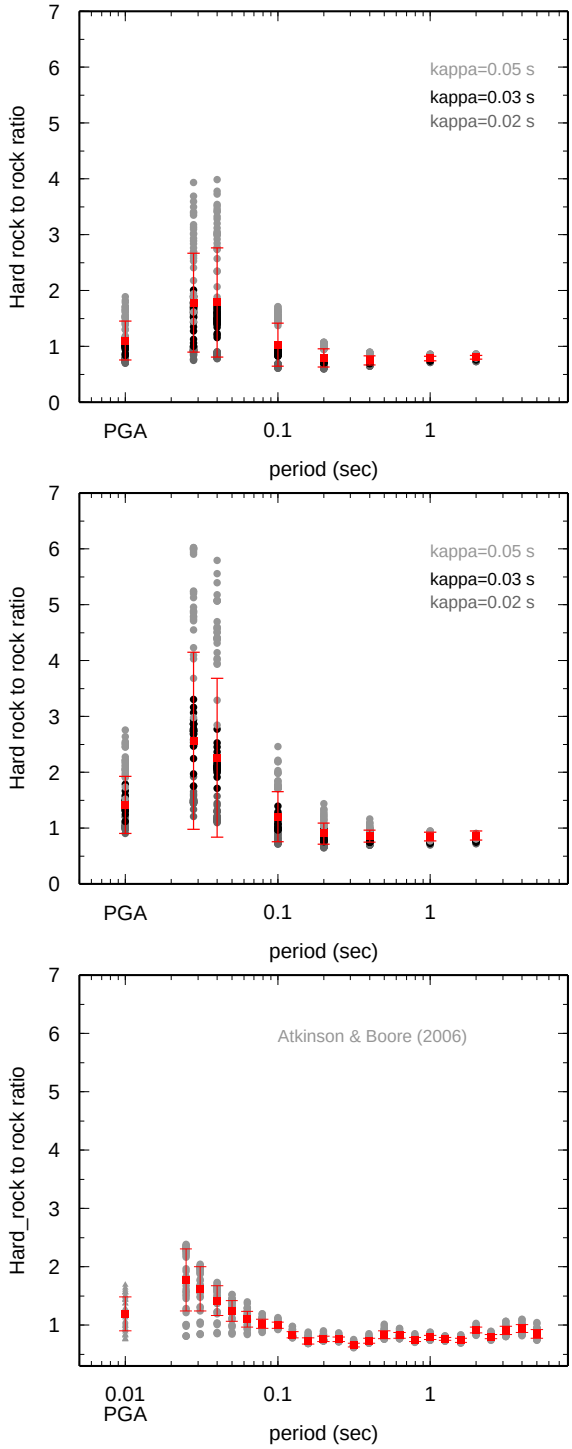

Figure 15: Ratios between the original model (top: Toro et al. [1997]; middle: Campbell [2003]) and the adjusted ones to several rock definitions (v_{S30}=800 m/s and κ=0.02 to 0.05 s). The ratios of the predictions for very hard rock over the predictions for rock using Atkinson and Boore [2006] GMPE are also shown (bottom). Average ratios and error bars are plotted in red.

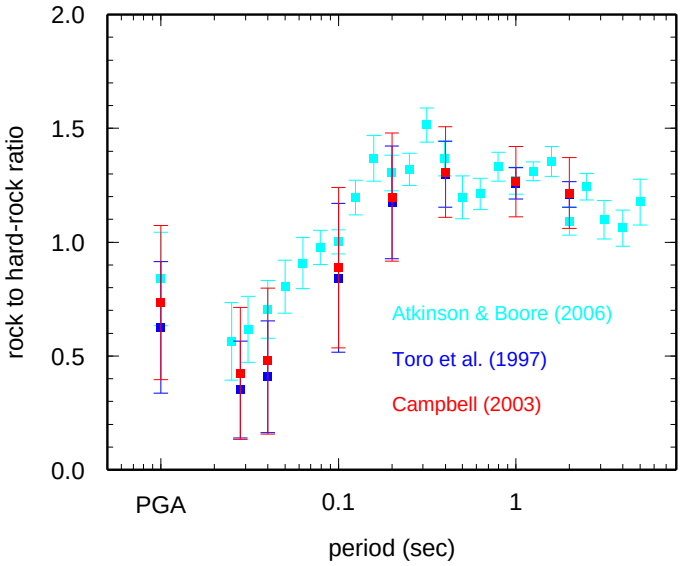

Figure 16: Average rock to very hard rock ratios estimated using: Atkinson and Boore [2006] GMPE (cyan), Toro et al. [1997] GMPE (blue), and Campbell [2003] GMPE (red).

It appears from Figure 16 that the results using Toro et al. [1997] GMPE and Campbell [2003] GMPE are consistent and similar. The final ratios have close mean and standard deviation at each period, while the ratios estimated from Atkinson and Boore [2006] presents higher values and lower standard deviation due to the low rock site κ these authors used. Finally, we suggest to keep and use the ratios computed with the Campbell [2003] since there is no distance limitations as in the case of Toro et al. [1997] (see text). The final ratios using Campbell [2003] GMPE can be used as a proxy to perform the very-hard to hard rock adjustment: motion estimated for a very hard rock site can be converted to motion expected for a rock site by multiplication of the response spectra by the period dependent adjustment factors given in Table 9. Further analysis using the other GMPEs for stable continental regions could help to check the stability of the ratio.

Table 9: Coefficients for the component conversion.

T (s)	Adjustment factor	σ
0.01	0.735106	0.338916
0.03	0.423049	0.289785
0.04	0.477379	0.320650
0.10	0.888509	0.352442
0.20	1.197291	0.281552
0.40	1.308267	0.198424
1.00	1.265762	0.154327
2.00	1.215779	0.155520

Acknowlegments

We would like to warmly thank John Douglas for sharing his Fortran programs for the estimation of the different GMPEs. The authors are also grateful to Jochen Woessner and to all the Share WP4 members (Sinan Akkar, Pierre-Yves Bard, Julian Bommer, Hilmar Bungum, Laurentiu Danciu, Elise Delavaud, John Douglas, Ezio Faccioli, Donat Faeh, Anne Lemoine, Kyriasis Pitilakis, Frank Scherbaum, Margaret Segou, Nikos Theodulidis, Graeme Weatherill) for the fruitful meetings and workshops we had together.

References

N. Abrahamson and W. Silva. Summary of the Abrahamson and Silva NGA ground-motion relations. *Earthquake Spectra*, 24(1):67–97, Feb 2008.

S. Akkar and J. J. Bommer. Empirical equations for the prediction of PGA, PGV and spectral accelerations in Europe, the Mediterranean region and the Middle East. *Seismol. Res. Lett.*, 82(2):195–206, Mar 2010.

N. N. Ambraseys, J. Douglas, S. K. Sarma, and P. M. Smit. Equations for the estimation of strong ground motions from shallow crustal earthquakes using data from

Europe and the Middle East: Horizontal peak ground acceleration and spectral acceleration. *Bull. Earthquake Eng.*, 3(1):1–53, 2005.

J. G. Anderson. Implication of attenuation for studies of the earthquake source. *Earthquake Source Mechanics, S. Das, J. Boatwright, and C. H. Scholz (Editors), American Geophysical Monograph 37*, pages 311–318, 1986.

G. M. Atkinson. Ground-motion prediction equations for Eastern North America from a referenced empirical approach: implications for epistemic uncertainty. *Bull. Seism. Soc. Am.*, 98(3):1304–1318, June 2008.

G. M. Atkinson and D. M. Boore. Empirical ground-motion relations for subduction-zone earthquakes and their application to Cascadia and other regions. *Bull. Seism. Soc. Am.*, 93(4):1703–1729, Aug 2003.

G. M. Atkinson and D. M. Boore. Earthquake ground-motion prediction equations for Eastern North America. *Bull. Seism. Soc. Am.*, 96(6):2181–2205, Dec 2006.

G. M. Atkinson and M. Macias. Predicted ground motions for great interface earthquakes in the Cascadia subduction zone. *Bull. Seism. Soc. Am.*, 99(3):1552–1578, June 2009.

K. Beyer and J. J. Bommer. Relationships between median values and between aleatory variabilities for different definitions of the horizontal component of motion. *Bull. Seism. Soc. Am.*, 96(4A):1512–1522, Aug 2006.

D. Bindi, L. Luzi, M. Massa, and F. Pacor. Horizontal and vertical ground motion prediction equations derived from the Italian Accelerometric Archive (ITACA). *Bull. Earthquake Eng.*, online:DOI 10.1007/s10518–009–9130–9, 2009.

J. J. Bommer, J. Douglas, and F. O. Strasser. Style-of-faulting in ground-motion prediction equations. *Bull. Earthquake Eng.*, 1:171–203, 2003.

J. J. Bommer, J. Douglas, F. Scherbaum, F. Cotton, H. Bungum, and D. Fäh. On the selection of ground-motion prediction equations for seismic hazard analysis. *Seismol. Res. Lett.*, 81(5):783–793, Sept. 2010.

D. M. Boore. Simulation of ground motion using the stochastic method. *Pure Appl. Geophys.*, 160:635–676, 2003.

D. M. Boore and G. M. Atkinson. Ground-motion prediction equations for the average horizontal component of PGA, PGV, and 5%-damped PSA at spectral periods between 0.01 and 10 s. *Earthquake Spectra*, 24(1):99–138, Feb 2008.

D. M. Boore and W. B. Joyner. Site amplifications for generic rock sites. *Bull. Seism. Soc. Am.*, 87(2):327–341, 1997.

D. M. Boore, J. Watson-Lamprey, and N. A. Abrahamson. Orientation-independent measures of ground motion. *Bull. Seism. Soc. Am.*, 96(4A):1502–1511, Aug 2006.

P. L. Bragato and D. Slejko. Empirical ground-motion attenuation relations for the Eastern Alps in the magnitude range 2.5-6.3. *Bull. Seism. Soc. Am.*, 95(1): 252–276, 2005.

K. W. Campbell. Prediction of strong ground motion using the hybrid empirical method and its use in the development of ground-motion (attenuation) relations in eastern North America. *Bull. Seism. Soc. Am.*, 93:1012–1033, 2003.

K. W. Campbell and Y. Bozorgnia. NGA ground motion model for the geometric mean horizontal component of PGA, PGV, PGD and 5% damped linear elastic response spectra for period ranging from 0.01 to 10 s. *Earthquake Spectra*, 24(1): 139–171, Feb 2008.

C. Cauzzi and E. Faccioli. Broadband (0.05 to 20 s) prediction of displacement response spectra based on worldwide digital records. *J. Seismology*, 12(4):453–475, Oct 2008.

A. M. Chandler, N. T. K. Lam, and H. H. Tsang. Near-surface attenuation modelling based on rock shear-wave velocity profile. *Soil Dyn. Earthq. Eng.*, 26:1004–1014, 2006.

B. S.-J. Chiou and R. R. Youngs. An NGA model for the average horizontal component of peak ground motion and response spectra. *Earthquake Spectra*, 24(1): 173–215, Feb 2008.

F. Cotton, F. Scherbaum, J. J. Bommer, and H. Bungum. Criteria for selecting and adjusting ground-motion models for specific target regions: Application to Central Europe and rock sites. *J. Seismology*, 10(2):doi:10.1007/s10950–005–9006–7, 2006.

F. Cotton, G. Pousse, F. Bonilla, and F. Scherbaum. On the discrepancy of recent European ground-motion observations and predictions from empirical models: analysis of KIK-net accelerometric data and point-sources stochastic simulations. *Bull. Seism. Soc. Am.*, 98(5):2244–2261, Oct 2008.

L. Danciu and G.-A. Tselentis. Engineering ground-motion parameters attenuation relationships for Greece. *Bull. Seism. Soc. Am.*, 97(1B):162–183, Feb 2007.

J. Douglas. Pre-selection of ground-motion prediction equations for WP4 of SHARE. Technical report, BRGM, Orlans, France, 2009. Report for the European project FP7-ENVIRONMENT-226967 "Seismic Hazard Harmonisation in Europe".

J. Douglas, H. Bungum, and F. Scherbaum. Ground-motion prediction equations for Southern Spain and Southern Norway obtained using the composite hybrid model perspective. *J. Earthq. Eng.*, 10(1):33–72, 2006.

J. Douglas, P. Gehl, L. F. Bonilla, and C. Gelis. A kappa model for mainland France. *Pure Appl. Geophys.*, pages doi:10.1007/s00024–010–0146–5, 2010.

S. Drouet, F. Cotton, and C. Beauval. Comparison of ground-motion prediction equations and selection for model testing. Technical report, LGIT/CNRS/Universit Joseph Fourier, Grenoble, France, 2010a. Report for the European project FP7-ENVIRONMENT-226967 "Seismic Hazard Harmonisation in Europe".

S. Drouet, F. Cotton, and P. Guéguen. v_{S30}, κ, regional attenuation and M_w from small magnitude events accelerograms. *Geophys. J. Int.*, 182(2):880–898, Aug 2010b.

S. Drouet, F. Cotton, and P. Guéguen. v_{S30} and κ from accelerometric data analysis. In *European Seismological Commission 32nd General Assembly, September 6-10, 2010, Montpellier, France*, 2010c.

D. Garcia, S. K. Singh, M. Herráiz, M. Ordaz, and J. F. Pacheco. Inslab earthquakes of Central Mexico: peak ground-motion parameters and response spectra. *Bull. Seism. Soc. Am.*, 95(6):2272–2282, Dec 2005.

I. M. Idriss. An NGA empirical model for estimating the horizontal spectral values generated by shallow crustal earthquakes. *Earthquake Spectra*, 24(1):217–242, Feb 2008.

E. Kalkan and P. Gülkan. Site-dependent spectra derived from ground motion records in Turkey. *Earthquake Spectra*, 20(4):1111–1138, Nov 2004.

T. Kanno, A. Narita, N. Morikawa, H. Fujiwara, and Y. Fukushima. A new attenuation relation for strong ground motion in Japan based on recorded data. *Bull. Seism. Soc. Am.*, 96(3):879–897, June 2006.

P.-S. Lin and C.-T. Lee. Ground-motion attenuation relationships for subduction-zone earthquakes in Northeastern Taiwan. *Bull. Seism. Soc. Am.*, 98(1):220–240, Feb 2008.

M. Massa, P. Morasca, L. Moratto, S. Marzorati, G. Costa, and D. Spallarossa. Empirical ground-motion prediction equations for Northern Italy using the weak- and strong-motion amplitudes, frequency content, and duration parameters. *Bull. Seism. Soc. Am.*, 98(3):1319–1342, June 2008.

G. H. McVerry, J. X. Zhao, N. A. Abrahamson, and P. G. Somerville. New Zealand acceleration response spectrum attenuation realtions for crustal and subduction zone earthquakes. *Bulletin of the New Zealand Society for Earthquake Engineering*, 39(4):1–58, 2006.

C. Özbey, A. Sari, L. Manuel, M. Erdik, and Y. Fahjan. An empirical attenuation relationship for Northwestern Turkey ground motion using a random effects approach. *Soil Dyn. Earthq. Eng.*, 24:115–125, Oct 2004.

K. L. Pankow and J. C. Pechmann. The SEA99 ground-motion predictive relations for extensional tectonic regimes: revisions and a new peak ground velocity relation. *Bull. Seism. Soc. Am.*, 94(1):341–348, Feb 2004.

F. Scherbaum, F. Cotton, and H. Staedtke. The estimation of minimum-misfit stochastic models from empirical ground-motion prediction equations. *Bull. Seism. Soc. Am.*, 96(2):427–445, 2006.

W. Silva, R. Darragh, N. Gregor, G. Martin, N. Abrahamson, and C. Kircher. Reassessment of site coefficients and near-fault factors for building code provisions. *Technical Report Program Element II: 98-HQ-GR-1010, Pacific Engineering and Analysis, El Cerrito, USA*, 1998.

V. Sokolov, K.-P. Bonjer, F. Wenzel, B. Grecu, and M. Radulian. Ground-motion prediction equations for the intermediate depth Vrancea (Romania) earthquakes. *Bull. Earthquake Eng.*, 6:367–388, Mar 2008.

B. Tavakoli and S. Pezeshk. Empirical-stochastic ground-motion prediction for Eastern North America. *Bull. Seism. Soc. Am.*, 95(6):2283–2296, Dec 2005.

G. R. Toro, N. A. Abrahamson, and J. F. Schneider. Model of strong ground motions for earthquakes in central eastern North America: best estimates and uncertainties. *Seismol. Res. Lett.*, 68:41–57, 1997.

R. R. Youngs, S.-J. Chiou, W. J. Silva, and J. R. Humphrey. Strong ground motion attenuation relationships for subduction zone earthquakes. *Seismol. Res. Lett.*, 68(1):58–73, Jan-Feb 1997.

J. X. Zhao, J. Zhang, A. Asano, Y. Ohno, T. Oouchi, T. Takahashi, H. Ogawa, K. Irikura, H. K. Thio, P. G. Somerville, Y. Fukushima, and Y. Fukushima. Attenuation relations of strong ground motion in Japan using site classification based on predominant period. *Bull. Seism. Soc. Am.*, 96(3):898–913, June 2006.

6 Annex

6.1 Coefficients of the Toro et al. [1997] adjusted models

The functional form of the Toro et al. [1997] GMPE is the following:

$$ln(Y) = c_1 + c_2(M-6) + c_3(M-6)^2 - c_4 ln(R_M) - (c_5 - c_4) max\left[ln\left(\frac{R_M}{100}\right), 0\right] - c_6 R_M \quad (4)$$

with $R_M = \sqrt{R_{jb}^2 + c_7^2}$ and R_{jb} the Joyner-Boore distance. The proposed coefficients below are giving $ln(Y)$ in m/s^2 while the original coefficients in Toro et al. [1997] are giving $ln(Y)$ in g. Note that T=0.0 s corresponds to PGA.

6.1.1 Very hard rock models

Table 10: Coefficients of the adjusted model for v_{S30}=2800 m/s and κ=0.002 sec.

Period (sec)	c_1	c_2	c_3	c_4	c_5	c_6	c_7
0.000	5.96	0.74	0.03	1.49	1.05	0.0023	9.0
0.028	6.65	0.76	0.02	1.45	1.82	0.0014	9.4
0.040	6.15	0.76	0.02	1.36	1.52	0.0021	8.9
0.100	4.62	0.78	0.01	1.02	0.42	0.0052	7.1
0.200	3.96	0.83	0.00	0.93	0.13	0.0049	6.6
0.400	3.27	1.05	-0.10	0.89	0.16	0.0036	6.4
1.000	2.29	1.41	-0.19	0.87	0.20	0.0025	6.3
2.000	1.52	1.83	-0.29	0.91	0.22	0.0018	6.7

Table 11: Coefficients of the adjusted model for v_{S30}=2800 m/s and κ=0.005 sec.

Period (sec)	c_1	c_2	c_3	c_4	c_5	c_6	c_7
0.000	4.99	0.76	0.02	1.32	0.85	0.0025	8.5
0.028	6.29	0.76	0.02	1.43	1.63	0.0015	9.3
0.040	5.93	0.77	0.01	1.36	1.43	0.0021	8.9
0.100	4.54	0.79	0.01	1.02	0.43	0.0051	7.1
0.200	3.92	0.83	0.00	0.93	0.14	0.0049	6.6
0.400	3.25	1.05	-0.10	0.89	0.16	0.0036	6.4
1.000	2.28	1.41	-0.19	0.87	0.20	0.0025	6.3
2.000	1.52	1.84	-0.29	0.91	0.22	0.0018	6.7

Table 12: Coefficients of the adjusted model for v_{S30}=2800 m/s and κ=0.01 sec.

Period (sec)	c_1	c_2	c_3	c_4	c_5	c_6	c_7
0.000	4.28	0.78	0.01	1.21	0.67	0.0028	8.1
0.028	5.64	0.77	0.01	1.38	1.31	0.0019	9.1
0.040	5.54	0.78	0.01	1.34	1.25	0.0021	8.9
0.100	4.41	0.79	0.01	1.03	0.43	0.0049	7.2
0.200	3.85	0.83	0.00	0.93	0.15	0.0048	6.7
0.400	3.22	1.05	-0.10	0.89	0.17	0.0036	6.4
1.000	2.28	1.41	-0.19	0.88	0.19	0.0025	6.3
2.000	1.52	1.84	-0.30	0.91	0.22	0.0018	6.7

Table 13: Coefficients of the adjusted model for v_{S30}=2600 m/s and κ=0.002 sec.

Period (sec)	c_1	c_2	c_3	c_4	c_5	c_6	c_7
0.000	5.96	0.74	0.03	1.49	1.05	0.0023	9.0
0.028	6.65	0.76	0.02	1.45	1.82	0.0014	9.4
0.040	6.15	0.76	0.02	1.36	1.52	0.0021	8.9
0.100	4.62	0.78	0.01	1.02	0.42	0.0052	7.1
0.200	3.96	0.83	0.00	0.93	0.13	0.0049	6.6
0.400	3.27	1.05	-0.10	0.89	0.16	0.0036	6.4
1.000	2.29	1.41	-0.19	0.87	0.20	0.0025	6.3
2.000	1.52	1.83	-0.29	0.91	0.22	0.0018	6.7

Table 14: Coefficients of the adjusted model for v_{S30}=2600 m/s and κ=0.005 sec.

Period (sec)	c_1	c_2	c_3	c_4	c_5	c_6	c_7
0.000	4.99	0.76	0.02	1.32	0.85	0.0025	8.5
0.028	6.29	0.76	0.02	1.43	1.63	0.0015	9.3
0.040	5.93	0.77	0.01	1.36	1.43	0.0021	8.9
0.100	4.54	0.79	0.01	1.02	0.43	0.0051	7.1
0.200	3.92	0.83	0.00	0.93	0.14	0.0049	6.6
0.400	3.25	1.05	-0.10	0.89	0.16	0.0036	6.4
1.000	2.28	1.41	-0.19	0.87	0.20	0.0025	6.3
2.000	1.52	1.84	-0.29	0.91	0.22	0.0018	6.7

Table 15: Coefficients of the adjusted model for v_{S30}=2600 m/s and κ=0.01 sec.

Period (sec)	c_1	c_2	c_3	c_4	c_5	c_6	c_7
0.000	4.28	0.78	0.01	1.21	0.67	0.0028	8.1
0.028	5.64	0.77	0.01	1.38	1.31	0.0019	9.1
0.040	5.54	0.78	0.01	1.34	1.25	0.0021	8.9
0.100	4.41	0.79	0.01	1.03	0.43	0.0049	7.2
0.200	3.85	0.83	0.00	0.93	0.15	0.0048	6.7
0.400	3.22	1.05	-0.10	0.89	0.17	0.0036	6.4
1.000	2.28	1.41	-0.19	0.88	0.19	0.0025	6.3
2.000	1.52	1.84	-0.30	0.91	0.22	0.0018	6.7

Table 16: Coefficients of the adjusted model for v_{S30}=2000 m/s and κ=0.002 sec.

Period (sec)	c_1	c_2	c_3	c_4	c_5	c_6	c_7
0.000	6.24	0.73	0.03	1.52	1.11	0.0022	9.0
0.028	6.84	0.75	0.02	1.44	1.87	0.0014	9.3
0.040	6.33	0.76	0.02	1.35	1.55	0.0022	8.8
0.100	4.77	0.78	0.01	1.01	0.41	0.0053	7.1
0.200	4.09	0.82	0.00	0.93	0.11	0.0050	6.6
0.400	3.37	1.05	-0.11	0.89	0.16	0.0036	6.4
1.000	2.36	1.41	-0.18	0.87	0.20	0.0025	6.3
2.000	1.58	1.83	-0.28	0.91	0.22	0.0018	6.7

Table 17: Coefficients of the adjusted model for v_{S30}=2000 m/s and κ=0.005 sec.

Period (sec)	c_1	c_2	c_3	c_4	c_5	c_6	c_7
0.000	5.22	0.75	0.02	1.34	0.89	0.0026	8.6
0.028	6.49	0.76	0.02	1.43	1.69	0.0015	9.3
0.040	6.11	0.76	0.01	1.35	1.46	0.0021	8.9
0.100	4.69	0.78	0.01	1.02	0.41	0.0052	7.1
0.200	4.04	0.82	0.00	0.93	0.12	0.0050	6.6
0.400	3.35	1.05	-0.10	0.89	0.16	0.0036	6.4
1.000	2.35	1.41	-0.19	0.87	0.20	0.0025	6.3
2.000	1.58	1.83	-0.29	0.91	0.22	0.0018	6.7

Table 18: Coefficients of the adjusted model for v_{S30}=2000 m/s and κ=0.01 sec.

Period (sec)	c_1	c_2	c_3	c_4	c_5	c_6	c_7
0.000	4.48	0.78	0.02	1.23	0.71	0.0028	8.2
0.028	5.86	0.77	0.01	1.38	1.37	0.0019	9.1
0.040	5.73	0.77	0.01	1.34	1.30	0.0021	8.9
0.100	4.56	0.79	0.01	1.02	0.42	0.0051	7.1
0.200	3.97	0.83	0.00	0.93	0.13	0.0049	6.6
0.400	3.31	1.05	-0.10	0.89	0.16	0.0036	6.4
1.000	2.35	1.41	-0.19	0.88	0.19	0.0025	6.3
2.000	1.57	1.84	-0.30	0.91	0.22	0.0018	6.7

6.1.2 Rock models

Table 19: Coefficients of the adjusted model for v_{S30}=800 m/s and κ=0.02 sec.

Period (sec)	c_1	c_2	c_3	c_4	c_5	c_6	c_7
0.000	4.34	0.78	0.01	1.15	0.58	0.0031	7.9
0.028	5.29	0.77	0.01	1.26	1.00	0.0025	8.5
0.040	5.56	0.77	0.01	1.30	1.06	0.0025	8.7
0.100	4.79	0.78	0.01	1.02	0.39	0.0052	7.1
0.200	4.28	0.82	0.00	0.92	0.10	0.0051	6.6
0.400	3.62	1.04	-0.10	0.89	0.14	0.0037	6.3
1.000	2.57	1.40	-0.18	0.88	0.19	0.0025	6.3
2.000	1.76	1.82	-0.29	0.92	0.22	0.0018	6.7

Table 20: Coefficients of the adjusted model for v_{S30}=800 m/s and κ=0.03 sec.

Period (sec)	c_1	c_2	c_3	c_4	c_5	c_6	c_7
0.000	3.56	0.83	0.00	1.02	0.58	0.0029	6.4
0.028	4.02	0.85	0.00	1.06	0.84	0.0026	6.7
0.040	4.39	0.83	0.00	1.13	0.87	0.0026	7.1
0.100	4.20	0.81	0.01	0.95	0.47	0.0047	6.1
0.200	3.89	0.83	0.01	0.87	0.19	0.0048	5.7
0.400	3.36	1.05	-0.10	0.85	0.21	0.0035	5.7
1.000	2.40	1.42	-0.20	0.84	0.24	0.0024	5.8
2.000	1.56	1.84	-0.30	0.87	0.27	0.0017	6.1

Table 21: Coefficients of the adjusted model for v_{S30}=800 m/s and κ=0.05 sec.

Period (sec)	c_1	c_2	c_3	c_4	c_5	c_6	c_7
0.000	3.03	0.89	-0.02	0.97	0.45	0.0029	6.2
0.028	3.20	0.92	-0.02	0.97	0.62	0.0027	6.2
0.040	3.33	0.91	-0.02	1.01	0.55	0.0028	6.4
0.100	3.67	0.84	0.00	0.95	0.40	0.0044	6.1
0.200	3.61	0.85	0.00	0.88	0.23	0.0045	5.7
0.400	3.21	1.05	-0.10	0.85	0.22	0.0035	5.7
1.000	2.34	1.42	-0.20	0.84	0.24	0.0024	5.8
2.000	1.52	1.86	-0.31	0.87	0.27	0.0017	6.0

6.2 Coefficients of the Campbell [2003] adjusted models

The functional form of the Campbell [2003] GMPE is the following:

$$ln(Y) = c_1 + c_2 M + c_3(8.5 - M)^2 + c_4 ln(R) + (c_5 + c_6 M) r_{rup} + f(r_{rup}) \quad (5)$$

with $R = \sqrt{r_{rup}^2 + (c_7 exp(c_8 M))^2}$ and:

$$f(r_{rup}) = \begin{cases} 0 \; for \; r_{rup} \leq r_1 \\ c_7(lnr_{rup} - lnr_1) \; for \; r_1 < r_{rup} \leq r_2 \\ c_7(lnr_{rup} - lnr_1) + c_8(lnr_{rup} - lnr_2) \; for \; r_2 < r_{rup} \end{cases} \quad (6)$$

The proposed coefficients below are giving $ln(Y)$ in m/s^2 while the original coefficients in Campbell [2003] are giving $ln(Y)$ in g. Note that T=0.0 s corresponds to PGA.

6.2.1 Very hard rock models

Table 22: Coefficients of the adjusted model for v_{S30}=2800 m/s and κ=0.002 sec.

Period (sec)	c_1	c_2	c_3	c_4	c_5	c_6	c_7	c_8	c_9	c_{10}
0.000	3.1852	0.819	-0.0211	-2.122	-0.00227	0.000297	0.996	0.378	1.940	-1.564
0.028	3.8205	0.791	-0.0208	-2.048	-0.00144	0.000294	1.112	0.366	1.540	-1.913
0.040	3.1677	0.782	-0.0209	-1.879	-0.00189	0.000289	0.913	0.393	1.603	-2.005
0.100	2.1332	0.759	-0.0243	-1.648	-0.00287	0.000233	0.628	0.448	1.829	-1.852
0.200	2.0433	0.715	-0.0544	-1.579	-0.00286	0.000175	0.572	0.456	1.834	-1.485
0.400	1.9062	0.622	-0.1113	-1.448	-0.00234	0.000135	0.510	0.452	1.614	-1.168
1.000	1.6656	0.513	-0.1983	-1.307	-0.00167	0.000127	0.501	0.440	1.284	-0.865
2.000	1.0483	0.478	-0.2496	-1.232	-0.00115	0.000115	0.472	0.450	1.094	-0.736

Table 23: Coefficients of the adjusted model for v_{S30}=2800 m/s and κ=0.006 sec.

Period (sec)	c_1	c_2	c_3	c_4	c_5	c_6	c_7	c_8	c_9	c_{10}
0.000	2.2542	0.805	-0.0276	-1.941	-0.00237	0.000284	0.844	0.405	1.967	-1.622
0.028	3.3606	0.788	-0.0231	-2.018	-0.00182	0.000301	1.048	0.375	1.622	-1.724
0.040	2.8863	0.777	-0.0228	-1.869	-0.00201	0.000300	0.889	0.398	1.616	-1.874
0.100	2.0642	0.753	-0.0256	-1.651	-0.00285	0.000251	0.635	0.446	1.821	-1.855
0.200	1.9855	0.715	-0.0544	-1.581	-0.00287	0.000182	0.572	0.456	1.834	-1.489
0.400	1.8338	0.630	-0.1099	-1.452	-0.00234	0.000137	0.503	0.455	1.621	-1.173
1.000	1.7140	0.508	-0.1997	-1.311	-0.00166	0.000126	0.493	0.443	1.291	-0.869
2.000	1.2271	0.452	-0.2554	-1.230	-0.00112	0.000110	0.475	0.448	1.090	-0.733

Table 24: Coefficients of the adjusted model for v_{S30}=2800 m/s and κ=0.01 sec.

Period (sec)	c_1	c_2	c_3	c_4	c_5	c_6	c_7	c_8	c_9	c_{10}
0.000	1.8864	0.791	-0.0335	-1.868	-0.00242	0.000275	0.783	0.417	2.000	-1.630
0.028	2.9087	0.785	-0.0260	-1.981	-0.00215	0.000302	0.973	0.387	1.732	-1.607
0.040	2.6055	0.773	-0.0251	-1.856	-0.00217	0.000308	0.858	0.403	1.647	-1.755
0.100	1.9983	0.747	-0.0270	-1.654	-0.00283	0.000270	0.641	0.445	1.814	-1.855
0.200	1.9374	0.713	-0.0548	-1.581	-0.00288	0.000190	0.574	0.455	1.832	-1.492
0.400	1.7849	0.633	-0.1093	-1.454	-0.00235	0.000138	0.500	0.456	1.624	-1.175
1.000	1.7366	0.504	-0.2005	-1.314	-0.00166	0.000125	0.487	0.445	1.296	-0.871
2.000	1.3595	0.433	-0.2599	-1.228	-0.00110	0.000106	0.478	0.446	1.087	-0.731

Table 25: Coefficients of the adjusted model for v_{S30}=2600 m/s and κ=0.002 sec.

Period (sec)	c_1	c_2	c_3	c_4	c_5	c_6	c_7	c_8	c_9	c_{10}
0.000	3.1852	0.819	-0.0211	-2.122	-0.00227	0.000297	0.996	0.378	1.940	-1.564
0.028	3.8205	0.791	-0.0208	-2.048	-0.00144	0.000294	1.112	0.366	1.540	-1.913
0.040	3.1677	0.782	-0.0209	-1.879	-0.00189	0.000289	0.913	0.393	1.603	-2.005
0.100	2.1332	0.759	-0.0243	-1.648	-0.00287	0.000233	0.628	0.448	1.829	-1.852
0.200	2.0433	0.715	-0.0544	-1.579	-0.00286	0.000175	0.572	0.456	1.834	-1.485
0.400	1.9062	0.622	-0.1113	-1.448	-0.00234	0.000135	0.510	0.452	1.614	-1.168
1.000	1.6656	0.513	-0.1983	-1.307	-0.00167	0.000127	0.501	0.440	1.284	-0.865
2.000	1.0483	0.478	-0.2496	-1.232	-0.00115	0.000115	0.472	0.450	1.094	-0.736

Table 26: Coefficients of the adjusted model for v_{S30}=2600 m/s and κ=0.006 sec.

Period (sec)	c_1	c_2	c_3	c_4	c_5	c_6	c_7	c_8	c_9	c_{10}
0.000	2.2542	0.805	-0.0276	-1.941	-0.00237	0.000284	0.844	0.405	1.967	-1.622
0.028	3.3606	0.788	-0.0231	-2.018	-0.00182	0.000301	1.048	0.375	1.622	-1.724
0.040	2.8863	0.777	-0.0228	-1.869	-0.00201	0.000300	0.889	0.398	1.616	-1.874
0.100	2.0642	0.753	-0.0256	-1.651	-0.00285	0.000251	0.635	0.446	1.821	-1.855
0.200	1.9855	0.715	-0.0544	-1.581	-0.00287	0.000182	0.572	0.456	1.834	-1.489
0.400	1.8338	0.630	-0.1099	-1.452	-0.00234	0.000137	0.503	0.455	1.621	-1.173
1.000	1.7140	0.508	-0.1997	-1.311	-0.00166	0.000126	0.493	0.443	1.291	-0.869
2.000	1.2271	0.452	-0.2554	-1.230	-0.00112	0.000110	0.475	0.448	1.090	-0.733

Table 27: Coefficients of the adjusted model for v_{S30}=2600 m/s and κ=0.01 sec.

Period (sec)	c_1	c_2	c_3	c_4	c_5	c_6	c_7	c_8	c_9	c_{10}
0.000	1.8864	0.791	-0.0335	-1.868	-0.00242	0.000275	0.783	0.417	2.000	-1.630
0.028	2.9087	0.785	-0.0260	-1.981	-0.00215	0.000302	0.973	0.387	1.732	-1.607
0.040	2.6055	0.773	-0.0251	-1.856	-0.00217	0.000308	0.858	0.403	1.647	-1.755
0.100	1.9983	0.747	-0.0270	-1.654	-0.00283	0.000270	0.641	0.445	1.814	-1.855
0.200	1.9374	0.713	-0.0548	-1.581	-0.00288	0.000190	0.574	0.455	1.832	-1.492
0.400	1.7849	0.633	-0.1093	-1.454	-0.00235	0.000138	0.500	0.456	1.624	-1.175
1.000	1.7366	0.504	-0.2005	-1.314	-0.00166	0.000125	0.487	0.445	1.296	-0.871
2.000	1.3595	0.433	-0.2599	-1.228	-0.00110	0.000106	0.478	0.446	1.087	-0.731

Table 28: Coefficients of the adjusted model for v_{S30}=2000 m/s and κ=0.002 sec.

Period (sec)	c_1	c_2	c_3	c_4	c_5	c_6	c_7	c_8	c_9	c_{10}
0.000	3.4195	0.821	-0.0198	-2.140	-0.00218	0.000283	1.025	0.373	1.920	-1.567
0.028	4.0055	0.795	-0.0199	-2.050	-0.00131	0.000276	1.118	0.365	1.535	-1.970
0.040	3.3297	0.786	-0.0200	-1.879	-0.00182	0.000270	0.913	0.394	1.608	-2.046
0.100	2.2503	0.765	-0.0235	-1.645	-0.00287	0.000211	0.620	0.450	1.837	-1.845
0.200	2.1615	0.716	-0.0541	-1.578	-0.00284	0.000164	0.569	0.457	1.836	-1.480
0.400	2.0057	0.622	-0.1112	-1.447	-0.00233	0.000132	0.510	0.452	1.614	-1.167
1.000	1.6773	0.522	-0.1961	-1.308	-0.00168	0.000128	0.499	0.441	1.286	-0.867
2.000	0.9599	0.500	-0.2440	-1.240	-0.00117	0.000120	0.463	0.455	1.105	-0.743

Table 29: Coefficients of the adjusted model for v_{S30}=2000 m/s and κ=0.006 sec.

Period (sec)	c_1	c_2	c_3	c_4	c_5	c_6	c_7	c_8	c_9	c_{10}
0.000	2.4359	0.809	-0.0258	-1.952	-0.00231	0.000272	0.861	0.402	1.954	-1.629
0.028	3.5486	0.791	-0.0221	-2.022	-0.00168	0.000284	1.059	0.373	1.606	-1.770
0.040	3.0519	0.781	-0.0218	-1.870	-0.00193	0.000282	0.892	0.397	1.616	-1.916
0.100	2.1810	0.758	-0.0247	-1.648	-0.00284	0.000230	0.627	0.448	1.829	-1.850
0.200	2.1018	0.717	-0.0541	-1.580	-0.00285	0.000171	0.569	0.457	1.836	-1.484
0.400	1.9349	0.629	-0.1098	-1.451	-0.00234	0.000134	0.503	0.455	1.621	-1.172
1.000	1.7373	0.514	-0.1980	-1.312	-0.00167	0.000127	0.492	0.444	1.293	-0.870
2.000	1.1442	0.473	-0.2502	-1.236	-0.00115	0.000115	0.468	0.452	1.100	-0.739

Table 30: Coefficients of the adjusted model for v_{S30}=2000 m/s and κ=0.01 sec.

Period (sec)	c_1	c_2	c_3	c_4	c_5	c_6	c_7	c_8	c_9	c_{10}
0.000	2.0418	0.795	-0.0315	-1.877	-0.00237	0.000265	0.795	0.414	1.989	-1.638
0.028	3.0990	0.787	-0.0248	-1.987	-0.00202	0.000287	0.989	0.384	1.709	-1.637
0.040	2.7734	0.777	-0.0240	-1.858	-0.00207	0.000291	0.864	0.402	1.641	-1.794
0.100	2.1146	0.752	-0.0260	-1.651	-0.00281	0.000248	0.634	0.446	1.821	-1.852
0.200	2.0527	0.715	-0.0544	-1.580	-0.00286	0.000178	0.571	0.456	1.835	-1.487
0.400	1.8855	0.633	-0.1092	-1.453	-0.00234	0.000135	0.500	0.456	1.624	-1.174
1.000	1.7684	0.509	-0.1991	-1.314	-0.00166	0.000126	0.488	0.445	1.296	-0.872
2.000	1.2829	0.452	-0.2550	-1.233	-0.00113	0.000111	0.472	0.450	1.096	-0.736

6.2.2 Rock models

Table 31: Coefficients of the adjusted model for v_{S30}=800 m/s and κ=0.02 sec.

Period (sec)	c_1	c_2	c_3	c_4	c_5	c_6	c_7	c_8	c_9	c_{10}
0.000	2.0736	0.776	-0.0376	-1.805	-0.00225	0.000210	0.744	0.423	2.022	-1.640
0.028	2.6986	0.783	-0.0297	-1.899	-0.00221	0.000223	0.844	0.408	1.904	-1.576
0.040	2.6558	0.777	-0.0267	-1.824	-0.00211	0.000240	0.796	0.415	1.722	-1.655
0.100	2.3586	0.753	-0.0265	-1.649	-0.00268	0.000216	0.624	0.449	1.828	-1.838
0.200	2.3632	0.717	-0.0542	-1.579	-0.00280	0.000156	0.564	0.458	1.840	-1.478
0.400	2.1661	0.637	-0.1080	-1.455	-0.00231	0.000127	0.496	0.457	1.629	-1.174
1.000	1.9029	0.523	-0.1954	-1.321	-0.00167	0.000128	0.479	0.449	1.307	-0.878
2.000	1.2437	0.486	-0.2458	-1.250	-0.00118	0.000121	0.456	0.457	1.120	-0.751

Table 32: Coefficients of the adjusted model for v_{S30}=800 m/s and κ=0.03 sec.

Period (sec)	c_1	c_2	c_3	c_4	c_5	c_6	c_7	c_8	c_9	c_{10}
0.000	1.8740	0.746	-0.0485	-1.760	-0.00225	0.000204	0.710	0.430	2.048	-1.614
0.028	2.0672	0.752	-0.0427	-1.793	-0.00236	0.000206	0.715	0.433	2.036	-1.565
0.040	2.0876	0.758	-0.0357	-1.769	-0.00237	0.000237	0.703	0.435	1.846	-1.536
0.100	2.2006	0.737	-0.0302	-1.655	-0.00263	0.000255	0.636	0.446	1.812	-1.832
0.200	2.2518	0.712	-0.0554	-1.580	-0.00282	0.000173	0.569	0.457	1.836	-1.485
0.400	2.0873	0.638	-0.1081	-1.456	-0.00232	0.000130	0.495	0.458	1.630	-1.175
1.000	1.9377	0.515	-0.1975	-1.323	-0.00166	0.000126	0.475	0.450	1.310	-0.879
2.000	1.4741	0.450	-0.2545	-1.242	-0.00114	0.000113	0.463	0.453	1.108	-0.743

Table 33: Coefficients of the adjusted model for v_{S30}=800 m/s and κ=0.05 sec.

Period (sec)	c_1	c_2	c_3	c_4	c_5	c_6	c_7	c_8	c_9	c_{10}
0.000	1.7367	0.696	-0.0677	-1.712	-0.00219	0.000195	0.680	0.435	2.067	-1.572
0.028	1.7176	0.684	-0.0677	-1.687	-0.00233	0.000181	0.647	0.445	2.084	-1.529
0.040	1.5379	0.699	-0.0608	-1.660	-0.00240	0.000203	0.586	0.461	1.969	-1.471
0.100	1.8933	0.707	-0.0391	-1.660	-0.00259	0.000317	0.640	0.446	1.799	-1.779
0.200	2.0447	0.700	-0.0580	-1.583	-0.00288	0.000213	0.581	0.453	1.827	-1.500
0.400	1.9447	0.636	-0.1089	-1.457	-0.00233	0.000136	0.494	0.458	1.630	-1.177
1.000	1.9418	0.508	-0.1997	-1.326	-0.00164	0.000123	0.469	0.453	1.316	-0.882
2.000	1.8235	0.394	-0.2679	-1.230	-0.00107	0.000100	0.473	0.447	1.091	-0.732

6.3 Bommer et al. (2010) article on the GMPE pre-selection criteria

On the Selection of Ground-Motion Prediction Equations for Seismic Hazard Analysis

Julian J. Bommer,[1] John Douglas,[2] Frank Scherbaum,[3] Fabrice Cotton,[4] Hilmar Bungum,[5] and Donat Fäh[6]

INTRODUCTION

A key element in any seismic hazard analysis is the selection of appropriate ground-motion prediction equations (GMPEs). In an earlier paper, focused on the selection and adjustment of ground-motion models for probabilistic seismic hazard analysis (PSHA) in moderately active regions—with limited data and few, if any, indigenous models—Cotton *et al.* (2006) proposed seven criteria as the basis for selecting GMPEs. Recent experience in applying these criteria, faced with several new GMPEs developed since the Cotton *et al.* (2006) paper was published and a significantly larger strong-motion database, has led to consideration of how the criteria could be refined and of other conditions that could be included to meet the original objectives of Cotton *et al.* (2006). In fact, about a dozen new GMPEs are published each year, and this number appears to be increasing. Additionally, Cotton *et al.* (2006) concluded that the criteria should not be excessively specific, tied to the state-of-the-art in ground-motion modeling at the time of writing and thus remaining static, but rather should be sufficiently flexible to be adaptable to the continuing growth of the global strong-motion database and the continued evolution of GMPEs.

The purpose of this paper is to present an update of these criteria, which formed a small section of the Cotton *et al.* (2006) paper but which are the exclusive focus of this study. The revised and extended list of selection criteria should be of use to those charged with conducting seismic hazard analyses, primarily as a way of avoiding unintended subjectivity in the process of assembling suites of GMPEs to be used in the hazard calculations. At the same time, the suite of criteria—which are actually for excluding GMPEs from a global set rather than selecting in the strict sense—may also be useful as a checklist for those developing new GMPEs.

1. Civil & Environmental Engineering, Imperial College London, U.K.
2. Earthquake Engineering Research Centre, University of Iceland, Selfoss, Iceland (on teaching leave from RNSC/RIS, BRGM, Orléans, France)
3. Institut für Geowissenschaften Universität Potsdam, Potsdam, German
4. LGIT, Université Joseph Fourier, Grenoble, France
5. NORSAR/ICG, Kjeller, Norway
6. Swiss Seismological Service, ETH, Zurich, Switzerland

OBJECTIVES OF GROUND-MOTION MODEL SELECTION

The two fundamental components of a PSHA are a model for the occurrence of future earthquakes in terms of magnitude, frequency, and location; and a model for the estimation of ground-motion parameters at a given site as a result of each earthquake scenario. The epistemic uncertainty in both components must be identified, quantified, and captured in the analysis, the most widely used tool for this purpose being the logic tree (*e.g.*, Kulkarni *et al.* 1984; Bommer and Scherbaum 2008). In order to capture the epistemic uncertainty in both median ground-motion predictions and their associated aleatory variability, it has become standard practice to include more than one GMPE in logic-tree formulations for PSHA (*e.g.*, Bommer *et al.* 2005).

The approach of Cotton *et al.* (2006) to populate the ground-motion branches of a logic-tree begins with the premise that to avoid availability traps (*e.g.*, Kahnemann *et al.* 1982), whereby an analyst may choose those models with which he or she is most familiar, the starting point should be to assemble a comprehensive list of all ground-motion models that meet the standard scientific quality criteria of international peer-reviewed journals and then eliminate those considered unsuitable. The first basis for exclusion of a model is that it is from a tectonic region that is not relevant to the location of the site for which the PSHA is being conducted. We believe that this should not be a basis for selection or exclusion on purely geographical criteria (*i.e.*, only using models derived for the host country or region) since several studies have concluded that there is no strong evidence for persistent regional differences in ground motions among tectonically comparable areas, at least in the range of moderate-to-large magnitude earthquakes (*e.g.*, Douglas 2007; Stafford *et al.* 2008), although some studies have found modest differences in ground-motion attenuation (for high-frequency response parameters) between active regions (Scasserra *et al.* 2009). Rather, this criterion would simply mean not including equations for subduction earthquakes in the analysis of hazard due to shallow crustal earthquakes, and vice versa. One should also exclude equations derived for volcanic areas for PSHA in a region that does not have this feature and models for deep Vrancea-type earthquakes for areas not affected by such events. In some cases, there may be a clear basis for other exclusions, such as in the United States where

doi: 10.1785/gssrl.81.5.783

models derived for western North America and for central and eastern North America (CENA) are each unlikely to be used for hazard analyses in the other region. However, beyond these cases, the issue of tectonic, rather than geographical, relevance will not generally be a sufficient basis to populate the logic-branches by itself.

All of the other exclusion criteria are then related to the inherent quality of the model and its applicability to the particular PSHA being conducted, in terms of ranges and definitions of both predicted and explanatory variables. These criteria cannot be completely decoupled from the consideration of tectonic relevance for the simple reason that when dealing with any type of seismicity other than active crustal earthquakes, the number of available GMPEs is limited. Therefore, while it is possible to be rather stringent with regard to quality and applicability criteria for GMPEs to be used in regions of shallow crustal seismicity, for subduction zones and particular areas such as the Vrancea region of Romania, the application of similarly rigorous exclusion criteria is likely to leave the analyst with no models at all. Using these criteria, stable continental regions (SCRs) are also less likely to be left with any models except for stochastic ones.

In terms of overall objectives, Cotton *et al.* (2006) stated that "ideally, the ground-motion selection process should result in the smallest set of independent models that capture, potentially after host-to-target conversions, the analyst's estimate of the range of possible ground motions in the target region." Two aspects of this statement have been reconsidered in the light of recent experience and developments, the first being to question the practice of applying full host-to-target conversions, using the hybrid approach of Campbell (2003) combined with the method of Scherbaum, Cotton *et al.* (2006) for obtaining equivalent stochastic parameters for empirical GMPEs. These approaches will nearly always be employed using local recordings of small-to-moderate magnitude earthquakes, because if there were sufficient large events recorded in the target region, then one would simply develop local equations. Without extending the discussion of this topic, which is somewhat outside the strict focus of this paper on ground-motion model selection procedures, many recent studies have cast doubt on the use of small-magnitude data as the basis for predicting motions from moderate-to-large magnitude earthquakes (*e.g.*, Bommer *et al.* 2007; Cotton *et al.* 2008; Atkinson and Morrison 2009; Chiou *et al.*, forthcoming). In summary, we are now inclined to believe that host-to-target conversions, beyond a V_s-κ adjustment to the reference site profile, may provide an apparent degree of precision in terms of improved local applicability of the equations, but at a high cost in terms of added uncertainty because of the problems in extrapolating magnitude scaling from small to large earthquakes. Also, the parameters needed for host-to-target conversions are also often poorly constrained, especially for target regions. If one accepts this conclusion, then the selection process should be implemented keeping in mind that models will not be subsequently adjusted to better match the characteristics of the target region.

The other aspect of the above statement cited from Cotton *et al.* (2006) that has been re-evaluated is the objective of obtaining the smallest suite of GMPEs possible that capture the potential range of future ground motions. The original rationale for this objective was to avoid model redundancy through having several models derived from overlapping datasets, notwithstanding that differences among such models, as is the case for example with the Next Generation Attenuation (NGA) equations (Abrahamson *et al.* 2008), may be a legitimate representation of epistemic uncertainty. Although the option always remains for the analyst to remove more equations if it is felt that model redundancy is an issue, an alternative approach is to assign weights to the logic-tree branches in a way that groups such models in the first instance and then redistributes their collective weight among the individual equations. For this purpose, while in the past any judgments regarding redundancy of models would have been based purely on the degree of overlap in their underlying datasets, tools have now been developed that allow the assessment of the degree of proximity of predictive models in terms of actual ground-motion distributions for appropriate ranges of predictor variables (*e.g.*, Scherbaum *et al.* 2009 and forthcoming). However, beyond these statements, considerations of host-to-target model adjustments and logic-tree branch weights are beyond the scope of this paper, which is intended to address only the question of model selection.

The remainder of the paper discusses the criteria that may be applied to exclude GMPEs from the global list assembled for consideration by the hazard analyst, after models that are from inappropriate tectonic regimes have been removed. Compendia of published empirical GMPEs for response spectral ordinates have been compiled by Douglas (2003, 2006, 2008), and these may provide a useful starting point for assembling the global list of candidate equations. The criteria are grouped under three broad headings, namely data issues, modeling issues, and model performance, although the separation into these categories is somewhat artificial, not least because of a degree of interdependence among some of the criteria. The paper concludes with a brief discussion of how these selection criteria may be adapted to keep abreast with the evolution of ground-motion modeling, and at the same time how the criteria could influence the latter by providing guidance on minimum standards for published ground-motion prediction equations.

DATA ISSUES

The starting point for deriving a ground-motion prediction equation is the dataset of ground-motion recordings that will be used either directly for regression analysis in the case of empirical models or the inversions that will provide the parameters for a stochastic model. Clearly it is important that any parameters used to characterize the earthquakes and the recordings must be determined in a consistent manner, using a unique definition or convention, for all of the recordings.

We also believe that the dataset should be presented as part of the model. Ideally, the presentation of the dataset will be in the form of a listing of the recordings, providing all of

the earthquake source parameters, source-to-site distances, and site classifications. However, it is also recognized that as the datasets used in the derivation of GMPEs become larger and larger, it may become cumbersome to provide so much information directly within the paper. Often the minimum that can be expected is a listing of the earthquakes represented in the dataset, together with their source parameters, and an indication of the number of recordings from each event, possibly with the range of distances over which these were obtained. When it is not possible to include such a table within the paper due to length considerations, it needs to be made available to users of the model in the form of an electronic supplement or a listing in an easily accessible publication such as a report that can be freely downloaded. Within the paper presenting the model itself, some basic statistics of the dataset, including a plot in magnitude-distance space (using different symbols for styles of faulting and/or site classes), are helpful for users to assess and understand the model. Ideally, the authors should make the data freely available, which would then allow their work to be reproduced and validated by others.

Predicted Ground-Motion Parameters

A site-specific PSHA will generally be conducted to determine seismic design loads for a specific engineering project, in which case there will be specific requirements with regard to the predicted ground-motion parameters that will influence the selection of GMPEs. For nearly all seismic design the principal parameter required is the response spectrum of absolute acceleration, usually with the nominal 5% of critical damping. Over the range of response periods relevant to most engineering projects, the difference between the true acceleration response (SA) and the pseudo-acceleration response (PSA) is generally not significant (*e.g.*, Chopra 1995), but when combining GMPEs in a logic-tree the difference should be considered, especially if very short or long response periods are being considered.

The main issue that needs to be addressed is whether the GMPE covers the full period range that will be required for the engineering analyses, especially if it will be necessary to define the complete response spectrum for the full period range. At the short-period end, most GMPEs provide an explicit equation for peak ground acceleration (PGA) and then acceleration response ordinates at a range of periods. If the highest response frequency required is not covered by a given equation, then provided there is a PGA equation it is possible to interpolate the coefficients to determine the missing values. This may require an assumption regarding the response frequency above which PSA is equal to PGA, which will depend on the stiffness of the site and the stress drop of the earthquake, among other factors. Estimates of this frequency generally lie in the range from 25 to 50 Hz, but for very hard rock conditions such as those typically represented in models for CENA, it may be closer to 100 Hz. Similarly, the coefficients for any specific intermediate response frequency not covered explicitly by the equations can be determined by interpolation of the coefficients against frequency (or its logarithm), but for complex models the behavior of the resulting equation should be carefully inspected before application since small variations in the coefficients can have a surprisingly large impact on the results (*e.g.*, Akkar and Bommer 2010).

All records in the dataset should be carefully processed, using uniform criteria and procedures to take account of high- and low-frequency noise. The derivation of a GMPE for response spectral ordinates should take account of the usable period range of each accelerogram, which will be determined mainly by the processing applied to the records (*e.g.*, Boore and Bommer 2005). At the other end of the frequency range, the highest usable frequency will depend on the instrument characteristics (hence analog recordings will have lower limiting values than digitally recorded accelerograms), the digitization interval, and any low-pass filtering applied to the records. (*e.g.*, Douglas and Boore 2010). The longest period for which spectral responses can be reliably calculated is determined by the high-pass filter cut off and is considerably shorter than this value for analog recordings (*e.g.*, Akkar and Bommer 2006). When regressions are performed, the spectral ordinates from each record should only be used down to the minimum usable frequency, and if this rule has not been followed then the equation should not be used beyond the clear limit of usable response periods.

A final consideration is the way that the two horizontal components from each accelerogram have been treated, since several different options have been used in the derivation of GMPEs. The choice of reference definition will be determined by the engineering analyses to be conducted downstream and the need for consistency between the manner in which the seismic loads are defined and how they are then applied to the structure in both response spectrum and time-history analysis. There is no need to exclude a model if it is based on a definition of the horizontal component definition different from that chosen for the PSHA, since simple conversions can be made for medians and associated standard deviations (Beyer and Bommer 2006; Watson-Lamprey and Boore 2007). A model may be excluded, however, if the horizontal component definition used is not explicitly stated and cannot be inferred from the publication describing the model definition.

Magnitude-Distance Ranges

Integrations in PSHA cover a range of range of magnitudes from the minimum considered to be of engineering importance (usually in the range M_w 4–5) to the maximum considered physically possible within each seismic source, M_{max}. Even in regions of relatively low seismic activity, M_{max} will often be assigned values up to at least M_w 6.5, even if these may be assigned relatively low weights on the logic-tree branches. Therefore, a GMPE needs to be applicable to this range of magnitudes, or at least to a range not too different from the integration limits of the PSHA calculations. The range of applicability of a predictive model is fundamentally controlled by the distribution of the data from which it is derived, so the upper and lower limits of magnitude of the dataset become important considerations in the selection process, and in particular the analyst will tend to exclude any equation in which the larg-

est magnitude represented is significantly smaller than M_{max}. Similar consideration may be given to the distance range of the model.

Excluding GMPEs that are not constrained for larger magnitudes will obviously tend to discriminate against the inclusion of local models for regions of low-to-moderate seismicity, which to some will seem counter-intuitive since it means not using in the PSHA those equations that are nominally most relevant to the setting of the site under consideration. However, as with the host-to-target region adjustments discussed earlier, the inclusion of such models can create the illusion of precision while actually adding considerable uncertainty because of the problems associated with extrapolation of magnitude scaling determined mainly from smaller events. This does not mean, however, that local small-magnitude datasets have no use at all, since they can be employed in several different ways to enhance the ground-motion model section of the logic-tree for a PSHA. For example, the data can be used to test the applicability of models from other regions, using techniques such as those proposed by Scherbaum, Schmedes, *et al.* (2004) and Scherbaum *et al.* (2009), although consideration must still be given to magnitude-scaling issues. Another option is to adjust one or more coefficients of a well-constrained model from another region, with more abundant data, to fit a locally recorded dataset (*e.g.*, Atkinson 2008). Equally, larger locally recorded datasets, although insufficient to derive sophisticated models with multiple explanatory parameters, may be used to test the implied magnitude, distance, and site scaling of global equations, making minor adjustments to some coefficients for local application if deemed necessary. An example of such an approach is the study of Scasserra *et al.* (2009) in which the NGA models were compared with Italian strong-motion data. Local datasets can also help to characterize stations' site transfer functions (*e.g.*, Edwards *et al.* 2008; Drouet *et al.* 2008). These site properties are useful to implement V_s-κ adjustments.

There is another potentially very important use for local datasets related to the recent discovery that empirical GMPEs tend to consistently over-predict ground motions at their lower magnitude limit (*e.g.*, Bommer *et al.* 2007; Atkinson and Morrison 2009). This is illustrated in Figure 1. Since this tendency to overpredict motions at the lower magnitude limit is consistently found in empirical GMPEs, it is believed that the overprediction arises not from data issues directly but on fitting the functional form over an insufficiently wide range of magnitudes to capture the change in scaling from linear at small magnitudes to non-linear for larger events. In order to overcome this problem in such a way as to have models adjusted to local conditions, Chiou *et al.* (forthcoming) have developed an approach to extending GMPEs so that predictions remain unchanged for larger magnitudes but fit those from target-region data in the smaller magnitude range.

The fact that a dataset extends between two limits in terms of both magnitude and distance, however, does not automatically mean that the resulting equation will be robustly constrained to provide predictions of ground motions for all of these magnitude and distance combinations, even without

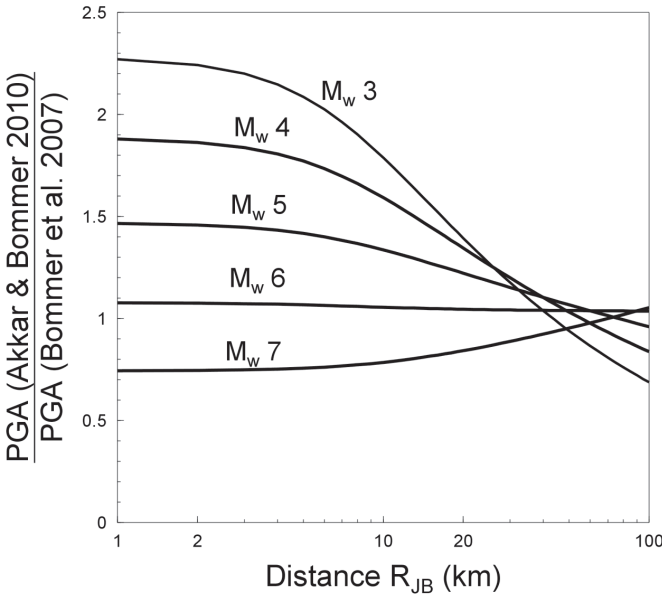

▲ **Figure 1.** Ratios of predicted median peak ground accelerations on rock sites from strike-slip earthquakes of different magnitudes obtained from the equation of Akkar and Bommer (2010), derived using data from M_w 5.0 to 7.6, to those from Bommer *et al.* (2007), which used the same data supplemented with additional data from M_w 3.0 to 5.0. Note that although M_w 5 is common to both datasets, the former equation predicts values 50% higher at short distances.

considering the "edge effects" (in other words, empirical models not performing well at the lower magnitude limit of the dataset from which they are derived) referred to in the previous paragraph. This consideration is relevant if the model has been derived with the primary focus on fitting an equation to observations rather than using these to constrain a model that can be used for robust predictions of ground motions from future scenarios that include but are not limited to those generating the dataset. One option for the hazard analyst is to consider the ability of the dataset to constrain the magnitude scaling and attenuation with distance over the range defined by the statistical confidence limits on the determination of mean values from the dataset, for which two simple measures could be used. The first is the average number of earthquakes in the dataset per unit of magnitude defining the total range, and the second the total number of records per 100 km of distance covered by the dataset. These numbers have been calculated for a large number of GMPEs for response spectral accelerations (for which the numbers of earthquakes and records, and the magnitude and distance ranges, were all reported) and are displayed in Figure 2 against year of publication of the model. These figures have been prepared using the information available in the reports of Douglas (2003, 2006, 2008).

Although these plots show that there are still some equations derived from very sparse datasets, the trend is clearly toward using larger and larger collections of strong-motion recordings (the rate of growth is somewhat concealed by the logarithmic *y*-axis). The question that the analyst needs to

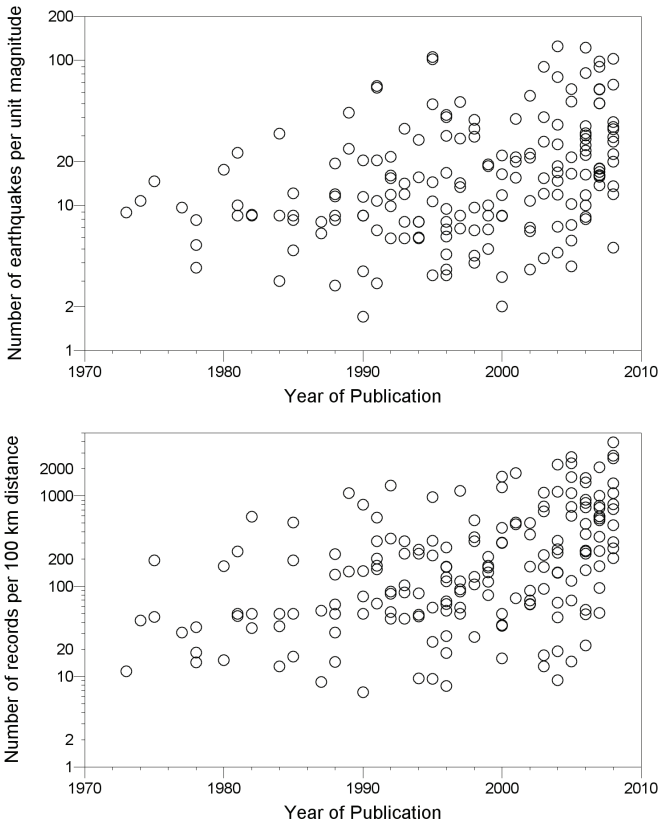

▲ **Figure 2.** Measures of the density of datasets to constrain the magnitude and distance dependence of ground-motion prediction models as a function of the year of publication.

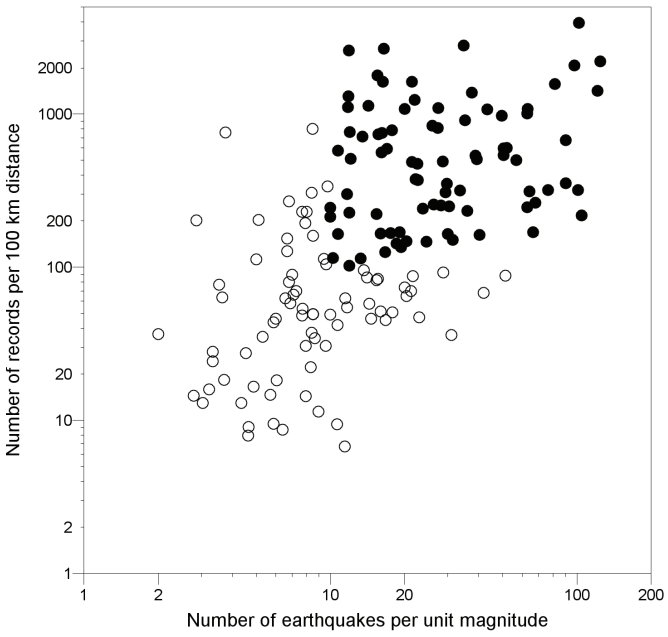

▲ **Figure 3.** Relationship between data density measures from Figure 2. The black circles correspond to models derived from datasets with at least 10 earthquakes for each unit of the magnitude range, and 100 records for every 100 km of the distance range.

address, in effect, is whether an equation derived from a dataset that could be classified as "small" compared to other contemporary models is justified? The important point here is that what appears to be an acceptable size for a strong-motion database now may have been impossible to achieve 30 years ago, and in turn may seem unacceptably small 10 or 20 years from now. As Figure 3 shows, the two parameters depicted in Figure 2 generally show a degree of correlation, but there is sufficient variability in this relationship to justify explicit consideration of both the number of earthquakes constraining magnitude dependence and the number of records constraining decay of ground-motion amplitudes with distance.

MODELING ISSUES

Once the analyst has duly considered the database from which the model has been derived and judged it to be at least adequate, the next criteria that may exclude an equation from use in the PSHA are related to the formulation and derivation of the model itself.

One option, as a prelude to specific considerations, is to drop any equation that has not been published in a peer-reviewed journal, since publication implies that it has passed some degree of scrutiny and technical challenge. Some flexibility may also need to be applied with such a criterion in order not to prevent the use of robust equations derived for specific projects or regions and published in the form of a technical report by a research institute with its own internal review system, although clearly one may have higher confidence in models published in reputable journals. The hazard analyst team will often possess similar review competence and should be allowed to exert the same, provided that their judgment is properly documented.

Predictor or Explanatory Variables

All GMPEs include earthquake magnitude and some measure of source-to-site distance as predictor variables in the model. The key issue is that the magnitude scale employed in the equation is consistent with that used to define earthquake activity rates in the seismic source model. These may require conversions for some of the GMPEs selected for inclusion in the logic-tree in a PSHA. The most commonly used scales have been surface-wave magnitude, M_s, and moment magnitude, M_w, and there are a number of empirical relationships between these scales that may be used to make the conversion, although increasingly modelers are adopting M_w. Many equations for smaller-magnitude earthquakes use local magnitude, M_L. The important point is that the variability associated with these relationships must be propagated into the sigma value of the GMPE for which the adjustment is made (Bommer *et al.* 2005). Although this is straightforward, the analyst may wish to limit the number of equations for which such adjustments are required since the sigma penalty is not insignificant (*e.g.*, Scherbaum *et al.* 2005), and in some sense the increase is artificial because it is not routinely found that equations derived in terms of M_s have higher variability than those derived as a

function of M_w, for example. Models that use local magnitude, M_L, to quantify earthquake size might be avoided by the hazard analyst, especially if from a different region than that for which the PSHA is being conducted. Even if the M_L scale is from the target region, the fact that this magnitude scale saturates at a relatively low value may be considered a reason to exclude the model, and unless there is a robust local M_L-M_w conversion available, compatibility issues are also likely to lead to such models being dropped. Also, M_L-M_w relations for magnitudes below 5 often show trends that, if extrapolated to larger magnitudes, could introduce significant biases.

In terms of distance metrics used in the ground-motion models, these need to be consistent with the manner in which earthquake scenarios are modeled within the seismic hazard computation code. Conversions can be made among different distance metrics (*e.g.*, Scherbaum, Schmedes, *et al.* 2004), but the sigma penalty is often very high and for this reason these adjustments should be avoided as much as possible (Scherbaum *et al.* 2005). However, this should not lead to GMPEs being excluded, since the solution to this problem lies in acquiring or developing a hazard code that is capable of modeling extended seismic sources in such a way that each of the commonly used distance metrics (*e.g.*, Abrahamson and Shedlock 1997) can be computed, and each equation used with its native distance measure. Nonetheless, the analyst may consider the use of point-source measures (*e.g.*, epicentral or hypocentral distance) as inappropriate metrics for the prediction of ground-motion amplitudes from larger earthquakes associated with fault ruptures tens or even hundreds of kilometers in length. Conversely, if the hazard analysis is to be performed with software that models earthquake occurrences within area sources as points without simulated fault ruptures for larger earthquakes (randomly oriented unless geological and stress-field information indicate a preferred strike), then in a sense it would be more appropriate to adopt GMPEs based on epicentral or hypocentral distance. If such software is used with modern equations employing R_{JB} or R_{rup} (see Abrahamson and Shedlock 1997 for definitions) as the distance metric, then the ground-motion variability needs to be increased in the near-source region to account for the difference in distance metrics; this could also be achieved by applying the empirical adjustments of Scherbaum, Schmedes, *et al.* (2004). Ideally, one should simply avoid performing PSHA calculations with software that cannot accommodate the native distance metric of each GMPE (Scherbaum, Bommer *et al.* 2006).

In addition to magnitude and distance, it is generally true that a parameter (or parameters) is included to model the influence of the near-surface materials, although there are some equations for which this is implicit by virtue of predicting ground motions only for a specific type of site (*e.g.*, rock). For those equations that do include one or more parameters to model the influence of site effects, the main consideration is whether the range of values that these parameters encompass can cover the target horizon at the site (which may be the foundation level or a deeper stratum if site response or soil-structure interaction analyses are to be conducted). The fact that a model does not include the site conditions in question need not, however, exclude it from the PSHA, since adjustments can be made, but the analyst will need to consider the uncertainty associated with such adjustments and will need to propagate this uncertainty through the hazard calculations. The main issue in this respect is that it will generally not be sufficient to apply only a correction from the reference V_{s30} of the GMPE to the target V_{s30} at the site, but to also adjust for differences in the near-surface attenuation parameter, κ. If this is not done, one is making the implicit assumption that only the uppermost 30 m at the reference and target sites are different, with the deeper kappa values being the same; these two parameters are coupled and should not be treated in isolation from one another. An important point to note is that applying an adjustment only for V_{s30} when applying CENA equations derived for sites with shear-wave velocities of 2–3 km/s, without a corresponding κ correction, can lead to ridiculously large and unrealistic high-frequency spectral accelerations.

A model may also be rejected by the analyst if it does not include the influence of a factor known to exert a marked influence on the ground motion, for which a range of values or classes is present in the underlying strong-motion dataset. An obvious example is the style of faulting, which is increasingly, but not universally, included as a predictor variable. If the seismic source characterization model specifies styles of faulting, then GMPEs that do not include this factor need to be adjusted, which can be done using, for example, the method proposed by Bommer *et al.* (2003). This approach requires that the distribution of the dataset among different styles of faulting can be determined, or that the dominant rupture mechanism represented by the model—such as reverse faulting for CENA GMPEs—can be assumed with some confidence.

Functional Form of Equation

The functional forms used for ground-motion prediction equations have evolved considerably, with some of the most recent models being rather cumbersome to implement as a result. As a consequence, the problem of balancing model complexity and data constraints becomes increasingly relevant for the generation of empirical ground-motion models (Kuehn *et al.* 2009). Although the criteria discussed in this section are related primarily to the exclusion of models considered to be excessively simple, one may also consider the issue of over-parameterization for already existing models. In other words, the analyst may decide that some models have attempted to constrain too many factors and too many influences on the ground motion. In a strict sense, the influence of each additional parameter can be unambiguously determined if it can be effectively decoupled from that of the other parameters already in the model. In other words, ideally one would like the distribution of the dataset with respect to each class or range of the additional parameter to be comparable with respect to the other model parameters. This consideration should take account of equations for which constraint from physical modeling was included in their derivation rather than relying entirely on fitting to empirical data, the main example of which are some of the NGA models.

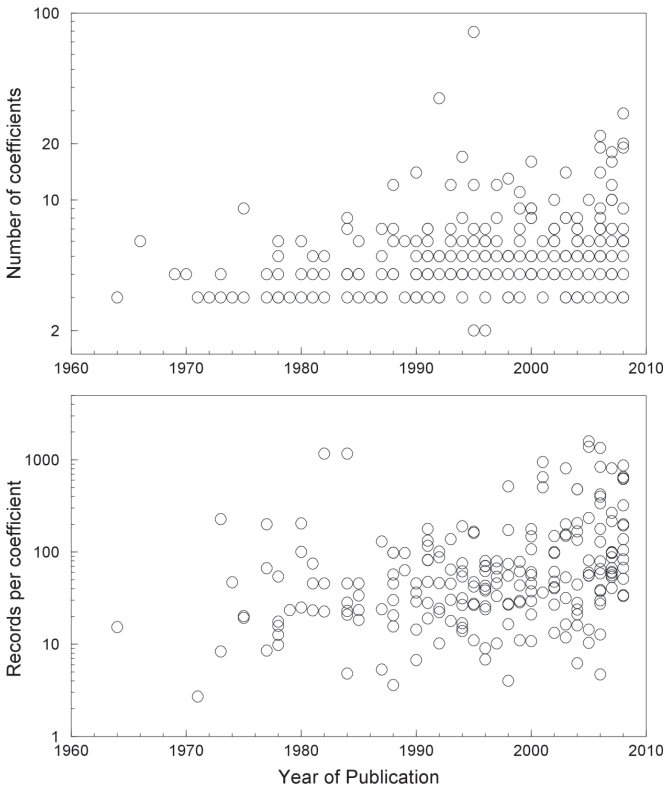

▲ **Figure 4.** Upper: The number of coefficients in ground-motion prediction equations against the year of publication. Lower: The total number of records in the dataset used to derive these GMPEs divided by the number of coefficients determined by regression analysis, against the year of publication.

Figure 4 shows both how the number of coefficients in models and the number of records used to constrain each coefficient of GMPEs has varied over time, again extracting the information from Douglas (2003, 2006, 2008). A few comments on these figures are in order, the first being that the highest number of coefficients (79) corresponds to the equation of Molas and Yamazaki (1995), which includes a separate term for each accelerograph station contributing to the dataset. Among recent equations, the European model of Akkar and Bommer (2010) has 12 coefficients whereas the NGA models of Boore and Atkinson (2008), Campbell and Bozorgnia (2008), and Abrahamson and Silva (2008) have 18, 19, and 20 coefficients, respectively, while the Chiou and Youngs (2008) model includes 29 coefficients. However, as noted above, the NGA models generally did not rely purely on fitting to empirical data to constrain the values of these parameters.

The average increase in the number of records per coefficient is much less pronounced than the ratios (earthquakes per unit magnitude, records per 100 km of distance) displayed in Figures 2 and 3, suggesting that model developers have become increasingly ambitious as the database available to them has expanded. This means that much more sophisticated models are being developed, but whether or not the available data justifies this degree of complexity is open to discussion; Kuehn *et al.* (2009) discuss the issue of possible over-fitting of ground-motion models.

Leaving this issue aside, the main reason a hazard analyst may exclude a GMPE is that its functional form does not lend itself well to extrapolation of the model across the full range of magnitudes and distances to be considered in the hazard integrations. This essentially means that the model should include non-linear scaling of ground-motion amplitudes with magnitude, and magnitude-dependent distance dependence; the latter can be included in various ways, including a magnitude-dependent multiplier on the distance-decay (geometrical-spreading) term or else through a magnitude-dependent depth or near-source term. If the dataset used to derive the model is from a narrow range of magnitudes, these features are unlikely to be captured well, but from earlier discussions such models are likely to have been rejected by this stage anyhow. In other cases, it is common for ground-motion modelers to perform tests of statistical significance for these terms and use these to determine whether or not they should be included. This raises the important question of whether the purpose of these models is primarily to explain a given set of strong-motion observations or to serve as the basis for predicting ground motions from future earthquake scenarios, including but also extending beyond those in the database. We believe that the latter is the real purpose of GMPEs, and even if non-linear magnitude scaling is not strongly revealed by our dataset, we need to ask what will happen in terms of predicted motions if, as will almost invariably be the case in PSHA, we push the equation to half a unit of magnitude (or more) above its supposed upper limit of applicability?

A hazard analyst may also give some consideration to other aspects of the functional form, such as how site response is modeled. Although very rarely done in modern equations, the inclusion of a single dummy variable taking three distinct values for three site classes (and thus fixing *a priori* the ratio of their influences on the ground motion) rather than using two binary variables could be the basis for excluding an equation. Depending on the particular application, an analyst may also have reservations about GMPEs not including non-linear site effects, even though these are often difficult to identify directly from strong-motion data and models that do include this feature may have other constraints (*e.g.*, Walling *et al.* 2008).

Regression Analysis for Empirical Models

If the model has survived the analyst's evaluation of the dataset used and the formulation of the model in terms of explanatory variables and their assumed relationship with the predicted ground-motion parameter, the next hurdle to be crossed is consideration of how the model has actually been derived. The main criterion that a hazard analyst is likely to invoke here is that the model should have been derived using one-stage or two-stage maximum likelihood regression (*e.g.*, Joyner and Boore 1993), or the random-effects method (*e.g.*, Abrahamson and Youngs 1992). Most strong-motion datasets show a correlation between magnitude and distance and also feature both poorly and well-recorded earthquakes. In addition, ground-motion variability

is composed of two terms: inter- and intra-event. These features mean that standard one-stage least-squares regression can lead to biased coefficients and, therefore, should be avoided for the derivation of GMPEs.

MODEL PERFORMANCE

A ground-motion model still in contention at this stage could be expected with confidence to be suitable for application to the PSHA, but the hazard analyst would be well advised to actually explore the model's performance across the range of magnitudes and distances (and other variables) to which it will be applied before adopting it for use in the hazard calculations. The first step is to consider the coefficients of the model and check that there are no physical inconsistencies (such as a positive coefficient on a quadratic magnitude term), but for complex functional forms it is difficult to judge the influence of any individual coefficient and one should be cautious about attributing too much physical significance to any term in such an equation.

The analyst therefore needs to actually inspect the model predictions, which can be done in a number of ways. Reproducing the figures of the original paper is an effective tool to assist in validating the analyst's implementation of the model. Plotting attenuation curves for individual parameters to visually inspect the dependence on magnitude, distance, and other parameters may be useful, but for spectral ordinates plotting the complete response spectra for different scenarios is likely to be more informative. The analyst should plot the median spectral ordinates but also other fractiles so that the influence of the aleatory variability (sigma) can be viewed as well. It is important that the response spectra are not only plotted for scenarios corresponding to the "comfort zone" of the equation (*i.e.*, within the magnitude-distance range of the data from which it is derived) but the GMPE should also be extended to the limits to which it will be applied in the PSHA calculations. This should hold for the sigma value as well, and may require the analyst to look even beyond the 84-percentile ordinates if significant contributions from epsilon (normalized standard deviations) greater than 1 are expected in the PSHA. When spectra are plotted for larger epsilon values at the lower and upper magnitude limits of the PSHA integrations, one can see the true stability and performance of the GMPE. This is particularly the case for those equations with heteroscedastic (*e.g.*, magnitude-dependent) sigma values (see, for example, Strasser *et al.* 2009). Many models have successfully incorporated magnitude-dependent sigma, some of the NGA models being good examples of this, but other models have been found to display somewhat erratic behavior when heteroscedastic variability was assumed. Akkar and Bommer (2010) discuss the unexpected results obtained in such circumstances, which prompted the revision of the heteroscedastic model of Akkar and Bommer (2007) by making the simplifying assumption of constant sigma at each response period.

In assessing the performance of a particular model, it can obviously be informative to compare the predicted spectral ordinates with those from other equations, although it is important to be wary of assuming that either model is exclusively the cause of any unexpected differences between two sets of predictions. Indeed, the basis for any expectations must be carefully examined. However, for models derived from comparable datasets or for the same region, one may reasonably expect some degree of agreement between the two sets of predictions. The visualization tools of Scherbaum *et al.* (forthcoming) provide a powerful way of checking if this is actually the case.

DISCUSSION AND CONCLUSIONS

This paper has presented a number of suggestions for criteria that can be used to select ground-motion prediction equations for use in PSHA. The basis of the approach is that this selection should neither be guided by familiarity with certain GMPEs, or even with their creators, nor by any particular preference that the analyst may have for a given model. Rather, the hazard analyst should begin with a comprehensive list of equations that meet the standard scientific quality criteria of international peer-reviewed journals and that cannot be excluded on the basis of clearly being from irrelevant tectonic settings to the PSHA in question, and then exclude those judged to be inappropriate on the basis of considerations of their quality, robustness, and suitability to the boundary conditions of the PSHA being conducted, in terms of magnitude-distance ranges and site characteristics. The exclusion criteria suggested in this paper are in no sense intended to be prescriptive, and hazard analysts should adapt and develop the criteria to suit each application. As noted earlier in the paper, the criteria will need to be adapted—and softened—as soon as one is considering subduction earthquakes or other tectonic regimes for which the number of published GMPEs is relatively small.

The criteria can in effect be considered as reflecting the state-of-the-art in ground-motion prediction, and trying to identify equations that fall significantly below this standard. Therefore, as what is state-of-the-art will continually evolve, the exclusion criteria must also be allowed to develop at the same time to continually reflect the best that can be done with the available strong-motion data and knowledge of ground-motion generation and propagation.

By way of illustration, we can apply a series of exclusion criteria that we consider to represent the current state-of-the-art in ground-motion modeling to the models for shallow crustal earthquakes available at the time of writing; for subduction zones, it would not be possible to apply the same strict criteria since there are relatively very few models currently available. The exclusion criteria proposed by the authors are as follows:

1. Model is derived for an inappropriate tectonic environment (such as subduction-zone earthquakes or volcanic regions).
2. Model not published in a Thomson Reuters ISI-listed peer-reviewed journal (although an exception can be made for an update to a model that did meet this criterion).
3. The dataset used to derive the model is not presented in an accessible format; the minimum requirement would be

a table listing the earthquakes and their characteristics, together with the number of records from each event.

4. The model has been superseded by a more recent publication.
5. The model does not provide spectral predictions for an adequate range of response periods, chosen here to be from 0.0 to 2.0 seconds.
6. The functional form lacks either non-linear magnitude dependence or magnitude-dependent decay with distance.
7. The coefficients of the model were not determined with a method that accounts for inter-event and intra-event components of variability; in other words, models must be derived using one- or two-stage maximum likelihood approaches or the random effects approach.
8. Model uses inappropriate definitions for explanatory variables, such as M_L or R_{epi}, or models site effects without consideration of V_{s30}.
9. The range of applicability of the model is too small to be useful for the extrapolations generally required in PSHA: $M_{min} > 5$, $M_{max} < 7$, $R_{max} < 80$ km.
10. Model constrained with insufficiently large dataset: fewer than 10 earthquakes per unit of magnitude or fewer than 100 records per 100 km of distance. The open circles in Figure 3 represent models failing this criterion.

Criteria nos. 6 and 8 are most effective at eliminating candidate models from further consideration, and collectively the application of these criteria leave only eight current models (from more than 150) passing on all 10 accounts, listed here in alphabetical order:

- Abrahamson and Silva (2008)
- Akkar and Bommer (2010)
- Atkinson and Boore (2006)
- Boore and Atkinson (2008)
- Campbell and Bozorgnia (2008)
- Chiou and Youngs (2008)
- Toro *et al.* (1997), as modified by Toro (2002)
- Zhao *et al.* (2006)

If one accepts the general approach presented in this paper, then it becomes inappropriate to develop and publish GMPEs that would subsequently be excluded from use in PSHA on the basis of not satisfying one or more of the requirements embodied in the criteria. With the preceding discussion in mind, Figure 5 presents a possible checklist, in the form of a flowchart, which we recommend for use by those planning to add to the large body of ground-motion prediction equations.

Clearly the application of excessively demanding criteria for GMPE selection would leave some important regions, such as SCRs, without indigenous relations, and in such cases other approaches have to be used, such as calibrated-theoretical (stochastic) methods, possibly combined with host-to-target conversions.

Recognizing that satisfying all of these criteria, either in the selection or in the development of GMPEs, may be rather onerous, Figure 5 indicates our view of their relative importance. We consider those shown in bold as indispensable, and these should always be given due consideration. Those in normal text are also very important but a greater degree of flexibility may be shown by the analyst for those models that do not fully satisfy these conditions. Those criteria shown in italics are the least important, and could be omitted if their inclusion became an impediment to the application in hand.

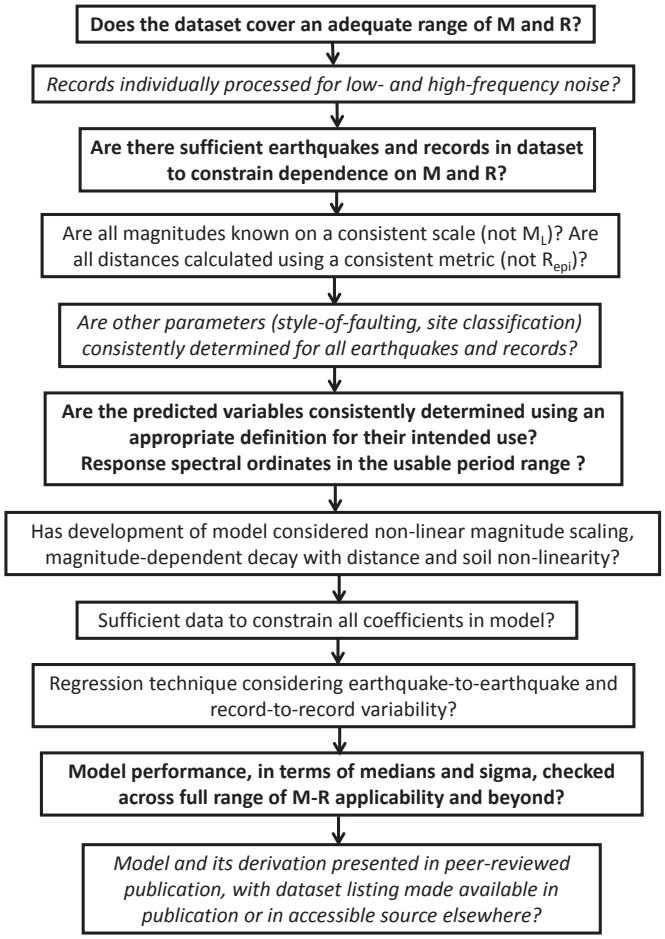

▲ **Figure 5.** Flowchart of considerations by ground-motion modelers in order to produce predictive equations that will be routinely applicable to state-of-the-art seismic hazard analyses. Those shown in bold text are considered indispensable; those in italics are the least important.

ACKNOWLEDGMENTS

We thank Jonathan Stewart for his insightful and constructive review comments, which have significantly improved the manuscript.

The authors are grateful to the organizers of the PEGASOS Refinement Project in Switzerland, particularly Drs. Philippe Renault and Norm Abrahamson, who provided the forum for the criteria presented in this paper to be developed and discussed. The ideas presented in this paper have also been discussed within the SHARE (Seismic Hazard Harmonization in Europe) project funded under contract 226967 of the EC-Research Framework Programme FP7.

John Douglas thanks Landsvirkjun and the University of Iceland for his one-year visiting professorship at the Earthquake Engineering Research Centre.

REFERENCES

Abrahamson, N., G. Atkinson, D. Boore, Y. Bozorgnia, K. Campbell, B. Chiou, I.M. Idriss, W. Silva & R. Youngs (2008). Comparisons of the NGA ground-motion relations. *Earthquake Spectra* **24** (1), 45-66.

Abrahamson, N. A., and K. M. Shedlock (1997). Overview. *Seismological Research Letters* **68** (1), 9–23.

Abrahamson, N. A., and W. Silva (2008). Summary of the Abrahamson and Silva NGA ground-motion relations. *Earthquake Spectra* **24** (1), 67–97.

Abrahamson, N. A., and R. R. Youngs (1992). A stable algorithm for regression analyses using the random effects model. *Bulletin of the Seismological Society of America* **82** (1), 505–510.

Akkar, S., and J. J. Bommer (2006). Influence of long-period filter cut-off on elastic spectral displacements. *Earthquake Engineering & Structural Dynamics* **35** (9), 1,145–1,165.

Akkar, S., and J. J. Bommer (2007). Prediction of elastic displacement response spectra at multiple damping levels in Europe and the Middle East. *Earthquake Engineering & Structural Dynamics* **36** (10), 1,275–1,301.

Akkar, S., and J. J. Bommer (2010). Empirical equations for the prediction of PGA, PGV, and spectral accelerations in Europe, the Mediterranean, and the Middle East. *Seismological Research Letters* **81** (2), 195–206.

Atkinson, G. M. (2008). Ground-motion prediction equations for eastern North America from a referenced empirical approach: Implications for epistemic uncertainty. *Bulletin of the Seismological Society of America* **98** (3), 1,304–1,318.

Atkinson, G. M., and D. M. Boore (2006). Earthquake ground-motion prediction equations for eastern North America. *Bulletin of the Seismological Society of America* **96** (6), 2,181–2,205.

Atkinson, G. M., and M. Morrison (2009). Observations on regional variability in ground-motion amplitude for small-to-moderate magnitude earthquakes in North America. *Bulletin of the Seismological Society of America* **99** (4), 2,393–2,409.

Beyer, K., and J. J. Bommer (2006). Relationships between median values and aleatory variabilities for different definitions of the horizontal component of motion. *Bulletin of the Seismological Society of America* **94** (4A), 1,512–1,522, and Erratum (2007), *Bulletin of the Seismological Society of America* **97** (5), 1,769.

Bommer, J.J., J. Douglas, and F. O. Strasser (2003). Style-of-faulting in ground motion prediction equations. *Bulletin of Earthquake Engineering* **1** (2), 171–203.

Bommer, J. J., and F. Scherbaum (2008). The use and misuse of logic-trees in PSHA. *Earthquake Spectra* **24** (4), 997–1009.

Bommer, J. J., F. Scherbaum, H. Bungum, F. Cotton, F. Sabetta, and N. A. Abrahamson (2005). On the use of logic trees for ground-motion prediction equations in seismic hazard assessment. *Bulletin of the Seismological Society of America* **95** (2), 377–389.

Bommer, J. J., P. J. Stafford, J. E. Alarcón, and S. Akkar (2007). The influence of magnitude range on empirical ground-motion prediction. *Bulletin of the Seismological Society of America* **97** (6), 2,152–2,170.

Boore, D. M., and G. M. Atkinson (2008). Ground-motion prediction equations for the average horizontal component of PGA, PGV, and 5%-damped PSA at spectral periods between 0.1 s and 10.0 s. *Earthquake Spectra* **24** (1), 99–138.

Boore, D. M., and J. J. Bommer (2005). Processing strong-motion accelerograms: Needs, options and consequences. *Soil Dynamics & Earthquake Engineering* **25** (2), 93–115.

Campbell, K. W. (2003). Prediction of strong ground motion using the hybrid empirical method and its use in the development of ground motion (attenuation) relations in eastern North America. *Bulletin of the Seismological Society of America* **93**, 1,012–1,033.

Campbell, K. W. and Y. Bozorgnia (2008). NGA ground motion model for the geometric mean horizontal component of PGA, PGV, PGD and 5%-damped linear elastic response spectra at periods ranging from 0.1 s to 10.0 s. *Earthquake Spectra* **24** (1), 139–171.

Chiou, B. S.-J., and R. R. Youngs (2008). An NGA model for the average horizontal component of peak ground motion and response spectra. *Earthquake Spectra* **24** (1), 173–215.

Chiou, B., R. Youngs, N. Abrahamson, and K. Addo (forthcoming). Ground-motion attenuation model for small-to-moderate shallow crustal earthquakes in California and its implications on regionalization of ground-motion prediction models. *Earthquake Spectra*.

Chopra, A. K. (1995). *Dynamics of Structures: Theory and Applications to Earthquake Engineering*. Englewood Cliffs, NJ: Prentice-Hall, 729 pp.

Cotton, F., G. Pousse, F. Bonilla, and F. Scherbaum (2008). On the discrepancy of recent European ground-motion observations and predictions from empirical models: Analysis of KiK-net accelerometric data and point-source stochastic simulations. *Bulletin of the Seismological Society of America* **98** (5), 2,244–2,261.

Cotton, F., F. Scherbaum, J. J. Bommer, and H. Bungum (2006). Criteria for selecting and adjusting ground-motion models for specific target applications: Applications to Central Europe and rock sites. *Journal of Seismology* **10** (2), 137–156.

Douglas, J (2003). Earthquake ground motion estimation using strong-motion records: A review of equations for the estimation of peak ground acceleration and response spectral ordinates. *Earth-Science Reviews* **61** (1/2), 43–104.

Douglas, J. (2006). *Errata of and Additions to "Ground Motion Estimation Equations 1964–2003*." Intermediary report BRGM/RP-54603-FR. Orléans, France: BRGM.

Douglas, J. (2007). On the regional dependence of earthquake response spectra. *ISET Journal of Earthquake Technology* **44** (1), 71–99.

Douglas, J. (2008). *Further Errata of and Additions to "Ground Motion Estimation Equations 1964–2003*." Final report RP-56187-FR. Orléans, France: BRGM.

Douglas, J., and D. M. Boore (2010). High-frequency filtering of strong-motion records.

Drouet, S., S. Chevrot, F. Cotton, and A. Souriau (2008). Simultaneous inversion of source spectra, attenuation parameters, and site responses: Application to the data of the French accelerometric network. *Bulletin of the Seismological Society of America* **98**, 198–219.

Edwards, B., A. Rietbrock, J. J. Bommer, and B. Baptie (2008). The acquisition of source, path and site effects from micro-earthquake recordings using *Q* tomography: Applications to the UK. *Bulletin of the Seismological Society of America* **98** (4), 1,915–1,935.

Joyner, W. B., and D. M. Boore (1993). Methods for regression analysis of strong-motion data. *Bulletin of the Seismological Society of America* **83** (2), 469–487.

Kahnemann, D., P. Slovic, and A. Tversky, eds. (1982). *Judgment under Uncertainty: Heuristics and Biases*. New York: Cambridge University Press, 555pp.

Kuehn, N., F. Scherbaum, and C. Riggelsen (2009). Deriving empirical ground-motion models: Balancing data constraints and physical assumptions to optimize prediction capability. *Bulletin of the Seismological Society of America* **99** (4), 2,335–2,347.

Kulkarni, R. B., R. R. Youngs, and K. J. Coppersmith (1984). Assessment of confidence intervals for results of seismic hazard analysis. In *Proceedings of the Eighth World Conference on Earthquake Engineering*, San Francisco, vol. 1, 263–270. Englewood Cliffs, NJ: Prentice Hall.

Molas, G. L., and F. Yamazaki (1995). Attenuation of earthquake ground motion in Japan including deep focus events. *Bulletin of the Seismological Society of America* **85** (5), 1,343–1,358.

Scasserra, G., J. P. Stewart, P. Bazzurro, G. Lanzo, and F. Mollaioli (2009). A comparison of NGA ground-motion prediction equa-

tions to Italian data. *Bulletin of the Seismological Society of America* **99** (5), 2,961–2,978.

Scherbaum, F., J. J. Bommer, H. Bungum, F. Cotton, and N. A. Abrahamson (2005). Composite ground-motion models and logic-trees: Methodology, sensitivities and uncertainties. *Bulletin of the Seismological Society of America* **95** (5), 1,575–1,593.

Scherbaum, F., J. J. Bommer, F. Cotton, H. Bungum, and F. Sabetta (2006). Ground-motion prediction in PSHA: A post-PEGASOS perspective. In *Proceedings of the First European Conference on Earthquake Engineering*, Geneva, paper no. 1312. Geneva: Symporg SA.

Scherbaum, F., F. Cotton, and P. Smit (2004). On the use of response spectral reference data for the selection of ground-motion models for seismic hazard analysis: the case of rock motion. *Bulletin of the Seismological Society of America* **94** (6), 2,164–2,185.

Scherbaum, F, F. Cotton, and H. Staedtke (2006). The estimation of minimum misfit stochastic models from empirical ground-motion equations. *Bulletin of the Seismological Society of America* **96** (2), 427–445.

Scherbaum, F., E. Delavaud, and C. Riggelsen (2009). Model selection in seismic hazard analysis: An information-theoretic perspective. *Bulletin of the Seismological Society of America* **99** (6), 3,234–3,247.

Scherbaum, F., N. M. Kuehn, M. Ohrnberger, and A. Koehler (forthcoming). Exploring the proximity of ground-motion models using high-dimensional visualization techniques. *Earthquake Spectra* **26** (4).

Scherbaum, F., J. Schmedes, and F. Cotton (2004). On the conversion of source-to-site distance measures for extended earthquake source models. *Bulletin of the Seismological Society of America* **94**, 1,053–1,069.

Stafford, P. J., F.O. Strasser, and J. J. Bommer (2008). An evaluation of the applicability of the NGA models to ground-motion prediction in the Euro-Mediterranean region. *Bulletin of Earthquake Engineering* **6** (2), 149–177.

Strasser, F. O., N. A. Abrahamson, and J. J. Bommer (2009). Sigma: Issues, insights, and challenges. *Seismological Research Letters* **80** (1), 40–56.

Toro, G. R., N. A. Abrahamson, and J. F. Schneider (1997). Models of strong ground motions from earthquakes in central and eastern North America: Best estimates and uncertainties. *Seismological Research Letters* **68** (1), 41–57.

Toro, G. R. (2002). *Modification of the Toro et al. (1997) Attenuation Equations for Large Magnitudes and Short Distances*. Risk Engineering Inc. report, unpublished.

Walling, M., W. Silva, and N. Abrahamson (2008). Nonlinear site amplification factors for constraining the NGA models. *Earthquake Spectra* **24** (1), 243–255.

Watson-Lamprey, J. A., and D. M. Boore (2007). Beyond Sa_{GMRotI}: Conversion to Sa_{Arb}, Sa_{SN}, and Sa_{MaxRot}. *Bulletin of the Seismological Society of America* **97** (5), 1,511–1,524.

Zhao, J. X., J. Zhang, A. Asano, Y. Ohno, T. Oouchi, T. Takahashi, H. Ogawa, K. Irikura, H.K. Thio, P.G. Somerville, Y. Fukushima, and Y. Fukushima (2006). Attenuation relations of strong ground motion in Japan using site classifications based on predominant period. *Bulletin of the Seismological Society of America* **96** (3), 898–913.

Civil & Environmental Engineering
Imperial College London
London SW7 2AZ, U.K.
j.bommer@imperial.ac.uk
(J. J. B.)

6.4 Douglas (2009) report on the GMPEs pre-selection

Pre-selection of ground-motion prediction equations for WP4 of SHARE

John Douglas

29th June 2009 (slightly revised 4th August 2009)

Within WP4 (Strong ground motion modelling) of SHARE it is planned to undertake selection, testing and possible modification of published ground-motion prediction equations (GMPEs) for use in the seismic hazard assessment of the wider European region within WP5 of SHARE. The first stage of this process is a pre-selection from the over 250 GMPEs that are currently available (Douglas, 2008) to retain a subset of the most recent and robust models. While making this pre-selection it is important to retain a sufficient number of models so that the potentially large epistemic uncertainty within the prediction of earthquakes ground motions is recognised. The purpose of this short report is to present a pre-selection of available models for all the seismotectonic regimes present in the wider European region. The wider European region can be divided into these broad classes:

- Stable continental regions (SCRs);
- Subduction zones;
- Active regions with shallow crustal seismicity;
- Volcanic zones;
- Areas of deep focus non-subduction earthquakes, such as Vrancea (Romania);
- Areas where the travel paths are mainly through oceanic crust, such as coastal Portugal.

Only models for the prediction of horizontal linear elastic response spectral ordinates for 5% damping are considered in this report since this is the focus of the seismic hazard assessments made in SHARE. In addition, mining-induced seismicity is not considered as a priority for SHARE and, therefore, no models for the prediction of shaking from mining-induced events are included. Note, however, that it some parts of Europe (e.g. southern Poland) mining-induced seismicity is the largest contribution to seismic hazard.

Pre-selection criteria

Due to the vast number of available GMPEs within the literature it is necessary to define criteria to winnow down the models to a more manageable number although recognising the necessity to retain sufficient models to account for epistemic uncertainty in the prediction of shaking. For this pre-selection it was decided to apply the seven criteria proposed by Cotton et al. (2006):

1. the model is from a clearly irrelevant tectonic regime;
2. the model is not published in an international peer-reviewed journal;
3. the documentation of model and its underlying dataset is insufficient;
4. the model has been superseded by more recent publications;
5. the frequency range of the model is not appropriate for engineering application;
6. the model has an inappropriate functional form;
7. the regression method or regression coefficients are judged to be inappropriate.

Criterion 1 was applied to retain only models relevant for the broad classes listed above (e.g. only subduction zone models were considered for these regions). Criterion 2 was applied to reject GMPEs that had not been published in a journal that is listed by ISI Web of Knowledge, which is a standard reference for bibliographic information. Criterion 3 was applied to reject

those studies that do not provide detailed information on the dataset used to derive the GMPEs presented. Criterion 4 has been applied to reject GMPEs for areas for which more recent models have been published using larger datasets even if the more recent models have not been derived by the same author teams. For example, the model of Field (2000) for southern California has been rejected since the data he used is a subset of the NGA database used by the NGA teams in developing their models. Criterion 5 leads to all peak ground acceleration (PGA)-only models being rejected as well as those that do not provide coefficients for periods less than 0.04s (25Hz) (that can be assumed to approximate PGA) and up to at least 2s (0.5Hz). This criterion removes models such as that by Ghasemi et al. (2009) who do not provide coefficients for periods less than 0.05s and the GMPEs by Bommer et al. (2007) who do not provide coefficients for periods greater than 0.5s. Criterion 6 has been applied to exclude models that do not use moment magnitude (M_w) (since there are difficulties and uncertainties in converting between other magnitude scales, especially M_L, and M_w, the standard magnitude scale for seismic hazard assessments) and to exclude models that do not allow the prediction of ground motions at rock sites (e.g. Crouse, 1991). Criterion 7 has been applied, in particular, to exclude those models based on simulations whose standard deviations were computed without taking into account modelling variability (e.g. Hwang & Huo, 1997).

These criteria have been applied to the empirical GMPEs listed in the reports of Douglas et al. (2004, 2006, 2008) plus the additional models published since the end of 2008 (or accidentally missed by these compilations). In addition, simulation-based GMPEs identified through a thorough literature search were considered. Note that only simulation-based GMPEs with fitted functional forms are considered since these are straightforward to use within seismic hazard assessment. Models derived using the hybrid empirical-stochastic approach of Campbell (2003) have also been considered although within SHARE this method maybe used to adjust some models. If this is done then it should not applied to these hybrid models but rather to the empirical GMPEs underlying these hybrid models.

The following sections list the GMPEs that have been retained for each seismotectonic regime. The models tested by Allen & Wald (2009) for Global ShakeMap purposes and those GMPEs used by Petersen et al. (2008) for the construction of the US National Seismic Hazard Maps are, in general, subsets of the models pre-selected here for SHARE.

Note that this pre-selection was performed in summer 2009. During the duration of the SHARE project many new GMPEs will be published (on average a dozen new models are published every year, according to the reports of J. Douglas) but it is not planned within SHARE to repeat this pre-selection to account for these models.

Stable continental regions (SCRs)

The following six models are pre-selected for stable continental regions:

- Atkinson (2008): Referenced empirical model for eastern North America
- Atkinson & Boore (2006): Extended stochastic model for eastern North America
- Campbell (2003): Hybrid model for eastern North America
- Douglas et al. (2006): Hybrid model for southern Norway
- Tavakoli & Pezeshk (2005): Hybrid model for eastern North America
- Toro et al. (1997): Stochastic model for eastern North America

A number of other models exist for SCRs but they fail one or more of the selection criteria, in particular the requirement of a publication in an ISI-listed journal.

Subduction zones

The following eight models are pre-selected for subduction zones:

- Atkinson & Boore (2003): Worldwide empirical
- Atkinson & Macias (2009): Simulation-based model for Cascadia (only for large magnitudes)
- Garcia et al. (2005): Only intraslab model for Mexico
- Kanno et al. (2006): Japan empirical
- Lin & Lee (2008): Taiwan empirical
- McVerry et al. (2006): New Zealand empirical
- Youngs et al. (1997): Worldwide empirical
- Zhao et al. (2006): Japan empirical

It should be noted that the epistemic uncertainty associated with the prediction of ground motions from subduction events seems to be higher than the uncertainty in the prediction of shaking from shallow crustal earthquakes (e.g. Atkinson & Macias, 2009).

Active regions with shallow crustal seismicity

These models derived for broad areas of shallow crustal seismicity are pre-selected:

- Abrahamson & Silva (2008): NGA model using worldwide data
- Ambraseys et al. (2005): Model using Mediterranean and Middle Eastern data
- Akkar & Bommer (2007): Model using Mediterranean and Middle Eastern data
- Boore & Atkinson (2008) : NGA model using worldwide data
- Campbell & Bozorgnia (2008) : NGA model using worldwide data
- Cauzzi & Faccioli (2008) : Model using worldwide data (mainly Japanese)
- Chiou & Youngs (2008): : NGA model using worldwide data
- Cotton et al. (2008): Model using Japanese data
- Idriss (2008): NGA model using worldwide data
- Kanno et al. (2006): Model using mainly Japanese data
- McVerry et al. (2006): Model using mainly New Zealand data (note that this was published in a non-ISI listed journal)
- Pankow & Pechmann (2004, 2006): Model using data from extensional regimes
- Zhao et al. (2006): Model using mainly Japanese data

The commonly-used model of Berge-Thierry et al. (2003) has not been pre-selected for SHARE due to its use of surface-wave magnitude (Ms), its non-consideration of the effect of style of faulting and its use of a binary soil/rock classification. In addition, it can be considered to have been superseded by more recent models using Mediterranean and Middle Eastern data (e.g. Ambraseys et al., 2005; Akkar & Bommer, 2007).

In addition, these regional models are of interest for particular areas although they are less robust than the models listed above since they are based on smaller less-well distributed datasets:

- Bindi et al. (2009): Italy
- Danciu & Tselentis (2007): Greece
- Douglas et al. (2006): Southern Spain (hybrid)
- Kalkan & Gülkan (2004, 2005): Turkey
- Massa et al. (2008): Northern Italy
- Özbey et al. (2004): NW Turkey

Note that a number of recent regional models fail the selection criteria of Cotton et al. (2006) since they use local magnitude and/or they are derived for a limited magnitude range.

Volcanic zones

Only this study explicitly mentions the prediction of ground motions in volcanic zones and passes the selection criteria of Cotton et al. (2006) (although it is not for the prediction of ground motion from volcano-associated earthquakes):

- McVerry et al. (2006)

Atkinson (2009) has recently published a report on the application of her referenced-empirical technique to Hawaiian data but this study has yet to be published as a journal article.

It is suggested here that, if the prediction of earthquake ground motions in volcanic zones is a priority for SHARE, a careful study of the difference between shaking in volcanic zones and other areas of active tectonics is made.

Areas of deep focus non-subduction earthquakes, such as Vrancea (Romania)

Only this model passes the selection criteria of Cotton et al. (2006) for this type of region (although the authors do not list the derived coefficients within their article):

- Sokolov et al. (2008)

Areas where the travel paths are mainly through oceanic crust, such as coastal Portugal

There are thought to be no available models for the prediction of ground motions in this type of area. Therefore, it is suggest that models for active zones and SCRs [as used by Vilanova & Fonseca (2007) for their hazard assessment of Portugal] are tested against data from these regions to check which models are most appropriate.

References

N. Abrahamson and W. Silva. Summary of the Abrahamson & Silva NGA ground-motion relations. Earthquake Spectra, 24(1):67–97, 2008. doi: 10.1193/1.2924360.

S. Akkar and J. J. Bommer. Prediction of elastic displacement response spectra in Europe and the Middle East. Earthquake Engineering and Structural Dynamics, 36(10):1275–1301, 2007b. doi: 10.1002/eqe.679.

T. I. Allen and D. J. Wald, Evaluation of ground-motion modeling techniques for use in Global ShakeMap – A critique of instrumental ground-motion prediction equations, peak ground motion to macroseismic intensity conversions, and macroseismic intensity predictions in different tectonic settings, Open-File Report 2009-1047, US Geological Survey, US Department of the Interior. 114 pp, 2009.

N. N. Ambraseys, J. Douglas, S. K. Sarma, and P. M. Smit. Equations for the estimation of strong ground motions from shallow crustal earthquakes using data from Europe and the Middle East: Horizontal peak ground acceleration and spectral acceleration. Bulletin of Earthquake Engineering, 3(1):1–53, 2005. doi: 10.1007/s10518-005-0183-0.

G. M. Atkinson. Ground-motion prediction equations for eastern North America from a referenced empirical approach: Implications for epistemic uncertainty. Bulletin of the Seismological Society of America, 98(3):1304–1318, Jun 2008. doi: 10.1785/0120070199.

G. M. Atkinson. Ground motion prediction equations for Hawaii from a referenced empirical approach, Final technical report 08HQGR0020, Mar 2009.

G. M. Atkinson and D. M. Boore. Empirical ground-motion relations for subduction zone earthquakes and their application to Cascadia and other regions. Bulletin of the Seismological Society of America, 93(4):1703–1729, 2003.

G. M. Atkinson and D. M. Boore. Earthquake ground-motion prediction equations for eastern North America. Bulletin of the Seismological Society of America, 96(6):2181–2205, 2006. doi: 10.1785/0120050245.

G. M. Atkinson and M. Macias. Predicted ground motions for great interface earthquakes in the Cascadia subduction zone. Bulletin of the Seismological Society of America, 99(3), 1552-1578, 2009. doi: 10.1785/0120080147.

Berge-Thierry, C., Cotton, F., Scotti, O., Griot-Pommera, D.-A., & Fukushima, Y. New empirical response spectral attenuation laws for moderate European earthquakes. Journal of Earthquake Engineering, 7(2), 193–222, 2003.

D. Bindi, L. Luzi, M. Massa and F. Pacor. Horizontal and vertical ground motion prediction equations derived from the Italian Accelerometric Archive (ITACA). Bulletin of Earthquake Engineering, 2009, in press. doi: 10.1007/s10518-009-9130-9.

D. M. Boore and G. M. Atkinson. Ground-motion prediction equations for the average horizontal component of PGA, PGV, and 5%-damped PSA at spectral periods between 0:01 s and 10:0 s. Earthquake Spectra, 24 (1):99–138, 2008. doi: 10.1193/1.2830434.

K. W. Campbell. Prediction of strong ground motion using the hybrid empirical method and its use in the development of ground-motion (attenuation) relations in eastern North America. Bulletin of the Seismological Society of America, 93(3):1012–1033, 2003.

K.W. Campbell and Y. Bozorgnia. NGA ground motion model for the geometric mean horizontal component of PGA, PGV, PGD and 5% damped linear elastic response spectra for periods ranging from 0:01 to 10 s. Earthquake Spectra, 24(1):139–171, 2008b. doi: 10.1193/1.2857546.

C. Cauzzi and E. Faccioli. Broadband (0.05 to 20 s) prediction of displacement response spectra based on worldwide digital records. Journal of Seismology, 12(4):453–475, Oct 2008. doi: 10.1007/s10950-008-9098-y.

B. S.-J. Chiou and R. R. Youngs. An NGA model for the average horizontal component of peak ground motion and response spectra. Earthquake Spectra, 24(1):173–215, 2008a. doi: 10.1193/1.2894832.

F. Cotton, F. Scherbaum, J. J. Bommer, and H. Bungum. Criteria for selecting and adjusting ground-motion models for specific target regions: Application to central Europe and rock sites. Journal of Seismology, 10(2):137–156, Apr 2006. doi: 10.1007/s10950-005-9006-7.

F. Cotton, G. Pousse, F. Bonilla, and F. Scherbaum. On the discrepancy of recent European ground-motion observations and predictions from empirical models: Analysis of KiK-net accelerometric data and point sources stochastic simulations. Bulletin of the Seismological Society of America, 98(5):2244–2261, Oct 2008. doi: 10.1785/0120060084.

C. B. Crouse. Ground-motion attenuation equations for earthquakes on the Cascadia subduction zones. Earthquake Spectra, 7(2):201–236, 1991.

L. Danciu and G.-A. Tselentis. Engineering ground-motion parameters attenuation relationships for Greece. Bulletin of the Seismological Society of America, 97(1B):162–183, 2007. doi: 10.1785/0120040087.

J. Douglas. Ground motion estimation equations 1964–2003: Reissue of ESEE Report No. 01-1: 'A comprehensive worldwide summary of strong-motion attenuation relationships for peak ground acceleration and spectral ordinates (1969 to 2000)' with corrections and additions. Technical Report 04-001-SM, Department of Civil and Environmental Engineering; Imperial College of Science, Technology and Medicine; London; U.K., Jan. 2004a. URL http://www3.imperial.ac.uk/civilengineering/research/researchnewsandreports/researchreports.

J. Douglas. Errata of and additions to 'Ground motion estimation equations 1964–2003'. Intermediary report RP-54603-FR, BRGM, Orl´eans, France, Dec 2006. URL http://www.brgm.fr/publication/rechRapportSP.jsp.

J. Douglas. Further errata of and additions to 'Ground motion estimation equations 1964–2003'. Final report RP-56187-FR, BRGM, Orléans, France, Dec 2008. URL http://www.brgm.fr/publication/rechRapportSP.jsp.

J. Douglas, H. Bungum, and F. Scherbaum. Ground-motion prediction equations for southern Spain and southern Norway obtained using the composite model perspective. Journal of Earthquake Engineering, 10(1):33–72, 2006.

E. H. Field. A modified ground-motion attenuation relationship for southern California that accounts for detailed site classification and a basin-depth effect. Bulletin of the Seismological Society of America, 90(6B):S209–S221, Dec 2000.

H. Ghasemi, M. Zare, Y. Fukushima, and K. Koketsu. An empirical spectral ground-motion model for Iran. Journal of Seismology, 2009. doi: 10.1007/s10950-008-9143-x. In press.

D. Garcia, S. K. Singh, M. Herr´aiz, M. Ordaz, and J. F. Pacheco. Inslab earthquakes of central Mexico: Peak ground-motion parameters and response spectra. Bulletin of the Seismological Society of America, 95(6):2272–2282, Dec 2005. doi: 10.1785/0120050072.

H. Hwang and J.-R. Huo. Attenuation relations of ground motion for rock and soil sites in eastern United States. Soil Dynamics and Earthquake Engineering, 16(6):363–372, 1997.

I. M. Idriss. An NGA empirical model for estimating the horizontal spectral values generated by shallow crustal earthquakes. Earthquake Spectra, 24(1):217–242, 2008. doi: 10.1193/1.2924362.

E. Kalkan and P. Gülkan. Site-dependent spectra derived from ground motion records in Turkey. Earthquake Spectra, 20(4):1111–1138, Nov 2004.

E. Kalkan and P. Gülkan. Erratum: Site-dependent spectra derived from ground motion records in Turkey. Earthquake Spectra, 21(1):283, Feb 2005.

T. Kanno, A. Narita, N. Morikawa, H. Fujiwara, and Y. Fukushima. A new attenuation relation for strong ground motion in Japan based on recorded data. Bulletin of the Seismological Society of America, 96(3):879–897, 2006. doi: 10.1785/0120050138.

P.-S. Lin and C.-T. Lee. Ground-motion attenuation relationships for subduction-zone earthquakes in northeastern Taiwan. Bulletin of the Seismological Society of America, 98(1):220–240, Feb 2008. doi:10.1785/0120060002.

M. Massa, P. Morasca, L. Moratto, S. Marzorati, G. Costa, and D. Spallarossa. Empirical ground-motion prediction equations for northern Italy using weak- and strong-motion amplitudes, frequency content, and duration parameters. Bulletin of the Seismological Society of America, 98(3):1319–1342, Jun 2008. doi: 10.1785/0120070164.

G. H. McVerry, J. X. Zhao, N. A. Abrahamson, and P. G. Somerville. New Zealand acceleration response spectrum attenuation relations for crustal and subduction zone earthquakes. Bulletin of the New Zealand Society for Earthquake Engineering, 39(4):1–58, Mar 2006.

C. Özbey, A. Sari, L. Manuel, M. Erdik, and Y. Fahjan. An empirical attenuation relationship for northwestern Turkey ground motion using a random effects approach. Soil Dynamics and Earthquake Engineering, 24(2):115–125, 2004.

K. L. Pankow and J. C. Pechmann. The SEA99 ground-motion predictive relations for extensional tectonic regimes: Revisions and a new peak ground velocity relation. Bulletin of the Seismological Society of America, 94(1):341–348, Feb 2004.

K. L. Pankow and J. C. Pechmann. Erratum: The SEA99 ground-motion predictive relations for extensional tectonic regimes: Revisions and a new peak ground velocity relation. Bulletin of the Seismological Society of America, 96(1):364, Feb 2006. doi: 10.1785/0120050184.

M. D. Petersen, A. D. Frankel, S. C. Harmsen, C. S. Mueller, K. M. Haller, R. L. Wheeler, R. L. Wesson, Y. Zeng, O. S. Boyd, D. M. Perkins, N. Luco, E. H. Field, C. J. Wills, and K. S.

Rukstales, Documentation for the 2008 Update of the United States National Seismic Hazard Maps. Open-File Report 2008-1128. U.S. Department of the Interior, U.S. Geological Survey. 61 p, 2008.

V. Sokolov, K.-P. Bonjer, F. Wenzel, G. Grecu & M. Radulian, Ground-motion prediction equations for the intermediate depth Vrancea (Romania) earthquakes. Bulletin of Earthquake Engineering, 6(3):367-388, 2008. doi: 10.1007/s10518-008-9065-6.

B. Tavakoli and S. Pezeshk. Empirical-stochastic ground-motion prediction for eastern North America. Bulletin of the Seismological Society of America, 95(6):2283–2296, Dec 2005. doi: 10.1785/0120050030.

G. R. Toro, N. A. Abrahamson, and J. F. Schneider. Model of strong ground motions from earthquake in central and eastern North America: Best estimates and uncertainties. Seismological Research Letters, 68(1):41–57, Jan/Feb 1997.

S. P. Vilanova and J. F. B. D. Fonseca. Probabilistic seismic-hazard assessment for Portugal. Bulletin of the Seismological Society of America, 97(5):1702-1717, Oct 2007. doi: 10.1785/0120050198.

R. R. Youngs, S.-J. Chiou, W. J. Silva, and J. R. Humphrey. Strong ground motion attenuation relationships for subduction zone earthquakes. Seismological Research Letters, 68(1):58–73, Jan/Feb 1997.

J. X. Zhao, J. Zhang, A. Asano, Y. Ohno, T. Oouchi, T. Takahashi, H. Ogawa, K. Irikura, H. K. Thio, P. G. Somerville, Y. Fukushima, and Y. Fukushima. Attenuation relations of strong ground motion in Japan using site classification based on predominant period. Bulletin of the Seismological Society of America, 96(3):898–913, 2006. doi: 10.1785/0120050122.

6.5 Drouet et al. (2010) article on French weak-motion data (v_{S30} and κ estimation)

Geophysical Journal International

Geophys. J. Int. (2010) doi: 10.1111/j.1365-246X.2010.04626.x

v_{S30}, κ, regional attenuation and M_{w} from accelerograms: application to magnitude 3–5 French earthquakes

Stéphane Drouet, Fabrice Cotton and Philippe Guéguen

LGIT, CNRS, LCPC, Université Joseph Fourier, BP 53, 38041 *Grenoble Cedex* 9, *France. E-mail: stephane.drouet@obs.ujf-grenoble.fr*

Accepted 2010 April 13. Received 2010 April 7; in original form 2009 November 5

SUMMARY

We investigate recordings from weak to moderate earthquakes, with magnitudes ranging between about 3 and 5, recorded by the French Accelerometric Network. *S*-wave spectra are modelled as a product of source, propagation and site terms. Inverting large data sets of multiple earthquakes recorded at multiple stations allows us to separate the three contributions. Source parameters such as moment magnitude, corner frequency and stress drop are estimated for each earthquake. We provide the first complete and homogeneous catalogue of moment magnitudes for France, for the events with magnitude greater than 3 that occurred between 1996 and 2006. Stress drops are found to be regionally dependent as well as magnitude dependent, and range from about 0.1 MPa (1 bar) to about 30 MPa (300 bars). The attenuation parameters show that, in France on a nationwide scale, variations of attenuation properties do exist. Site transfer functions are also computed, giving the level of amplification at different frequencies with respect to the response of a generic rock site (characterized by an average 30 m *S*-wave velocity, v_{s30}, of 2000 m s^{-1}). From these site terms, we compute the high-frequency fall-off parameter κ [modelled as exp $(-\pi\kappa f)$, with f the frequency] for 76 stations. We also determine rock stations v_{s30} and we show the κ–v_{s30} relationship for 21 rock stations.

Key words: Fourier analysis; Earthquake ground motions; Earthquake source observations; Body waves; Seismic attenuation; Site effects.

GJI Seismology

1 INTRODUCTION

Ground-motion prediction equations are usually obtained from regression analysis of strong ground-motion data (see Douglas 2003, for a review). In areas of moderate-to-low seismic activity, it is common to have few recorded strong ground motions. As a consequence, the prediction of the expected ground motion for hypothetical future earthquakes is often performed through stochastic simulations (Boore 2003), or by selecting and adjusting empirical models from other regions (e.g. Cotton *et al.* 2006). In this context, Campbell's hybrid empirical approach (Campbell 2003; Campbell & Bozorgnia 2004) provides a methodological framework to adapt ground-motion prediction equations to arbitrary target regions, by using response spectral host-to-target-region conversion functions. The purpose of those transfer functions is the removal of the effects of the host region characteristics in terms of attenuation, geometrical spreading, average stress drop, site effect, etc., and their replacement by the equivalent effects for the target region. This can improve the overall usefulness of a particular empirical model for a target region of interest. A small number of observed ground-motion records can then help to rank the adjusted ground motion models in a systematic and comprehensible way (e.g. Scherbaum *et al.* 2004).

Several issues related to source, path and local site effects must be resolved before one can properly select, adjust and rank allogeneous models in low-seismicity areas.

(1) Recent ground-motion prediction equations use the moment magnitude scale. Compatibility must therefore be achieved between this moment magnitude scale and the magnitude scale describing the earthquakes used for ground-motion prediction in Probabilistic Seismic Hazard Analysis (PSHA). However, there is currently no systematic moment magnitude (M_{w}) determination in many countries, and generally only local magnitudes (M_{L}) are estimated homogeneously since the 1960s. For example, calibration of the relationship between M_{w} and M_{L} is currently an issue for French PSHA analysis: the local magnitudes estimated in France are known to be higher than the M_{L} of neighbouring countries (Braunmiller *et al.* 2005); and large discrepancies exist between the M_{w} and M_{L} estimated from punctual studies of specific earthquakes (Dufumier 2002).

(2) No consensus exists on the regional dependence of ground motion (Douglas 2007). Differences between recent ground-motion prediction equations derived in the United States and in Europe are slight (Campbell & Bozorgnia 2006; Stafford *et al.* 2008). However, intensity studies have long since shown a regional dependence of the attenuation of intensity with distance (e.g. Bakun & Scotti 2006). Recent studies of regional weak motions (e.g. Bay *et al.* 2003; Akinci *et al.* 2006; Malagnini *et al.* 2007; Drouet *et al.* 2008a; Edwards *et al.* 2008; Atkinson & Morrison 2009) confirm that clear regional particularities exist in terms of attenuation and/or stress drop. There is then a need to analyse the regional variation of ground

motion and the scaling of both geometrical spreading and stress drops with magnitude (e.g. Bay *et al.* 2005; Cotton *et al.* 2008).

(3) The average 30 m shear wave velocity (v_{s30}) is widely used as the number characterizing the site effect in the context of ground-motion prediction equations. There is then a need to characterize the v_{s30} at the stations of the target region. This value is usually determined from direct borehole or geophysical measurements. However, the associated cost of these measurements is high (some thousands or tens of thousands of euros depending on the method used), and as such there is a real interest to develop cheaper alternative methods. As most PSHA studies are performed for rock conditions, it is particularly crucial to obtain these measurements for rock stations.

(4) In addition to v_{s30}, one other site parameter, the high-frequency decay (κ or $f_{\max}$), has a primary influence on the adjustments required (Cotton *et al.* 2006). That decay has been observed and modelled through two different ways: the κ model [Anderson & Hough 1984, $\exp(-\pi\kappa\ f)$]; and the $f_{\max}$ model {Hanks 1982; Boore 2003, $[(1+(f/f_{\max})^8]^{-1/2}$}. Those studies demonstrate that the high-frequency decay is mainly a site term. A source dependency of κ has been demonstrated by Papageorgiou & Aki (1983) or Purvance & Anderson (2003) however this source component has a smaller effect than the site component. The clear dependence of κ on the site suggests a potential relationship between κ and v_{s30}. However, to our knowledge, only the Silva *et al.* (1998) and Chandler *et al.* (2006) papers investigate such a relationship.

The development and improvement of accelerometric networks provide an opportunity to analyse these issues. In Europe, several networks have recorded high-quality small-to-moderate events (http://itaca.mi.ingv.it/ItacaNet/, http://www-rap.obs.ujf-grenoble.fr/, http://www.seismo.ethz.ch/). The advantage of these weak-motion databases compared with the international strong ground-motion databases, such as the NGA (Next Generation Attenuation of ground motions) database, is the homogeneous coverage of a unique region. This allows the recovery of path and site terms. So in this study, we use data from the French Accelerometric Network (RAP, Pequegnat *et al.* 2008) to analyse source, path and site effects for three different tectonic regions (French Pyrenees, French Alps and Rhine Graben). We compute moment magnitudes and corner frequencies for 161 events and deliver a moment magnitude catalogue of French earthquakes recorded between 1996 and 2006 in these tectonic regions. Our inversion procedure also characterizes the geometric and anelastic attenuation parameters for these three tectonic regions. We finally describe the site transfer functions of 76 accelerometric stations. A new method, developed to analyse these site transfer functions, allows the determination of κ and v_{s30} at the rock stations. This new $\kappa - v_{s30}$ relationship is finally presented and discussed. Those results supersede those from our previous studies (Drouet *et al.* 2005, 2008a) as the amount of data has more than doubled and the inversion is performed for a wider frequency range (now up to 30 Hz compared to 15 Hz). Moreover, the inversion procedure has been modified to work with acceleration spectra rather than displacement spectra (reducing the processing used) and the site terms are determined relative to a quantified reference (i.e. a rock site with $v_{S30} = 2000$ m s^{-1}).

2 DATA

The French Accelerometric Network (Réseau Accélérométrique Permanent, RAP) has been operating since 1996. Today more than 100 stations cover the national French territory providing high-quality data, even for small events, which is freely available at the National Data Center RAP-NDC: http://www-rap.obs.ujf-grenoble.fr/ (Pequegnat *et al.* 2008).

On the basis of the RAP recordings, three regional data sets for France have been constructed (Fig. 1). The records of earthquakes with local magnitude greater than 3 are kept if at least three different recordings with a distance greater than 15 km are available. These are the same criteria as in a previous paper (Drouet *et al.* 2008a) however the number of analysed spectra has since more than doubled. The final data set is composed of 72 earthquakes in the Alps (Table 1), 23 in the Rhine Graben (Table 2) and 66 in the Pyrenees (Table 3). The hypocentral information comes from the French national network RéNaSS, whereas local magnitudes are given by two national agencies: RéNaSS and LDG ($M_{\rm ren}$ and $M_{\rm ldg}$). Fig. 1 shows the locations of the three regions within France and the earthquakes, stations and paths for each region.

Each three-component recording has been visually inspected and the *P*- and *S*-wave arrival times have been picked. As in Drouet *et al.* (2008a), a 5 s time window is used to select the direct *S* waves for all the distances, and acceleration Fourier spectra are computed. The spectra are then smoothed between 0.5 and 30 Hz using a Konno–Ohmachi procedure (Konno & Ohmachi 1998). Noise spectra are similarly computed, using the pre-recorded window before the *P*-wave arrivals. The north–south and east–west components (of signal and noise) are combined, to get a single horizontal component, as follows:

$$S(H) = \sqrt{S(E)^2 + S(N)^2}. \tag{1}$$

A minimum signal-to-noise (S/N) ratio of 3 is imposed at each frequency. Consequently, some points between 0.5 and 30 Hz might be missing in some spectra. To minimize this problem, a minimum of 60 per cent of the total number of frequencies with S/N ratio above 3 must be included in a record.

3 METHOD

The *S*-wave acceleration spectrum $A_{ijk}(r_{ij}, f_k)$ can be written as the product of a source, a propagation and a station term.

$$A_{ijk}(r_{ij}, f_k) = \Omega_i(f_k)\, D_{ij}(r_{ij}, f_k)\, S_j(f_k), \tag{2}$$

where r_{ij} is the hypocentral distance from earthquake i to station j and f_k the frequency. We adopt the far-field acceleration spectrum given by Brune's model (Brune 1970, Brune 1971).

$$\Omega_i(f_k) \sim \frac{(2\pi f_k)^2\, M_{0_i}}{\left[1 + \left(\frac{f_k}{f_{c_i}}\right)^2\right]}, \tag{3}$$

where M_{0_i} is the seismic moment and f_{c_i} the corner frequency of event i.

Attenuation involves anelastic decay and geometrical spreading.

$$D_{ij}(r_{ij}, f_k) = \exp\left(-\frac{\pi r_{ij} f_k}{Q(f_k) v_S}\right) \times \frac{1}{r_{ij}^{\gamma}}, \tag{4}$$

where v_S is the average *S*-wave velocity along the path and $Q(f_k) = Q_0 \times f_k^{\alpha}$ is the frequency-dependent quality factor. Note that the geometrical spreading may differ from the classical r_{ij}^{-1} form through the coefficient γ. We expect γ to be greater than 1, because downward reflections from layer interfaces (e.g. Frankel 1991) and scattering (e.g. Gagnepain-Beyneix 1987) can result in a geometrical loss of energy.

Considering the moderate magnitudes of the largest analysed events and the minimum frequency of 0.5 Hz, a minimum hypocentral distance of 15 km was required, for the far-field approximation to be valid (e.g. Aki & Richards 2002).

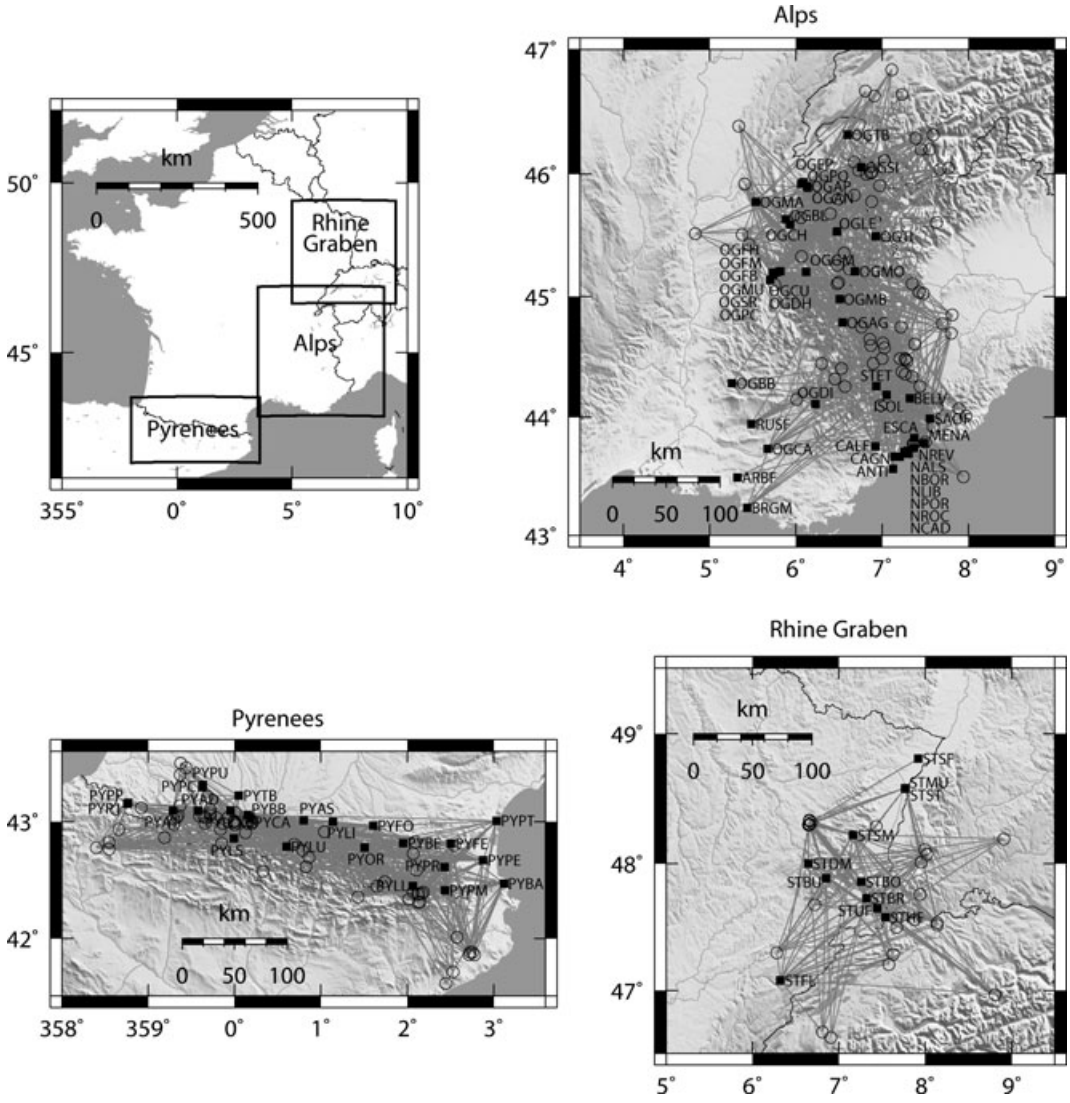

Figure 1. Maps of the earthquakes (circles), stations (squares) and paths (lines) used in this study for the three data sets: Alps, Rhine Graben and Pyrenees (see the map of France, top left frame).

$S_j(f_k)$ is the site effect at the station j. This term is equal to unity for all frequencies in the absence of site effect ('rock' site conditions). The so-called $f_{\max}$ effect (Hanks 1982) or κ effect (Anderson & Hough 1984) describes the observed strong attenuation of the high-frequencies. Although the origin of this effect is not completely understood an important contribution comes from the high intrinsic attenuation in the most superficial layers (Hanks 1982). Drouet *et al.* (2008a) used frequencies up to 15 Hz to avoid or limit the $f_{\max}$ effect. In this study, we assume that this effect is a site term (Hanks 1982) and that it will be resolved in the $S_j(f_k)$ parameter elements without using any extra parameters.

Eq. (2) may thus be rewritten as

$$y_{ijk} = m_{0_i} - \log_{10}\left[\left(\frac{(2\pi f_k)^2}{1+\left(\frac{f_k}{f_{c_i}}\right)^2}\right)\right] - \gamma \log_{10}(r_{ij}) - \frac{\pi r_{ij} f_k}{\log_e(10) Q_0 f_k^{\alpha} v_S} + s_{jk}, \quad (5)$$

where

$$y_{ijk} = \log_{10}\left[A_{ijk}(r_{ij}, f_k)\right], \quad (6)$$

$$m_{0_i} = \log_{10}\left[M_{0_i} \times \frac{2R_{\theta\phi}}{4\pi\rho\beta^3}\right], \quad (7)$$

$$s_{jk} = \log_{10}\left[S_j(f_k)\right], \quad (8)$$

with $R_{\theta\phi}$ the source radiation pattern, assumed to be constant ($R_{\theta\phi} = 0.55$ for S waves, Boore & Boatwright 1984), ρ the density, β the S-wave velocity of the medium at the source and v_S the S-wave velocity along the path (we assume $\beta = v_S = 3.5\,\mathrm{km\,s^{-1}}$ and $\rho = 2800\,\mathrm{kg\,m^{-3}}$). The factor 2 in eq. (7) accounts for the free surface reflection at the station assuming a quasi-vertical incidence. This is exact for *SH* and a reasonable approximation for quasi-vertical *SV* (Aki & Richards 2002).

Additionally, we want to compute 'absolute' site effects; thus we normalize the input spectra to a common reference accounting for crustal amplification. To do this, a generic rock velocity profile with depth associated with a v_{s30} of 2000 $\mathrm{m\,s^{-1}}$ (Boore & Joyner 1997; Cotton *et al.* 2006) is computed together with the corresponding amplification spectrum. Examples of generic amplifications computed from generic profiles with different v_{s30} values and for a *SH*-wave

Table 1. Earthquakes analysed for the Alps.

Number	Date	Hour	Latitude	Longitude	Depth (km)	M_{ldg}	M_{ren}	Number of records	Distance range (km)	M_w	f_c
1	15-05-1997	00:24:05	45.23	6.62	3	3.8	4.1	4	49/93	3.2	1.58
2	03-10-1997	15:03:35	44.32	6.45	6	3.8	4.0	4	39/101	3.3	2.86
3	31-10-1997	04:23:44	44.26	6.57	2	4.7	4.8	10	63/201	4.0	1.11
4	06-11-1997	12:39:49	44.41	6.53	2	3.6	3.7	4	79/103	3.2	2.29
5	08-11-1997	01:56:09	44.07	7.89	2	–	4.1	6	28/213	3.5	3.35
6	30-03-1998	20:49:00	46.64	7.23	10	–	3.2	3	75/165	2.8	6.27
7	11-04-1998	11:05:03	44.61	7.38	10	4.0	3.8	9	54/168	3.5	2.99
8	06-05-1998	12:02:26	44.15	6.01	10	–	3.2	4	20/118	3.0	3.01
9	13-05-1998	21:11:55	44.45	6.30	5	–	3.1	3	38/86	2.6	5.34
10	09-12-1998	22:08:16	46.20	7.45	2	3.4	3.5	5	55/136	3.1	2.19
11	11-01-1999	03:36:37	45.10	5.76	2	4.2	4.1	11	60/196	3.5	3.26
12	14-02-1999	05:57:55	46.84	7.11	2	4.7	3.8	9	70/233	4.0	1.79
13	25-04-1999	20:36:50	45.91	6.97	2	–	3.0	6	23/123	2.8	3.08
14	30-04-1999	20:59:11	44.01	7.97	2	–	3.2	4	33/89	3.1	3.31
15	10-06-1999	16:16:12	45.65	6.06	2	–	3.1	4	34/104	2.8	3.18
16	28-08-1999	15:03:15	45.26	6.48	2	–	3.3	6	17/63	3.2	2.91
17	13-09-1999	23:27:11	45.51	5.38	10	4.0	3.5	11	33/170	3.2	4.27
18	01-11-1999	17:22:35	43.78	7.36	4	–	3.3	3	27/137	2.8	3.80
19	01-04-2000	01:21:39	45.04	7.43	5	3.1	3.0	6	61/132	3.1	4.39
20	05-04-2000	08:38:22	45.52	4.84	2	3.4	3.2	6	61/161	3.0	5.77
21	31-05-2000	07:46:08	44.75	7.22	10	3.5	3.2	9	55/150	3.2	4.69
22	10-06-2000	02:44:31	44.47	7.29	5	3.5	3.2	9	37/145	3.1	4.32
23	26-06-2000	19:29:18	44.45	6.90	2	3.6	3.3	11	21/183	3.3	2.49
24	19-08-2000	08:37:26	46.10	6.68	10	4.0	3.5	8	27/126	3.4	2.41
25	19-12-2000	14:20:50	43.78	7.37	5	3.7	3.4	4	27/131	3.6	1.04
26	20-12-2000	05:45:15	43.78	7.37	5	3.2	3.0	4	27/131	3.2	1.32
27	25-01-2001	02:17:15	46.03	6.73	6	3.3	3.0	9	34/123	2.8	5.33
28	23-02-2001	22:19:42	46.11	7.03	7	3.9	3.6	10	41/144	3.3	4.21
29	25-02-2001	01:22:31	46.11	7.02	7	3.5	3.2	7	40/144	3.1	2.56
30	14-03-2001	07:09:53	43.50	7.94	7	4.1	3.8	8	48/154	3.6	3.28
31	30-05-2001	22:43:51	45.80	6.49	6	3.6	3.3	12	30/113	2.9	5.64
32	01-07-2001	19:37:20	44.58	7.03	5	3.7	3.4	12	37/178	3.3	2.75
33	09-07-2001	22:50:03	46.04	7.67	7	3.4	3.3	3	108/169	3.0	4.39
34	16-10-2001	04:18:30	45.11	6.48	6	3.4	3.1	7	16/105	3.0	2.68
35	26-01-2002	07:35:47	44.36	7.27	5	3.5	3.0	8	30/149	3.2	3.35
36	21-04-2002	17:57:17	45.61	7.63	5	3.5	3.3	4	90/165	3.1	3.16
37	06-05-2002	06:42:53	44.49	7.27	5	3.5	3.0	6	37/154	3.1	5.95
38	31-05-2002	16:50:34	46.29	7.39	5	3.6	3.5	4	106/155	3.2	3.40
39	04-02-2003	20:49:41	46.05	7.77	5	3.6	3.4	7	90/177	3.1	4.06
40	10-03-2003	13:25:06	44.85	7.81	10	3.5	3.1	7	96/175	3.0	6.74
41	29-04-2003	04:55:08	46.32	7.59	5	4.2	3.9	12	76/192	3.5	3.61
42	25-05-2003	23:03:32	45.12	6.50	5	4.0	3.6	23	16/172	3.4	1.85
43	10-06-2003	22:59:47	44.78	7.70	5	3.8	3.4	19	84/250	3.2	5.81
44	17-08-2003	22:31:51	44.65	6.86	5	3.4	3.2	6	44/195	3.1	3.07
45	01-09-2003	19:28:11	44.26	7.44	5	3.7	3.4	8	32/198	3.4	2.03
46	16-10-2003	16:23:26	44.62	7.01	5	3.4	3.1	7	41/115	3.0	4.22
47	02-12-2003	17:08:23	46.39	5.34	5	3.1	3.0	4	70/137	2.7	8.64
48	09-12-2003	18:03:07	45.33	6.07	5	3.1	3.0	11	24/65	2.8	3.07
49	20-12-2003	03:29:41	44.49	7.21	5	3.6	3.3	21	34/195	3.2	3.23
50	21-12-2003	01:35:57	44.49	7.00	5	3.5	3.1	10	27/125	3.2	2.46
51	28-01-2004	20:09:22	45.43	5.46	5	3.8	3.3	16	33/123	3.1	3.90
52	18-02-2004	14:26:02	46.63	6.91	10	3.5	3.3	4	65/143	3.0	4.98
53	18-02-2004	14:31:59	46.67	6.81	10	3.8	3.5	5	69/180	3.1	4.52
54	14-05-2004	00:30:35	45.03	7.48	10	4.0	3.6	19	66/174	3.4	2.89
55	12-06-2004	04:44:35	45.78	6.88	10	3.7	3.2	8	34/108	3.0	4.32
56	03-12-2004	22:28:59	44.34	7.35	5	3.1	3.1	5	81/155	2.8	6.48
57	25-03-2005	23:19:28	44.48	7.27	5	3.9	3.5	20	37/202	3.5	3.30
58	02-04-2005	04:33:52	44.75	6.76	5	3.5	3.1	17	18/150	3.2	3.83
59	10-04-2005	08:04:38	45.36	6.56	5	3.8	3.4	14	20/93	3.2	2.60
60	12-06-2005	21:16:15	45.11	7.35	5	3.3	3.1	9	54/173	3.0	4.30
61	08-09-2005	11:27:18	46.01	6.87	10	5.3	4.9	22	41/329	4.4	1.14
62	08-09-2005	11:53:11	46.02	6.88	5	3.5	3.2	5	40/88	2.7	7.55
63	08-09-2005	14:10:03	46.00	6.82	5	3.5	3.2	6	39/118	3.0	3.92
64	10-09-2005	13:25:29	44.60	6.87	5	3.6	3.2	9	38/168	3.3	2.43

Table 1. *(Continued)*

Number	Date	Hour	Latitude	Longitude	Depth (km)	M_{ldg}	M_{ren}	Number of records	Distance range (km)	M_w	f_c
65	04-10-2005	13:37:15	44.38	7.23	5	3.0	3.0	9	26/92	2.8	6.72
66	31-10-2005	03:39:58	45.68	6.40	5	4.1	3.6	17	31/243	3.2	2.88
67	20-12-2005	23:57:34	44.10	6.99	5	3.8	3.5	15	19/219	3.7	0.66
68	11-01-2006	10:32:08	45.92	5.41	5	4.1	3.7	7	19/280	3.5	1.43
69	02-09-2006	01:21:31	43.92	7.59	10	4.3	4.0	17	20/248	3.8	2.61
70	11-09-2006	15:04:11	44.70	7.80	5	3.7	3.3	11	71/187	3.2	5.70
71	24-10-2006	17:31:49	43.92	7.59	5	3.8	3.6	12	17/185	3.3	3.76
72	22-11-2006	15:54:32	45.83	6.68	6	3.3	3.0	10	26/97	2.7	6.51

Note: Date and localization are from the RéNaSS network. M_{ldg} and M_{ren} are local magnitudes from LDG and RéNaSS. The number and the distance range of recordings are also indicated, as well as the moment magnitudes and corner frequencies determined in this study.

Table 2. Same as Table 1 for the Rhine Graben.

Number	Date	Hour	Latitude	Longitude	Depth (km)	M_{ldg}	M_{ren}	Number of records	Distance range (km)	M_w	f_c
1	13-11-2000	16:30:40	47.21	7.58	11	3.8	3.6	4	42/117	3.2	5.25
2	22-02-2003	20:41:05	48.31	6.66	10	5.9	5.4	9	36/140	4.5	1.98
3	22-02-2003	20:54:25	48.32	6.68	10	3.7	3.4	3	38/87	3.1	6.46
4	23-02-2003	04:53:47	48.30	6.66	10	3.4	3.2	8	34/104	2.8	6.25
5	24-02-2003	00:35:41	48.30	6.65	10	3.3	3.1	5	34/89	2.7	7.11
6	04-03-2003	19:08:11	48.33	6.66	10	3.6	3.4	6	38/97	2.9	7.68
7	22-03-2003	13:36:17	48.19	8.91	5	4.8	4.5	5	122/171	3.9	2.69
8	24-03-2003	07:54:22	47.68	6.72	10	3.6	3.4	7	26/70	3.0	8.45
9	06-05-2003	21:59:46	46.97	8.81	5	4.2	3.8	7	127/200	3.4	3.71
10	24-08-2003	12:43:40	47.76	7.94	10	3.1	3.1	4	47/144	2.7	13.21
11	31-08-2003	05:38:57	47.56	7.88	10	3.3	3.1	5	27/105	2.9	11.15
12	16-02-2004	09:58:27	48.34	6.66	10	3.5	3.3	7	39/143	2.9	7.50
13	18-02-2004	14:26:02	46.63	6.91	10	3.5	3.3	3	126/178	3.0	6.83
14	18-02-2004	14:31:59	46.67	6.81	10	3.8	3.5	5	59/175	3.1	5.62
15	23-02-2004	17:31:21	47.30	6.28	10	5.5	5.1	9	26/181	4.2	3.37
16	13-03-2004	20:00:18	48.01	7.95	10	3.5	3.3	8	55/161	2.9	7.96
17	21-06-2004	23:10:02	47.50	7.67	21	-	3.8	8	25/115	3.4	5.41
18	28-06-2004	23:42:29	47.54	8.14	20	4.2	4.1	8	57/148	3.5	5.86
19	05-12-2004	01:52:39	48.11	8.00	10	5.2	4.9	8	55/171	4.1	3.40
20	12-05-2005	01:38:05	47.29	7.63	10	4.3	3.9	6	43/110	3.5	6.24
21	13-05-2005	19:44:07	48.07	8.02	10	3.5	3.2	7	61/169	2.9	8.73
22	03-11-2005	00:18:07	48.29	7.43	5	3.8	3.3	3	22/159	3.0	3.25
23	12-11-2005	19:31:16	47.52	8.14	10	4.3	3.8	3	106/147	3.3	7.72

with vertical incidence are shown in Fig. 2. We assume here that a v_{s30} of 2000 m s^{-1} is representative of hard rock sites for France.

In addition to eq. (5), a reference condition is also needed to remove the trade-off between seismic moments and site effects, which are the two constant parameters that control the amplitude of the spectrum (Andrews 1986; Field & Jacob 1995). As in Drouet *et al.* (2008a), we impose that the average of the logarithms of the site effects at each frequency over a number of stations is 0.

$$\sum_{j \text{ in list of reference stations}} s_{jk} = 0; \quad for\ all\ k. \tag{9}$$

The 'list of reference stations' has to be defined: the common practice is to use either all the stations, or a subset of stations located on rock. We choose the second option, beginning by identifying the rock stations. In a first inversion, we use all the stations within the reference list. From the obtained results, the stations showing the least amplification, and with a reasonably flat response, are identified as rock sites and kept in the final list of reference stations. The final inversion is then performed, using this additional information.

A system of equations must then be solved where the unknowns are the following: the m_{0_i} value (related to seismic moment) and the corner frequency f_{c_i} for each event i; the site term s_{jk} for each station j and each frequency k and the attenuation parameters Q_0, α and γ.

We use an iterative Gauss–Newton inversion scheme, based on the derivatives of y_{ijk} with respect to the parameters, to linearize the problem at each iteration and converge to the solution (Tarantola 2004; Drouet *et al.* 2008a).

4 RESULTS

4.1 Residuals

Fig. 3 shows the residuals (difference between the logarithms of observed and modelled amplitudes) for all the records and all the frequencies obtained after the inversion for the three regions (top of Fig. 3). The residuals from the three regions are combined in the bottom frames of Fig. 3. The amount of data is about the same for the Alps and the Pyrenees, whereas it is about three times smaller for the Rhine Graben. However, the distributions still have the same shape and also have similar standard deviations, that is, $\sigma = 0.26$,

Table 3. Same as Table 1 for the Pyrenees.

Number	Date	Hour	Latitude	Longitude	Depth (km)	M_{ldg}	M_{ren}	Number of records	Distance range (km)	M_w	f_c
1	04-06-2001	19:17:57	43.01	0.16	10	3.6	3.6	3	50/191	3.5	9.44
2	12-12-2001	12:10:52	43.12	−1.08	9	3.3	3.5	3	31/93	3.3	12.64
3	14-12-2001	18:28:54	42.87	−0.81	2	3.5	3.6	5	26/115	3.3	4.85
4	16-05-2002	14:56:33	42.94	−0.16	10	4.8	4.8	12	18/251	4.0	4.92
5	16-05-2002	15:14:44	42.82	−0.15	10	4.4	4.2	11	16/249	3.8	6.00
6	19-05-2002	04:44:13	42.99	0.15	10	3.8	3.8	10	22/198	3.4	7.23
7	11-06-2002	18:56:40	41.88	2.73	5	3.0	3.0	5	64/106	2.8	10.14
8	13-06-2002	10:42:32	41.86	2.78	5	3.2	3.4	6	68/130	3.0	11.01
9	21-06-2002	02:26:30	41.86	2.72	5	3.7	3.6	11	66/251	3.5	6.67
10	08-07-2002	09:46:48	42.99	−0.34	10	3.3	2.8	4	17/77	3.1	7.69
11	05-09-2002	20:42:15	43.05	−0.40	10	4.1	4.1	6	39/239	3.5	5.41
12	09-12-2002	13:44:54	43.02	0.19	5	3.7	3.3	5	21/191	3.2	7.14
13	11-12-2002	20:09:52	43.04	−0.33	5	4.3	4.4	5	24/153	3.8	4.99
14	12-12-2002	17:59:49	43.11	−0.28	10	4.9	4.6	9	15/263	4.0	4.87
15	13-12-2002	06:00:23	43.06	−0.28	5	3.3	2.9	4	20/150	2.9	10.95
16	16-12-2002	16:20:26	42.58	0.33	10	3.3	3.3	7	43/173	3.0	6.84
17	18-12-2002	17:58:08	43.00	0.21	10	3.2	2.4	5	25/109	2.9	8.15
18	21-01-2003	18:00:59	43.05	−0.36	10	4.6	4.4	11	28/277	3.8	5.16
19	26-02-2003	03:32:58	42.38	2.12	10	4.4	4.1	14	28/246	3.8	4.12
20	10-03-2003	00:54:38	42.39	2.14	10	3.1	3.0	6	27/101	2.8	6.91
21	03-10-2003	23:40:18	42.73	2.07	10	3.5	3.5	9	38/158	3.0	7.74
22	26-10-2003	08:28:32	41.88	2.76	5	3.0	3.3	3	65/89	2.9	10.03
23	03-02-2004	21:16:14	42.70	0.86	10	3.7	3.7	13	25/188	3.3	6.65
24	01-06-2004	16:50:19	42.39	2.17	5	4.4	4.1	6	33/109	3.5	4.24
25	04-06-2004	04:56:51	42.40	2.19	5	3.5	3.6	7	21/97	3.2	5.28
26	18-07-2004	02:16:02	42.92	1.04	10	3.8	3.7	12	15/178	3.5	5.55
27	22-07-2004	20:15:59	43.01	0.14	10	3.4	3.1	6	20/115	2.9	9.58
28	18-09-2004	12:52:15	42.78	−1.60	2	5.2	5.3	14	51/380	4.6	1.78
29	18-09-2004	19:58:29	42.94	−1.34	5	3.5	3.7	3	25/125	3.3	3.45
30	21-09-2004	15:48:05	42.34	2.02	5	5.1	4.8	14	45/239	4.2	2.94
31	21-09-2004	18:12:49	42.32	2.15	5	2.9	3.0	6	17/82	2.7	9.34
32	23-09-2004	09:50:18	42.31	2.13	10	3.5	3.5	7	20/108	3.2	5.05
33	23-09-2004	09:58:06	42.40	2.07	10	4.0	3.9	9	39/170	3.5	5.14
34	30-09-2004	13:09:05	42.77	−1.45	10	4.6	5.2	8	47/243	4.1	2.30
35	07-10-2004	06:16:29	42.83	−1.45	5	3.9	3.9	4	67/242	3.7	3.32
36	27-11-2004	22:22:02	43.04	−0.08	10	3.7	3.5	8	22/211	3.2	7.50
37	02-12-2004	18:11:18	41.61	2.45	5	3.3	3.5	5	99/152	3.2	5.91
38	15-01-2005	07:13:06	42.76	0.79	10	3.6	3.7	12	19/141	3.4	8.30
39	09-02-2005	15:20:45	42.01	2.58	10	3.5	3.7	6	66/124	3.2	6.78
40	15-02-2005	16:31:12	42.99	0.20	5	3.3	3.4	7	23/110	3.0	10.54
41	26-02-2005	20:36:49	42.62	0.83	5	3.7	3.7	17	27/189	3.4	6.70
42	15-06-2005	21:27:50	43.04	−0.67	5	3.5	3.5	8	21/258	3.3	8.22
43	17-06-2005	04:06:48	43.04	−0.21	5	3.3	3.0	5	15/144	2.9	10.10
44	16-07-2005	09:52:53	43.40	−0.63	5	3.5	3.4	3	34/59	3.4	2.03
45	05-11-2005	00:30:08	42.91	0.13	5	3.7	3.5	8	25/192	3.5	8.30
46	27-12-2005	21:33:22	42.36	1.43	5	3.8	3.8	10	47/140	3.4	3.90
47	07-02-2006	14:59:19	42.49	1.74	5	3.7	3.8	7	27/76	3.2	5.83
48	24-03-2006	07:19:20	42.80	2.55	5	3.1	3.3	5	23/60	2.9	7.08
49	29-03-2006	12:44:57	43.14	−0.63	5	3.3	3.3	4	18/60	3.2	6.64
50	04-05-2006	09:13:05	42.98	−0.70	5	3.3	3.3	4	26/73	3.3	5.71
51	04-05-2006	09:42:06	43.03	−0.70	5	3.4	3.6	5	24/73	3.4	6.70
52	08-05-2006	21:47:56	42.83	2.10	5	3.6	3.6	6	36/123	3.2	6.71
53	20-05-2006	05:36:06	43.00	0.00	5	3.7	3.5	7	16/161	3.2	6.75
54	02-06-2006	08:41:55	43.08	−0.28	5	3.5	3.2	4	19/39	3.0	7.73
55	25-07-2006	19:10:37	42.59	2.11	5	2.9	3.1	4	26/84	2.7	8.30
56	04-09-2006	05:44:22	42.45	1.65	5	3.0	3.0	3	39/58	2.9	7.08
57	24-10-2006	00:04:12	43.50	−0.62	5	3.6	3.2	6	29/65	3.4	3.41
58	04-11-2006	16:44:57	43.22	−0.31	6	3.8	3.8	5	17/42	3.4	6.30
59	14-11-2006	07:40:09	43.06	−0.65	11	3.2	3.0	5	21/67	3.0	6.11
60	17-11-2006	18:19:50	43.08	0.01	11	5.4	4.9	17	16/213	4.5	2.88
61	18-11-2006	20:34:19	42.98	0.01	6	3.6	3.1	8	15/125	3.2	6.10
62	18-11-2006	22:17:27	42.98	0.00	6	3.3	3.1	8	15/126	3.0	7.81

Table 3. *(Continued)*

Number	Date	Hour	Latitude	Longitude	Depth (km)	M_{ldg}	M_{ren}	Number of records	Distance range (km)	M_w	f_c
63	19-11-2006	13:16:12	43.00	0.00	6	3.5	3.2	8	15/126	3.2	7.00
64	20-11-2006	04:01:45	43.01	0.00	6	3.2	3.0	6	25/60	3.0	9.29
65	16-12-2006	08:17:01	42.99	−0.13	5	4.1	4.1	11	18/214	3.6	6.67
66	22-12-2006	12:14:58	43.46	−0.56	5	3.5	3.2	6	23/74	3.3	4.22

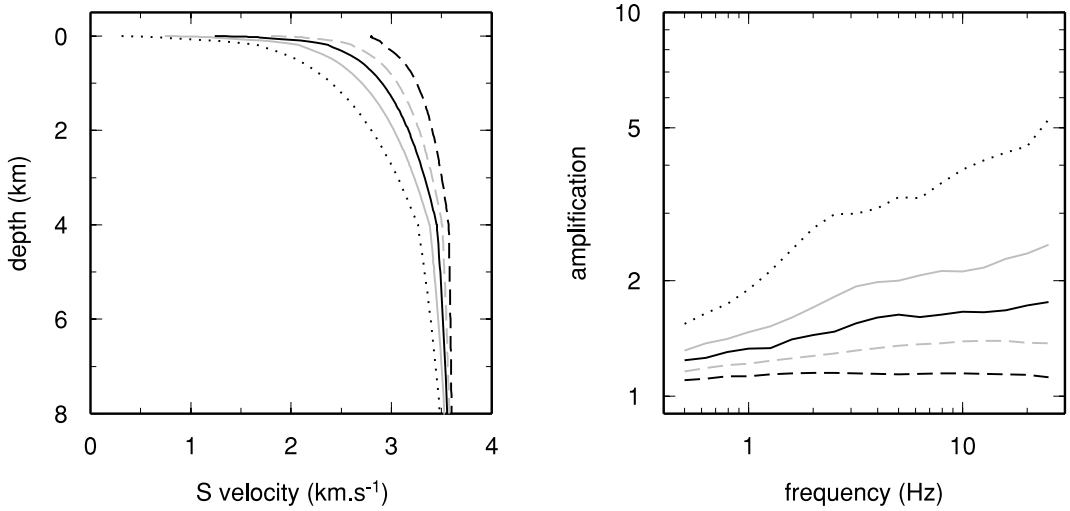

Figure 2. Left-hand side: generic rock velocity profiles (e.g. Boore & Joyner 1997; Cotton *et al.* 2006) with different v_{s30} values: 500 m s^{-1} (black dotted line), 1000 m s^{-1} (grey line), 1500 m s^{-1} (black line), 2000 m s^{-1} (grey dashed line) and 3000 m s^{-1} (black dashed line). Right-hand side: generic amplifications resulting from the profiles on the left for vertically incident *SH* waves, using a Haskell–Thomson procedure.

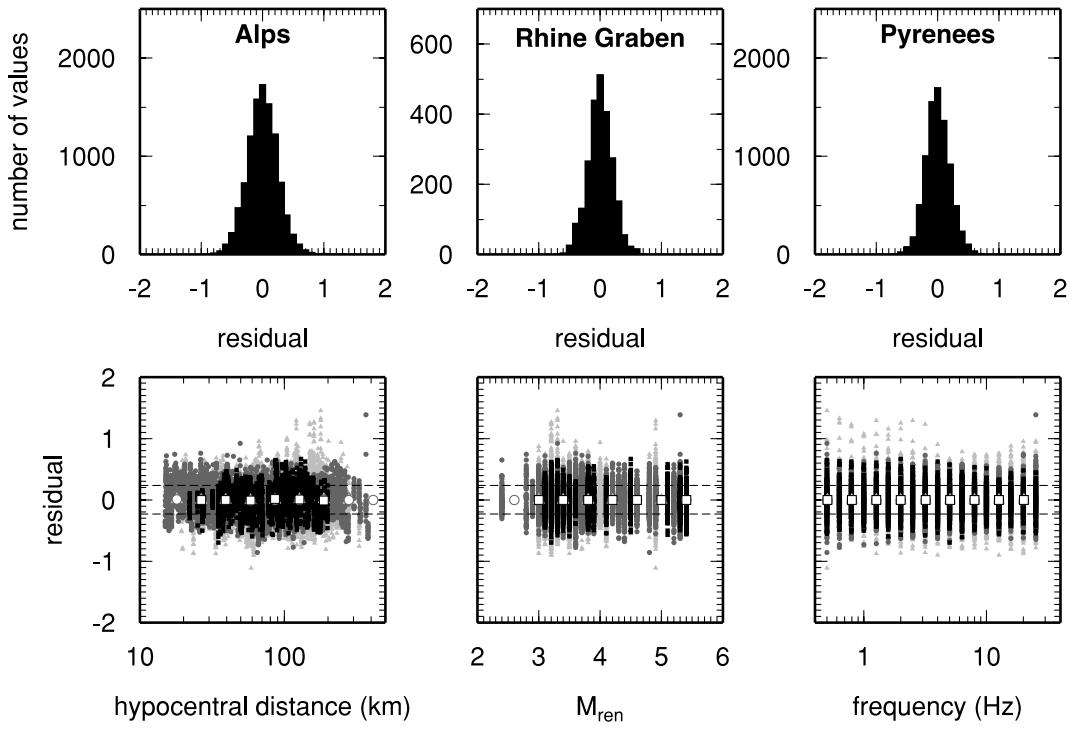

Figure 3. Top panels: distributions of residuals for each region after the inversion. Bottom panels: plots of the residuals (Alps: light grey triangles, Rhine Graben: black squares and Pyrenees: grey circles) as a function of distance (left-hand panel), local magnitude (middle panel) and frequency (right-hand panel). Dashed lines show the one standard deviation of the whole residuals distribution. Large white filled symbols are average residuals over a number of distances, magnitude and frequency bins.

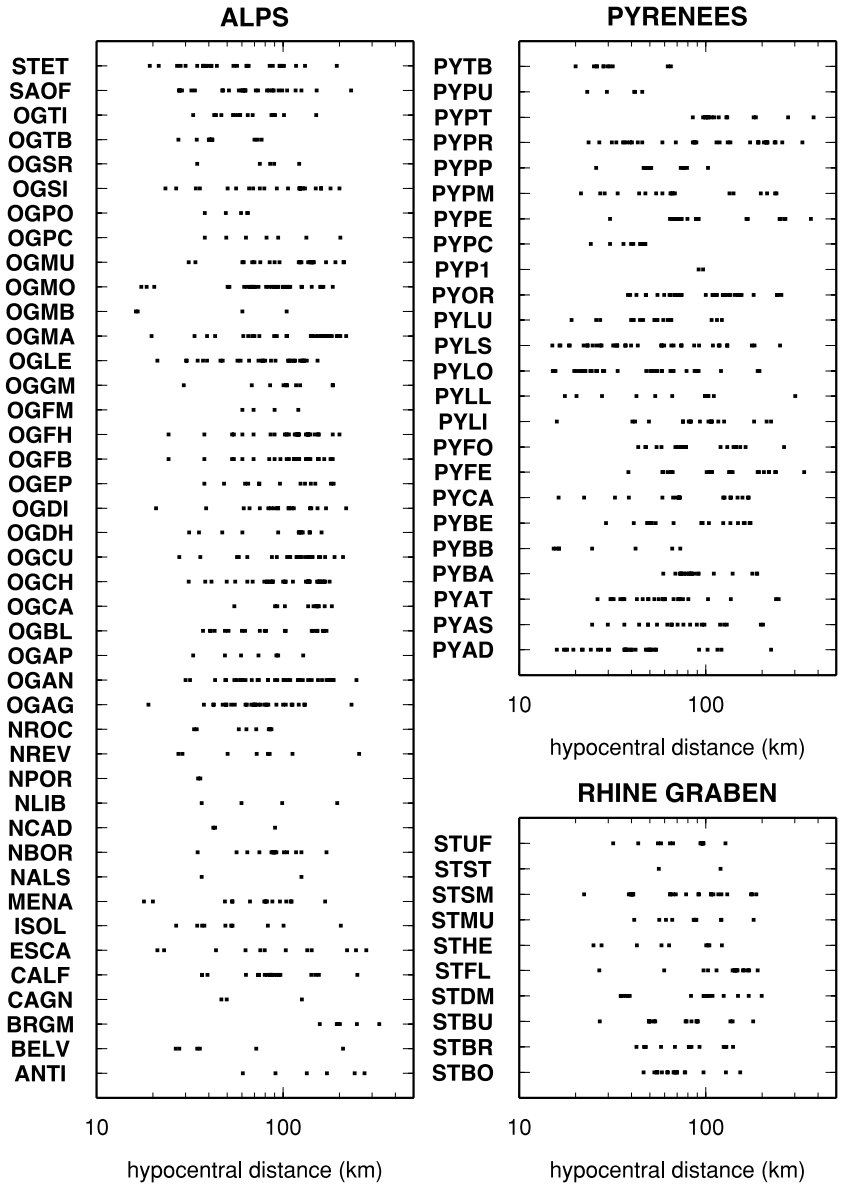

Figure 4. Hypocentral distance distribution at the stations in each region.

0.20 and 0.20, for the Alps, the Pyrenees and the Rhine Graben, respectively.

At the bottom of Fig. 3 the residuals are plotted as function of the distance, the magnitude and the frequency for the three data sets. The standard deviation computed for the three data sets simultaneously is $\sigma = 0.23$. Fig. 4 shows that the distance distribution is fairly homogeneous at each station for the three regions. Figs 3 and 4 show that there is no obvious trend for the residuals with either distance, magnitude or frequency, indicating that no bias is included during the inversion process.

4.2 Regional attenuations

The results for the three attenuation parameters γ, Q_0 and α are given in Table 4 for the three regions. The standard deviations are relatively small, except for Q_0 and α in the Rhine Graben where the limited number of recordings lead to higher uncertainty in the attenuation parameters.

Table 4. Inverted attenuation parameters.

Region	γ	Q_0	α
Alps	1.06 ± 0.01	336 ± 15	0.32 ± 0.02
Rhine Graben	1.06 ± 0.01	1163 ± 247	0.19 ± 0.07
Pyrenees	1.19 ± 0.01	790 ± 31	0.15 ± 0.01

Those attenuation parameters, especially the Q values, are the most difficult parameters to invert because small variations of Q_0 and α lead to almost unchanged amplitudes, mainly at low frequency and short distance. The main attenuation models valid for the investigated regions that were found in the literature are: Thouvenot (1983) ($Q_0 = 436$, $\alpha = 0.25$) and Drouet *et al.* (2008a) ($Q_0 = 322$, $\alpha = 0.2$) for the Alps; Modiano & Hatzfeld (1982) ($Q_0 = 250$, $\alpha = 0.0$), Gagnepain-Beyneix (1987)1 ($Q_0 = 30$, $\alpha = 1.1$), Gagnepain-Beyneix (1987)2 ($Q_0 = 142$, $\alpha = 0.7$) and Drouet *et al.* (2008a) ($Q_0 = 376$, $\alpha = 0.5$) for the Pyrenees. Two other models exist for the whole of France: Nicolas *et al.* (1982) ($Q_0 = 100$,

$\alpha = 0.8$) and Campillo & Plantet (1991) ($Q_0 = 320, \alpha = 0.5$). Note that the original model of Thouvenot (1983) is valid for *P* waves ($Q = 756 \times f^{0.25}$), and it was converted assuming $Q_S = Q_P/\sqrt{3}$ and $\alpha_S = \alpha_P$.

To test the adequacy of the attenuation models, we filtered the times-series for each earthquake in each region around four central frequencies: 1, 5, 10 and 25 Hz. The peak ground acceleration (PGA) values for the east–west and north–south components, corrected for the Brune's source model using the inverted seismic moments and corner frequencies, and scaled to have amplitude 1 at 40 km, are plotted against distance in Fig. 5. The attenuation models: $\exp[-\pi f R_{ij}/(Q_0 f^{\alpha} v_S)]/R_{ij}^{\gamma}$ using γ-values from Table 4 together

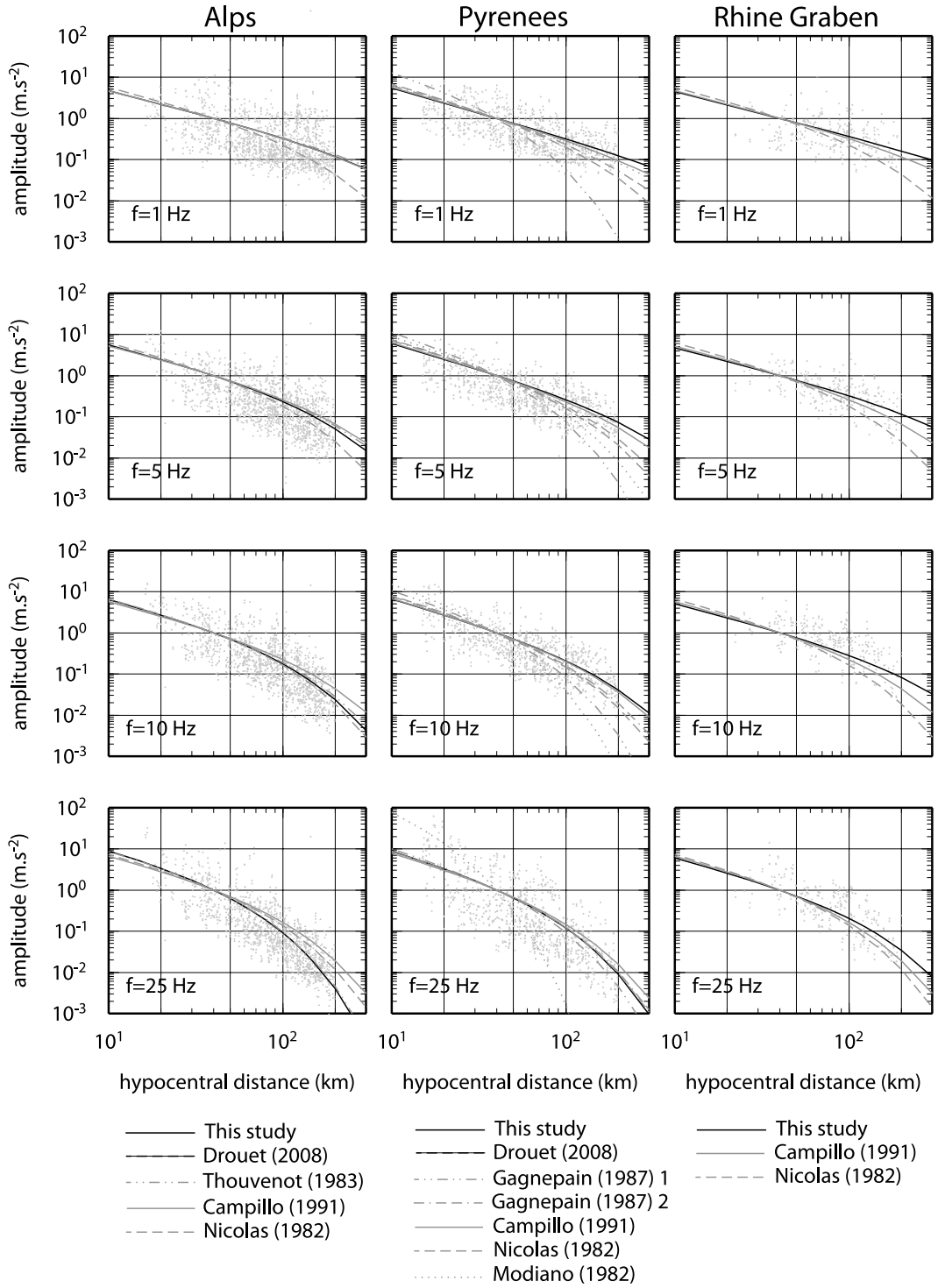

Figure 5. Peak-ground acceleration of the filtered time-series (east–west: triangles; north–south: circles) for four different frequencies in each region. The attenuation models are the *Q*-models described in the text, associated with the γ-values of Table 4. Note that the amplitudes are scaled to get an amplitude equal to 1 at 40 km.

with Q_0- and α-values from Table 4 or from the literature are also plotted in Fig. 5. These results show that most of the models fit equally well the data.

Looking at Fig. 5, we can however draw some conclusions concerning the different models. Models with a low Q_0 (below 300) and no frequency dependence lead to an overestimation of attenuation for the high frequencies at long distance, for example, Modiano & Hatzfeld (1982) for the Pyrenees at 25 Hz. The same conclusion would be observed for the Alps and the Rhine Graben, should such models exist, suggesting that Q is frequency dependent. One can also reject models with a frequency dependence greater than 1, for example, the first model by Gagnepain-Beyneix (1987) leads to lower attenuation at high frequency than at low frequency, which is opposite to the usual observations in this frequency band (0.5–30 Hz). The Nicolas *et al.* (1982) model gives a slight overestimation of attenuation at low frequencies but gives an overall reasonable fit. Consequently, we suggest an upper bound of 0.8 for the frequency dependence in the three regions if it is associated with a low Q_0. Our analysis also supports the idea that the frequency dependence is higher in the Alps than in the other two regions, as shown by the data in Fig. 5.

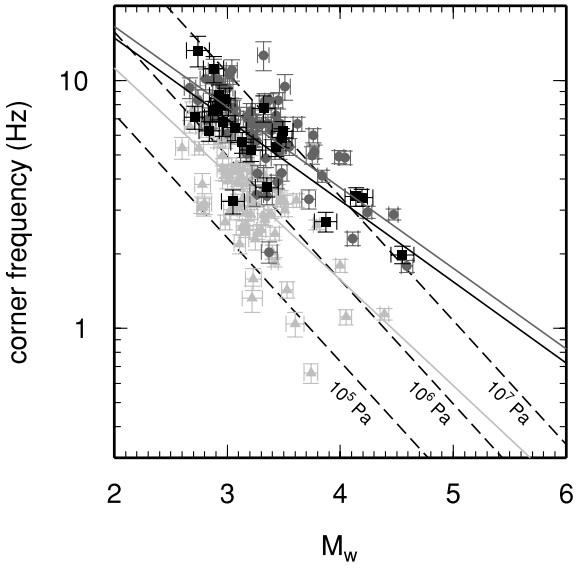

Figure 7. Corner frequencies as a function of moment magnitudes. Solid lines show the regressions determined in this study for the Alps (light grey), the Rhine Graben (black) and the Pyrenees (dark grey). Dashed lines show constant stress drops of 0.1, 1 and 10 MPa (1, 10 and 100 bars).

4.3 Source parameters

Moment magnitudes are determined from the seismic moments using the Hanks & Kanamori (1979) relationship

$$M_{\mathrm{w}} = \frac{\log_{10}(M_0) - 9.1}{1.5}. \tag{10}$$

Fig. 6 shows a comparison of the moment magnitude scale determined in this study and two local magnitude scales used in France (M_{ldg} and M_{ren}). The solid black lines show the regressions obtained in this study

$$M_{\mathrm{w}} = 0.42(\pm 0.10) + 0.77(\pm 0.03) \times M_{\mathrm{ldg}} \tag{11}$$

$$M_{\mathrm{w}} = 0.43(\pm 0.10) + 0.80(\pm 0.03) \times M_{\mathrm{ren}}. \tag{12}$$

Those relations are close to that obtained by Drouet *et al.* (2008a), which are also shown in Fig. 6.

To test our moment magnitude scale, we search through the catalogue of the Swiss Seismological Service (http://www.seismo.ethz.ch/) for the events where a moment magnitude has been computed using the waveform inversion technique of surface waves. Fig. 6 displays the comparison for the 29 earthquakes for which the information was available. It shows that from magnitude 3 to 5, the two independent methods give equivalent values. The regression between the two magnitude scales gives

$$M_{\mathrm{w}} = 0.24(\pm 0.16) + 0.90(\pm 0.05) \times M_{\mathrm{w\text{-}ETH}}. \tag{13}$$

Fig. 7 shows the corner frequencies as a function of the moment magnitudes. Lines of constant stress drop of 0.1, 1 and 10 MPa (1, 10 and 100 bars) are indicated. In this case, a regional dependence of the relationship between corner frequency and moment magnitude is apparent. The regression give the following relationships for the three different regions:

$$Alps : \log_{10}(f_c) = 1.91(\pm 0.08) - 0.43(\pm 0.03) \times M_{\mathrm{w}}, \tag{14}$$

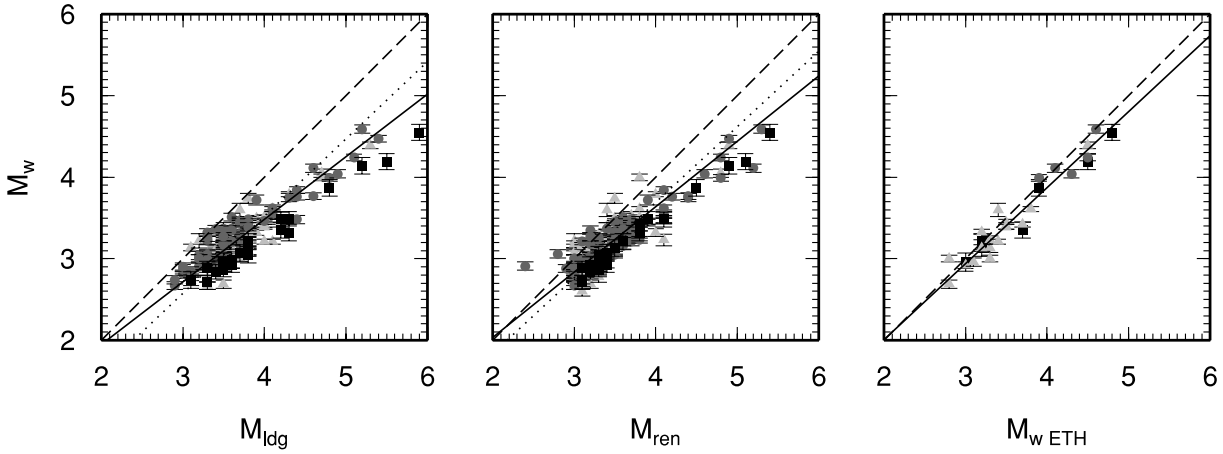

Figure 6. Inverted moment magnitudes as a function of LDG local magnitudes (left-hand panel), ReNaSS local magnitudes (middle panel) and ETH moment magnitudes (right-hand panel), for the Alps (light grey triangles), the Rhine Graben (black squares) and the Pyrenees (grey circles). Solid lines show the regressions determined in this study, dotted lines show the regressions from Drouet *et al*. (2008a) and dashed lines correspond the one-to-one relationship.

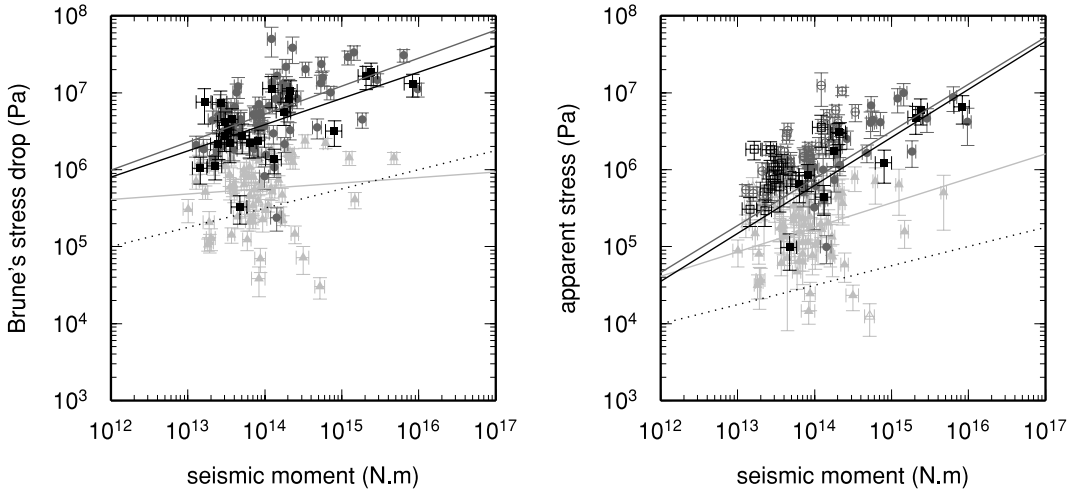

Figure 8. Brune's stress drops as a function of seismic moments (left-hand panel), and apparent stresses as a function of seismic moments (right-hand panel). Solid lines show the regressions determined in this study for the Alps (light grey), the Rhine Graben (black) and the Pyrenees (dark grey). Dotted lines show the dependency of $\Delta\sigma$ and σ_a on seismic moment [originally developed for σ_a: $\sigma_a \propto M_0^{0.25}$ Mayeda & Walter (1996) and extrapolated to $\Delta\sigma$ assuming proportionality between $\Delta\sigma$ and σ_a Bay *et al.* (2005)]. Open symbols in the right-hand frame do not fulfill the conditions $\frac{f_c}{2} \geq f_{\min}$ or $5 \times f_c \leq f_{\max}$ (see text).

$$RhineGraben : \log_{10}(f_c) = 1.83(\pm 0.14) - 0.33(\pm 0.04) \times M_w, \quad (15)$$

$$Pyrenees : \log_{10}(f_c) = 1.87(\pm 0.08) - 0.33(\pm 0.02) \times M_w. \quad (16)$$

The inverted moment magnitudes and corner frequencies for each earthquake are reported in Tables 1–3.

From the inverted seismic moments and corner frequencies, Brune's stress drops are computed using the Brune (1970) relationship.

$$\Delta\sigma = \frac{7}{16} M_0 \left(\frac{f_c}{0.37 v_S} \right)^3. \quad (17)$$

As a consequence of the regional dependence of the corner frequency–moment magnitude relationship, the mean stress drop values are also regionally dependent. The mean stress drop for the three data sets equals to 4.9 MPa (49 bars) whereas values of 0.9, 5.7 and 8.9 MPa (9, 57 and 89 bars) are found for the Alps, Rhine Graben and Pyrenees individually. The computed Brune's stress drops are shown in Fig. 8.

We also computed apparent stress, defined as

$$\sigma_a = \frac{2\mu E}{M_0}, \quad (18)$$

where E is the radiated seismic energy assumed to be equal the to S-wave radiated energy. In reality P waves also carry some radiated energy however this energy is estimated to be less than 10 per cent of the total energy (Abercrombie 1995; Mayeda & Walter 1996). Here, E will denote the S-wave energy. μ, the shear modulus, is taken as 3.4×10^{10} Pa.

E is estimated from the integration of the squared velocity source spectra (obtained by integration of the acceleration source spectra) in the frequency domain (Mayeda & Walter 1996)

$$E = \frac{R_{\theta\phi}}{4\pi\rho v_S^5} \times \int_{f_1}^{f_2} V(f)^2 \mathrm{d}f. \quad (19)$$

Here $V(f)$ is computed from the original data, corrected for site and propagation effects, and averaged for each earthquake over all the stations. As most of the energy is radiated at around the corner frequency, Abercrombie (1995) suggests that f_1 should be less than half the corner frequency and that f_2 should be greater than five times the corner frequency. Another study (Ide & Beroza 2001) computed a correction function to account for missing high frequencies in the integration which arises from recording limitations. The apparent stresses shown in Fig. 8 are all adjusted using the Ide & Beroza (2001) method; earthquakes which do not fulfill the condition proposed by Abercrombie (1995) are indicated as open symbols.

Standard deviations on Brune's stress drop are estimated from the corner frequency and seismic moment standard deviations. Similarly, standard deviations on apparent stress are estimated from the energy and seismic moment standard deviations. Note that the standard deviations of energy are relatively high. This is because they combine the uncertainty linked to source spectra retrieval (via path and site effects corrections) with the uncertainty from averaging the source spectra over all the stations.

Both Brune's stress drop and the apparent stress show an increase with increasing seismic moment (Fig. 8). The increase is almost linear in a log–log space and flattens towards higher values of seismic moment. If one extrapolates the results to high magnitudes, then unrealistically high stress drops would be obtained. Thus this flattening of the curves is expected. Mayeda & Walter (1996) have already observed a scaling of apparent stress with seismic moment: $\sigma_a \propto M_0^{0.25}$, which can be extrapolated to Brune's stress drop assuming proportionality between apparent stress and Brune's stress drop. The scalings observed here are of the same order of magnitude. One other interesting result is the regional dependence of the stress drop, which is lower in the Alps than in the other two regions. One possible explanation is the pre-dominant extensional regime in the Alps. This will be discussed later.

4.4 Site effects

4.4.1 Site transfer functions

As shown by previous studies, the site amplifications are the most stable parameters coming out of an inversion such as the one

presented in this paper, because they are less sensitive to the trade-off between parameters (Field & Jacob 1995; Drouet *et al.* 2008a). In addition, several studies (Field & Jacob 1995; Bonilla *et al.* 1997; Drouet *et al.* 2008a; Bindi *et al.* 2009) have shown similarities between the calculated site effects from an inversion method, and those computed using other common methods (such as the spectral ratios with reference station or the horizontal-to-vertical spectral ratios). More specifically, Drouet *et al.* (2008a) have shown a semblance of the site effects estimated from these different methods at stations PYLO and OGDH. The inversion results are also similar to the theoretical amplifications computed from a layered soil model in Drouet *et al.* (2008b).

The main difficulty is in defining the reference used. In this study, all the spectra have been corrected for crustal amplification using a generic rock site with a $v_{s30} = 2000\,\mathrm{m\,s^{-1}}$ as the reference. This methodology allows us to compare the site effects obtained from independent inversions (i.e. for the three regions). After a first trial inversion, the stations that are kept in the list of reference stations (as explained in section 3) are: CALF, ISOL, NBOR, OGAN, OGCH, OGFB, OGGM, OGLE, OGMU, SAOF and STET for the Alps; STSM for the Rhine Graben; PYAS, PYLI, PYLL and PYLO for the Pyrenees. Fig. 9 shows that no systematic bias with distance or magnitude affect the residuals obtained at the reference stations for two selected frequencies (1 and 10 Hz). Such bias would be observed

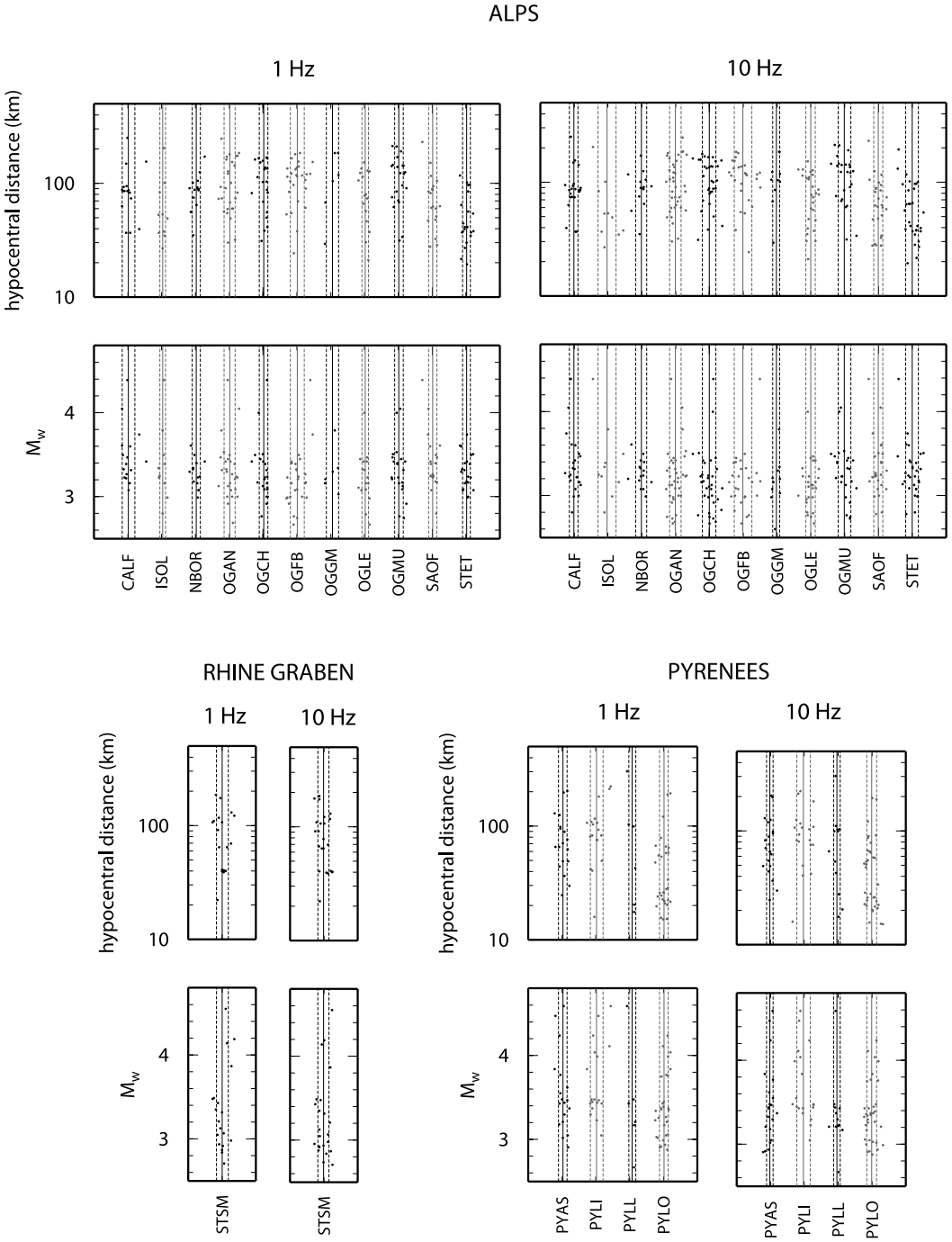

Figure 9. Distribution of the residuals versus hypocentral distance and magnitude for two frequencies: 1 and 10 Hz, for the reference stations in each region.

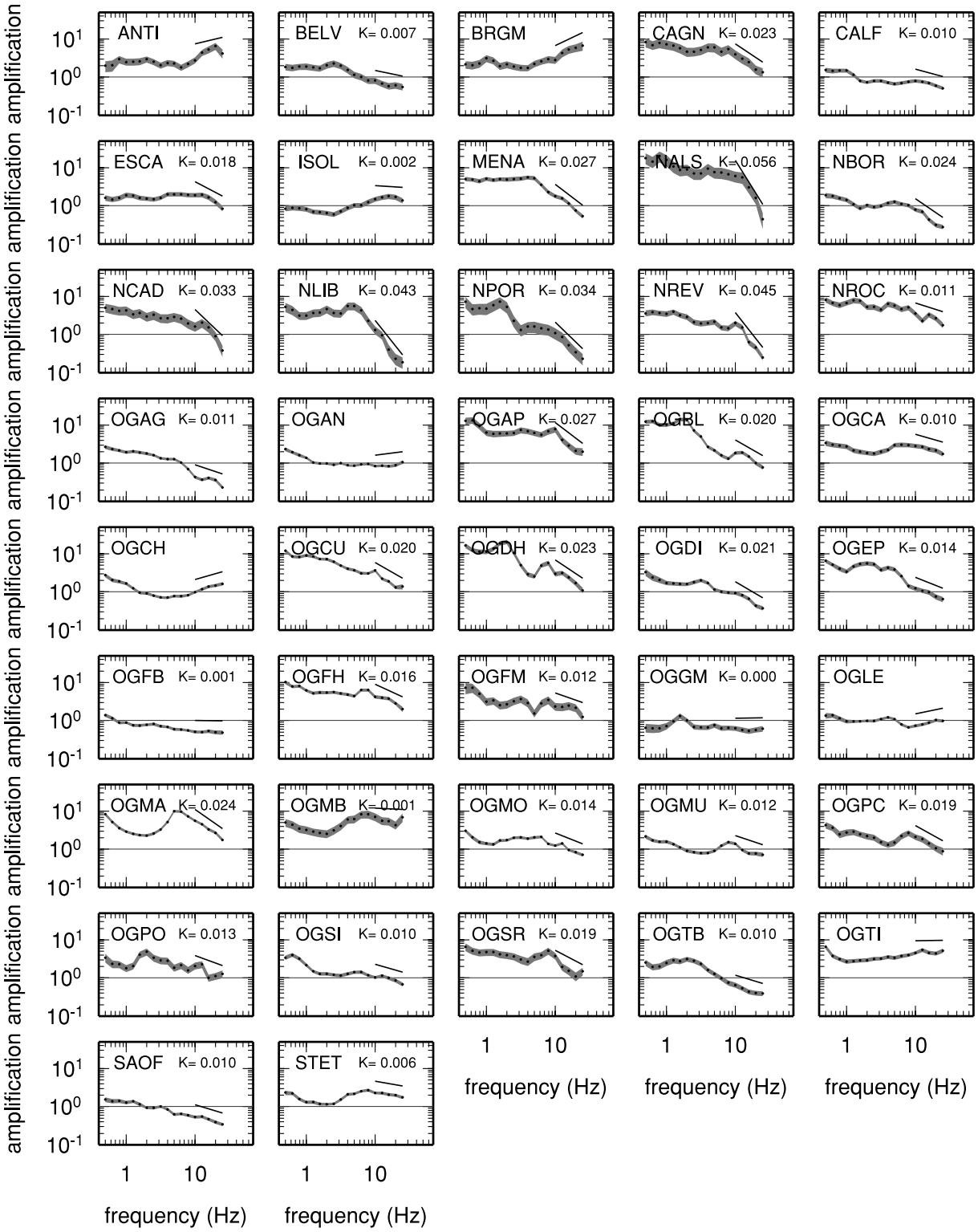

Figure 10. Site transfer functions ± one standard deviation for the horizontal component (black line and dark grey shaded area) for the stations in the Alps. Solid lines indicate the regression of the high frequency part of the transfer functions, which leads to the κ-values indicated on top of each frame.

if all the reference stations were affected by strong fall-offs at high frequencies.

Figs 10–12 show, for each region, the site transfer functions for the different stations. The largest amplifications in the frequency range 1–5 Hz are obtained for stations in the Alpine Valleys (e.g. NALS, NPOR, OGAP, OGBL, OGDH among others), reaching amplifications greater than 10. The stations in the Rhine Graben area present lower amplifications above 1 Hz, however Fig. 11 suggests that high amplification occurs at low frequency (below 1 Hz). This could be linked to a large-scale structure like the Rhine Graben. Some of the Pyrenean stations are also characterized by large amplifications below 10 Hz, however the most striking feature

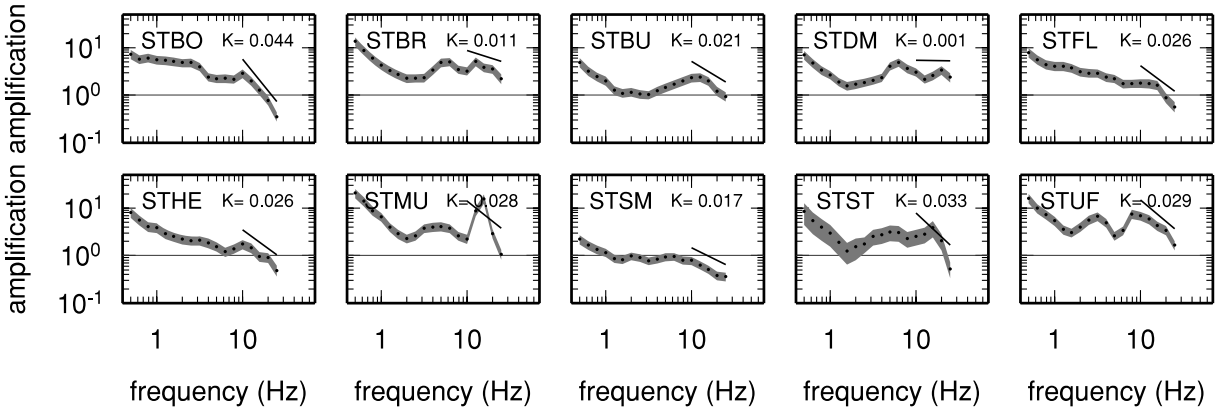

Figure 11. Same as Fig. 10 for the stations in the Rhine Graben.

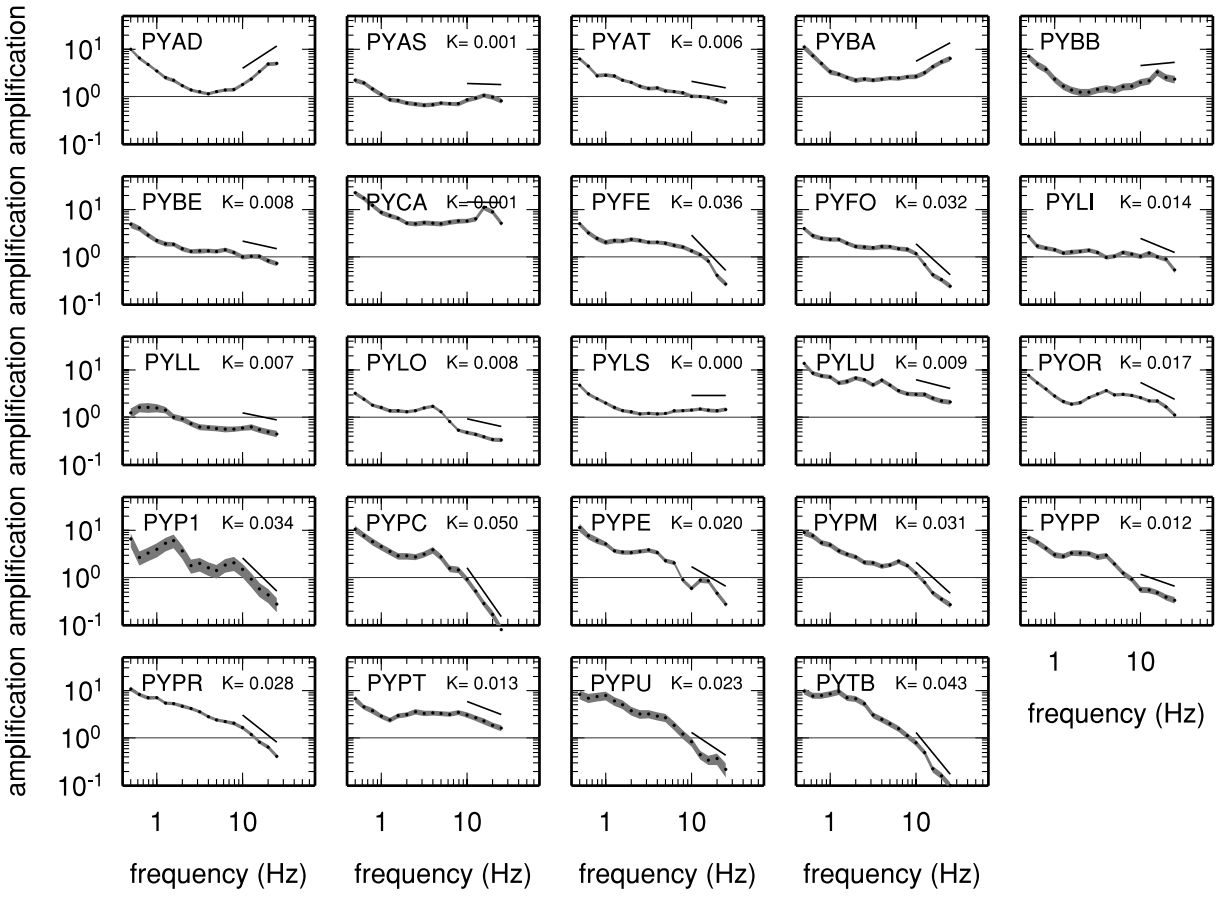

Figure 12. Same as Fig. 10 for the stations in the Pyrenees.

is the high attenuation observed at high frequencies (above 10 Hz) at most of the stations. Some studies have shown that scattering is very strong in this region (Gagnepain-Beyneix 1987) which could explain the observed rapid high-frequency decay.

4.4.2 Kappa (κ)

From these curves, we also compute the κ values by regression of the high-frequency part of the transfer functions ($f \geq 10$ Hz). Similar to Anderson & Hough (1984), we model the high-frequency attenuation through $\exp(-\pi\kappa f)$, however in our case the κ values are independent of distance since the inversion procedure has already accounted for this. The computed values of κ are indicated in Figs 10–12 next to the station name. For some of the stations, we see that the peaks in the transfer function are probably leading to a biased κ (e.g. NCAD, STST or PYPE). This effect has already been analysed theoretically by Parolai & Bindi (2004). For a few stations, the procedure also gave positive slopes, in which case no κ is computed because it would have been a negative value. However, for most of the stations, a good fit is obtained and the κ-values range between 0 and 0.05, which is the usual range of variation for κ.

The Anderson & Hough (1984) method has recently been applied to the French data by Douglas *et al.* (2010) and the results are summarized in Table 5. Although there is a clear correlation between the κ-values from both methods, ours are pre-dominantly lower,

Table 5. κ-values from Douglas *et al.* (2010) (from their constrained weighted regression, i.e. after correction for regional attenuation) compared to κ-values from this study.

Station	κ Douglas *et al.* (2010)	κ This study
OGMO	0.035	0.014
OGMU	0.027	0.012
OGSI	0.023	0.010
PYAT	0.016	0.006
PYFE	0.030	0.036
PYLO	0.021	0.008
PYLS	0.008	0.000
PYOR	0.015	0.017
PYPR	0.025	0.028

except for stations PYFE, PYOR and PYPR. The difference may be the result of data processing and attenuation correction. In our case, we first separate source, path and site effects using data for all the stations in the 0.5–30 Hz frequency band. Then in a second step, we estimate κ by regression of the high-frequency part ($\geq$10 Hz) of the site transfer functions. Douglas *et al.* (2010) used a higher frequency band from 2–12 to 20–50 Hz depending on the quality of the data to determine a κ_r which depends on distance, because it includes the effect of attenuation. They made attenuation correction at a regional scale using the slope of the κ_r distance curves, before the final κ-value for each station is computed. Consequently, the attenuation correction term is estimated using only high-frequency data in Douglas *et al.* (2010). Our results are also likely to be less affected by source effects, because again the inversion process deconvolves all the terms.

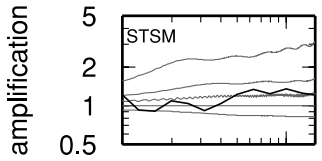

Figure 14. Same as Fig. 13 for the stations in the Rhine Graben.

4.4.3 v_{s30}

We develop a new method to infer some information about the mean shear wave velocity over the uppermost 30 m (v_{s30}). We have computed the ratios between the generic rock site amplifications for different v_{s30}-values (shown in Fig. 2) with respect to the generic rock site amplifications for $v_{s30} = 2000\ \mathrm{m\,s^{-1}}$. We then compare these ratios with the inverted site transfer functions (which are also relative to the generic rock site amplifications for $v_{s30} = 2000\ \mathrm{m\,s^{-1}}$), corrected for the κ effect. This comparison is shown for the rock stations in Figs 13–15. Then we assign to each rock station in France the v_{s30}-value that minimizes the misfit between the site transfer function and the generic amplification curves (see Table 6). A quality criteria, estimated visually, is also given in Table 6 which describes the level of confidence we give to the estimated v_{s30}-values ('+++' for a good fit, '++' for an intermediate fit and '+' for a poor fit).

Our results show that stations identified as rock stations from superficial geological investigations can be split in three categories depending on the v_{s30}-value: (1) soft rock: v_{s30} from 500 to 1000 m s^{-1}; (2) intermediate rock: v_{s30} from 1000 to 2000 m s^{-1} and (3) hard rock: v_{s30} above 2000 m s^{-1}. From Table 6 it is clear that stations located on alluvial deposits (BELV), or moraines (PYFO) are included in the soft-rock category. PYLO is an outlier located on Moraines but with a relatively high v_{s30}(1500 m s^{-1}). This

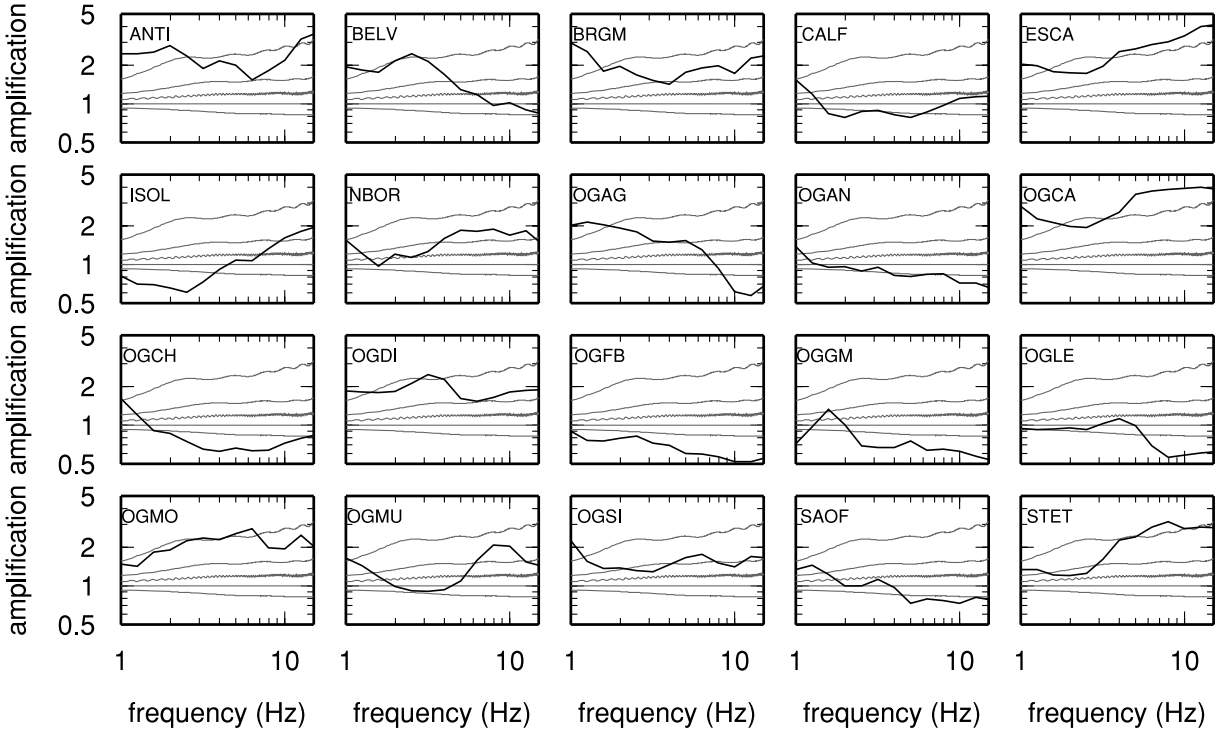

Figure 13. Site transfer functions for the rock stations in the Alps after correction of κ (black lines) compared with the ratios between generic amplifications for $v_{s30} = 500$, 1000, 1500, 2000 and 3000 m s^{-1} with respect to generic amplification for $v_{s30} = 2000$ m s^{-1} (grey lines).

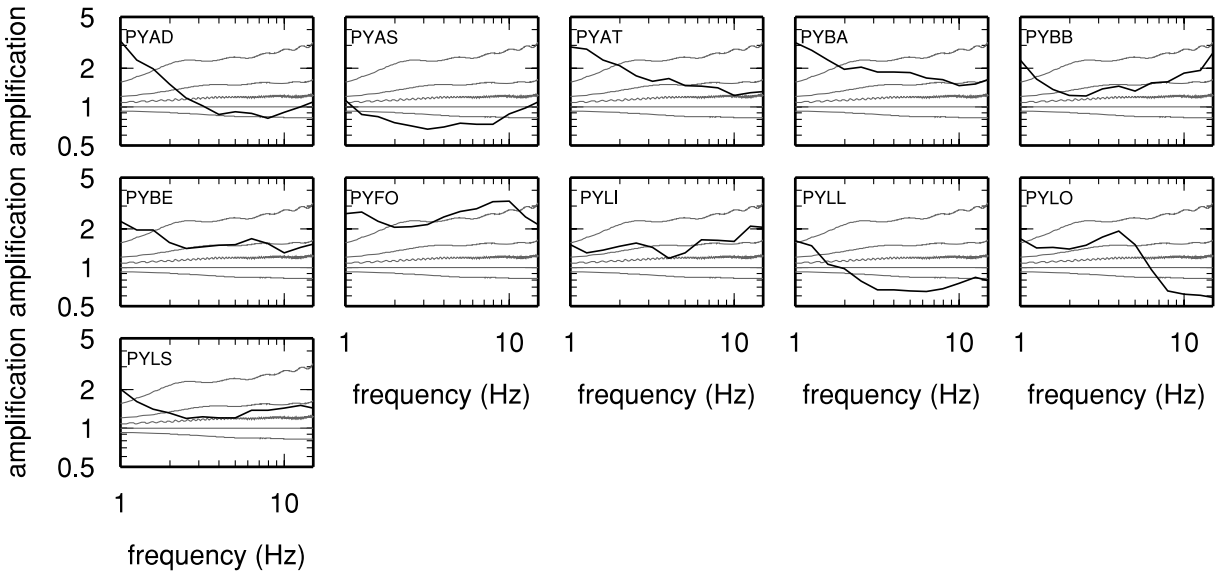

Figure 15. Same as Fig. 13 for the stations in the Pyrenees.

Table 6. v_{s30}-values determined from Figs 13 to 15.

Station	v_{s30} (m s^{-1})	Quality	Geology
Alps			
ANTI	500	++	Dolomites (Upper and Middle Jurassic)
BELV	1000	+	Alluvium (undetermined age)
BRGM	500	++	Limestone
CALF	2000	++	Limestone (Callovian)
ESCA	500	+++	Limestone (Senonian)
ISOL	2000	+	Metamorphic crystalline massifs
NBOR	1000	++	Limestone (Portlandian)
OGAG	1500	+	Limestone (Dogger)
OGAN	3000	+++	Limestone (Barremian, Aptian)
OGCA	500	+++	Limestone (Valanginian)
OGCH	3000	++	Limestone (Tithonian)
OGDI	500	++	Limestone (Hettangian, Sinemurian, Pliensbachian)
OGFB	3000	+++	
OGGM	3000	++	Limestone (Pliensbachian, Toarcian)
OGLE	3000	++	Metamorphic crystalline massifs
OGMO	500	+++	Gypseous formation (Triassic)
OGMU	1000	+	Limestone (Oxfordian, Kimmeridgian)
OGSI	1000	+++	Limestone (Barremian, Aptian)
SAOF	3000	++	Sandstone (Mesozoic)
STET	500	++	Rock fragments above metamorphic crystalline massifs
Rhine Graben			
STSM	1500	++	
Pyrenees			
PYAD	1500	+	Limestone (Aptian)
PYAS	3000	+++	Gneiss
PYAT	1000	++	Marlstone (Albian)
PYBA	500	++	Limestone
PYBB	1000	++	Flysh (Albian, Cemonian)
PYBE	1000	++	Marlstone (Albian)
PYFO	500	+++	Moraines (Würm)
PYLI	1000	+++	Limestone (Aptian)
PYLL	3000	++	Gneiss (Precambrian)
PYLO	1500	+	Moraines (Würm)
PYLS	1000	++	Calcareous schistose formation (Carboniferous)

station is located on a slope of a hill and topographic site effects have been observed (strong deamplification above 5 Hz, Dubos 2003). The stations located on metamorphic crystalline massifs (OGLE, ISOL) or on gneiss (PYAS, PYLL) are in the hard-rock category. One interesting station is STET, located on rock fragments above metamorphic crystalline massifs. As Fig. 13 shows, this station exhibits high amplification above 2–3 Hz, whereas the part of the curve below 2–3 Hz suggests a high v_{s30}. Finally, for the stations

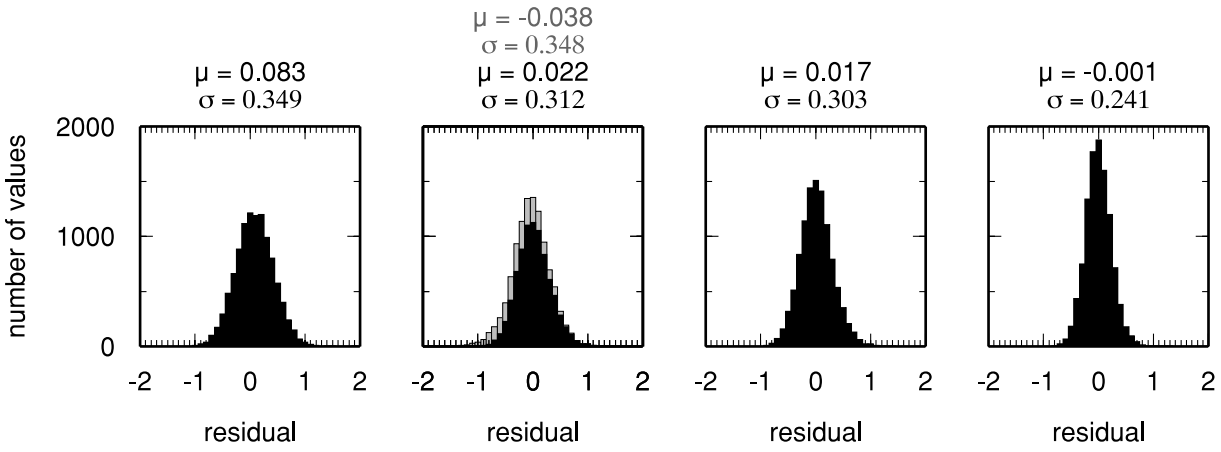

Figure 16. Distributions of residuals for the rock stations tabulated in Table 6, computed without site correction (first frame), using a site correction based on v_{s30} (second frame), using a site correction based on v_{s30} and κ (third frame) and with a site correction based on the inverted site amplification curves (fourth frame). On top of each frame, the median and standard deviation of the corresponding normal distribution are shown. The grey distribution in the second frame corresponds to all the frequencies while the black distribution results from frequencies lower than 10 Hz.

located on limestone, which appear in each of the rock categories, there is a large variability of the response.

To check the reliability of the v_{s30} estimates, we tried to quantify the reduction of the residuals linked with the use of these estimates as a proxy for site effects. We computed modelled spectra using the inverted seismic moments, corner frequencies and propagation parameters. Site effects were handled in four ways: no correction; correction using generic amplification curves based on the computed v_{s30} for each station; correction using generic amplification curves based on the computed v_{s30} for each station plus correction of κ and correction using the inverted site specific amplification curves. Fig. 16 shows the four distributions of residuals corresponding to these four cases. One can see the reduction in standard deviation at each step, from 0.35 without site correction to 0.24 with site specific site corrections. From Fig. 16 one can also see that the correction based on v_{s30} only improves the residuals below 10 Hz (median closer to zero and lower standard deviation), while the combined correction of v_{s30} and κ results in a global improvement for all the frequencies.

Finally, we compare the κ–v_{s30} couples we computed for the rock stations in France with the results obtained in California by Silva *et al.* (1998) (Fig. 17). The uncertainties linked with the estimation of both κ and v_{s30} are very high as shown by the error bars in Fig. 17. Looking at these results one cannot draw a clear conclusion about the correlation between kappa-values and v_{s30}. A recent paper by Campbell (2009) shows that the kappa-values are strongly dependent on the sediment thickness for soft sites. κ may thus also depend on deep structures at rock sites, which could explain the low level of correlation with v_{s30}, a value that describes superficial properties of the soil.

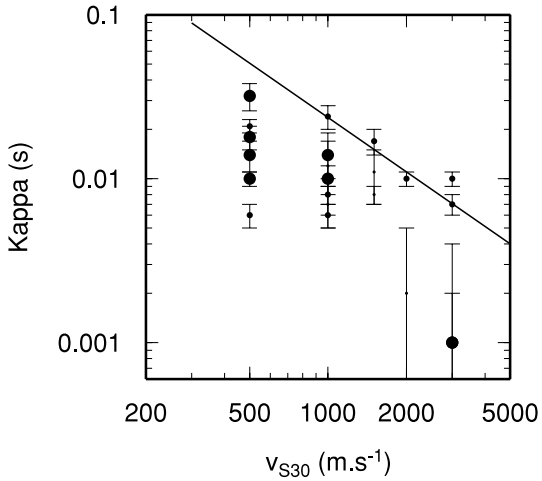

Figure 17. Plot of the v_{s30} versus the κ-values (circles) compared with the relationship derived by Silva *et al.* (1998). The size of the symbol refers to the quality of the v_{s30} as given in Table 6.

5 DISCUSSION AND CONCLUSION

We modified the method proposed by Drouet *et al.* (2008a) to separate source, path and site effects from the far-field *S*-wave Fourier spectra in three different tectonic regions of France (Pyrenees, Alps and Rhine Graben). The inversion is performed using acceleration spectra instead of the displacement spectra from the original method, and higher frequencies are now included (30 Hz instead of 15 Hz). All the spectra are corrected for crustal amplification so that the reference site is a generic rock site with $v_{s30} = 2000$ m s^{-1}. The κ values are computed by regression of the high-frequency part ($f \geq 10$ Hz) of the transfer functions.

The moment magnitudes resulting from our analysis show a good agreement, throughout the whole magnitude range, with the available moment magnitudes determined by the ETH Zürich. Our inverted moment magnitudes are linearly correlated to the local magnitude of French seismological agencies. In the range 2.5–5.5, local magnitude values are higher than our moment magnitude determinations. This discrepancy increases with the size of earthquakes. This point has already been observed in Deichmann (2006), Drouet *et al.* (2008a) and Edwards *et al.* (2008). We finally provide the first complete and homogeneous catalogue of moment magnitudes for France, for the events with magnitude greater than 3 that occurred between 1996 and 2006. Propagation and site terms determined in this study can also be used to estimate the moment magnitudes of any new event.

We observe an increase with magnitude for both Brune's stress drop and the apparent stress. Such increase has already been proposed by Mayeda & Walter (1996) and Kanamori & Rivera (2004) ($\Delta\sigma \propto M^{0.25}$). Resulting stress drops are lower in the Alps than in the other two regions (Pyrenees and Rhine Graben). This regional

variation could be explained by differences in the style of faulting. Events in the French Alps are located in a region with pre-dominant normal focal mechanisms (Sue *et al.* 1999; Kastrup *et al.* 2004). Events in the Pyrenees and Rhine Graben are usually characterized by strike-slip or reverse focal mechanisms (Eva *et al.* 1998; Rigo *et al.* 2005).

Our results show a regional dependence of the attenuation (for both geometric and anelastic attenuation). The Alps area is characterized by higher attenuation than the Rhine Graben or the Pyrenees areas, a conclusion also reached by Bakun & Scotti (2006) from their analysis of intensity data. However, large variations in the absolute value of Q lead to similar amplitude decays with distance (see the different models in Fig. 5). More data are then needed to constrain accurate values of Q.

The local site transfer functions have been determined and κ-values have been derived for each station. These κ determinations are based on the spectral high-frequency regression of the site transfer functions. An original method to determine v_{s30} for the rock stations is also proposed; comparing the resulting transfer functions with ratios of generic site amplifications allows us to estimate v_{s30}.

From this analysis, we then provide a v_{s30} range for the rock stations of the French accelerometric network (see Table 6). Our individual v_{s30}–κ estimates are compared with the Californian relationship developed by Silva *et al.* (1998). At first glance, the results suggest a correlation between v_{s30} and κ. However, considering the large uncertainties in both v_{s30} and κ estimates, the correlation becomes less clear. Additionally, Campbell (2009) showed that κ is strongly dependent on the thickness of the sedimentary layers for soft sites. This study provides a methodology to rapidly and easily estimate v_{s30} and κ for any rock station. Such data are needed to further test any correlation between v_{s30} and κ and understand the physical origin of κ at rock sites.

ACKNOWLEDGMENTS

The authors would like to warmly thank all the participants to the RAP program who were providing really high quality data. This work has been partly supported by the European Commission through the following projects: FP7-ENVIRONMENT-226967 entitled 'Seismic Hazard Harmonization in Europe'; and FP7-PEOPLE-248182 entitled 'Ground-motion modelling for seismic hazard assessment in regions with moderate-to-low seismic activity'. The authors thank David Halliday (GJI editor), John Douglas and Luca Malagnini (GJI reviewers) for their critical reviews and encouraging comments, which greatly helped to improve the manuscript as well as Sylvia Hales (GJI Editorial Assistant) for her helpful assistance. The authors are also grateful to François Thouvenot, Emmanuel Chaljub and Mathieu Causse for their careful internal reviews of this manuscript, as well as to Chris Van Houtte for his thorough check of the grammar and spelling of the text.

REFERENCES

Abercrombie, R.E., 1995. Earthquake source scaling relationships from −1 to 5 M_L using seismograms recorded at 2.5 km depth, *J. geophys. Res.,* **100,** 24 015–24 036.

Aki, K. & Richards, P.G., 2002. *Quantitative Seismology*, 2nd edn, University Science Books, Sausalito, California, 700 pp.

Akinci, A., Malagnini, L., Hermann, R.B., Gok, R. & Srensen, M.B., 2006. Ground motion scaling in the Marmara region, Turkey, *Geophys. J. Int.,* **166,** 635–651.

Anderson, J.G. & Hough, S.E., 1984. A model for the shape of the fourier amplitude spectrum of acceleration at high frequencies, *Bull. seism. Soc. Am.,* **74**(5), 1969–1993.

Andrews, D.J., 1986. Objective determination of source parameters and similarity of earthquakes of different size, in *Earthquake Source Mechanics*, pp. 259–267, eds Das, S., Boatwright, J. & Scholz, C.H., American Geophysical Monograph 37.

Atkinson, G.M. & Morrison, M., 2009. Observations on regional variability in ground-motion amplitudes for small-to-moderate earthquakes in North America, *Bull. seism. Soc. Am.,* **99**(4), 2393–2409.

Bakun, W.H. & Scotti, O., 2006. Regional intensity attenuation models for France and the estimation of magnitude and location of historical events, *Geophys. J. Int.,* **164,** 596–610.

Bay, F., Fäh, D., Malagnini, L. & Giardini, D., 2003. Spectral shear-wave ground-motion scaling in Switzerland, *Bull. seism. Soc. Am.,* **93**(1), 414–429.

Bay, F., Wiemer, S., Fäh, D. & Giardini, D., 2005. Predictive ground motion scaling in Switzerland: best estimates and uncertainties, *J. Seismol*, **9,** 223–240.

Bindi, D. *et al.*, 2009. Site amplifications observed in the Gubbio Basin, Central Italy: hints for lateral propagation effects, *Bull. seism. Soc. Am.,* **99**(2A), 741–760.

Bonilla, L.F., Steidl, J.H., Lindley, G.T., Tumarkin, A.G. & Archuleta, R.J., 1997. Site amplification in the San Fernando Valley, California: variability of site-effect estimation using the S-wave, coda and H/V methods, *Bull. seism. Soc. Am.,* **87**(3), 710–730.

Boore, D.M., 2003. Simulation of ground motion using the stochastic method, *Pure appl. Geophys.,* **160,** 635–676.

Boore, D. & Boatwright, J., 1984. Average body-wave radiation coefficients, *Bull. seism. Soc. Am.,* **74**(5), 1615–1621.

Boore, D.M. & Joyner, W.B., 1997. Site amplifications for generic rock sites, *Bull. seism. Soc. Am.,* **87**(2), 327–341.

Braunmiller, J., Deichmann, N., Giardini, D., Wiemer, S. & the SED Magnitude Working Group, 2005. Homogeneous moment-magnitude calibration in Switzerland, *Bull. seism. Soc. Am.,* **95**(1), doi:10.1785/0120030245.

Brune, J.N., 1970. Tectonic stress and the spectra of seismic shear waves from earthquakes, *J. geophys. Res.,* **75**(26), 4997–5009.

Brune, J.N., 1971. Correction, *J. geophys. Res.,* **76**(20), 5002.

Campbell, K.W., 2003. Prediction of strong ground motion using the hybrid empirical method and its use in the development of ground-motion (attenuation) relations in eastern North America, *Bull. seism. Soc. Am.,* **93,** 1012–1033.

Campbell, K.W., 2009. Estimates of shear-wave Q and κ_0 for unconsolidated and semiconsolidated sediments in Eastern North America, *Bull. seism. Soc. Am.,* **99**(4), 2365–2392.

Campbell, K.W. & Bozorgnia, Y., 2004. Erratum, *Bull. seism. Soc. Am.,* **94**(6), 2417.

Campbell, K.W. & Bozorgnia, Y., 2006. Next Generation Attenuation (NGA) empirical ground motion models: can they be used in Europe? *1st European Conference on Earthquake Engineering and Seismology*, 3–8 September 2006, Geneva, Switzerland, paper no. 458.

Campillo, M. & Plantet, J.-L., 1991. Frequency dependence and spatial distribution of seismic attenuation in France: experimental results and possible interpretations, *Phys. Earth planet. Inter.,* **67,** 48–64.

Chandler, A.M., Lam, N.T.K. & Tsang, H.H., 2006. Near-surface attenuation modelling based on rock shear-wave velocity profile, *Soil Dyn. Earthq. Eng.,* **26,** 1004–1014.

Cotton, F., Scherbaum, F., Bommer, J.J. & Bungum, H., 2006. Criteria for selecting and adjusting ground-motion models for specific target regions: application to Central Europe and rock sites, *J. Seismol*, **10**(2), doi:10.1007/s10950–005–9006–7.

Cotton, F., Pousse, G., Bonilla, F. & Scherbaum, F., 2008. On the discrepancy of recent European ground-motion observations and predictions from empirical models: analysis of KIK-net accelerometric data and point-sources stochastic simulations, *Bull. seism. Soc. Am.,* **98**(5), 2244–2261.

Deichmann, N., 2006. Local magnitude, a moment revisited, *Bull. seism. Soc. Am.,* **96**(4A), doi:10.1785/0120050115.

Douglas, J., 2003. Earthquake ground motion estimation using strong-motion records: a review of equations for the estimation of peak ground acceleration and response spectral ordinates, *Earth-Sci. Rev.,* **61,** 43–104.

Douglas, J., 2007. On the regional dependence of earthquake response spectra, *ISET J Earthq Technol*, **44**(1), 71–99.

Douglas, J., Gehl, P., Bonilla, L.F. & Gelis, C., 2010. A kappa model for mainland France, *Pure appl. Geophys.,* doi:10.1007/s00024-010-0146-5.

Drouet, S., Souriau, A. & Cotton, F., 2005. Attenuation, seismic moment, and site effects for weak-motion events: application to the Pyrenees, *Bull. seism. Soc. Am.,* **95**(5), 1731–1748.

Drouet, S., Chevrot, S., Cotton, F. & Souriau, A., 2008a. Simultaneous inversion of source spectra, attenuation parameters, and site responses: application to the data of the French accelerometric network, *Bull. seism. Soc. Am.,* **98**(1), doi:10.1785/0120060215.

Drouet, S., Triantafyllidis, P., Savvaidis, A. & Theodulidis, N., 2008b. Comparison of site effects estimation methods using the Lefkas (Greece) 2003 earthquake aftershocks, *Bull. seism. Soc. Am.,* **98**(5), 2349–2363.

Dubos, N., 2003. Contribution à l'évaluation du risque sismique dans les Pyrénées centrales, *Thèse*, Université Paul Sabatier, Toulouse III, France.

Dufumier, H., 2002. Synthesis of magnitude and focal mechanism computations for the $M \geq 4.5$ earthquakes in France for the period 1995-2000, *J. Seismol*, **6,** 163–181.

Edwards, B., Rietbrock, A., Bommer, J.J. & Baptie, B., 2008. The acquisition of source, path, and site effects from microearthquake recordings using Q tomography: application to the United Kingdom, *Bull. seism. Soc. Am.,* **98**(4), doi:10.1785/0120070127.

Eva, C., Pastore, S. & Deichmann, N., 1998. Evidence for ongoing extensional deformation in the western Swiss Alps and thrust-faulting in the southwestern Alpine foreland, *J. Geodyn*, **26**(1), 27–43.

Field, E.H. & Jacob, K.H., 1995. A comparison and test of various site-response estimation techniques, including three that are not reference-site dependent, *Bull. seism. Soc. Am.,* **85**(4), 1127–1143.

Frankel, A., 1991. Mechanisms of seismic attenuation in the crust: scattering and anelasticity in New York State, South Africa, and southern California, *J. geophys. Res.,* **96**(B4), 6269–6289.

Gagnepain-Beyneix, J., 1987. Evidence of spatial variations of attenuation in the western Pyrenean range, *Geophys. J. R. astr. Soc.,* **89,** 681–704.

Hanks, T.C., 1982. $f_{\max}$, *Bull. seism. Soc. Am.,* **72**(6), 1867–1879.

Hanks, T.C. & Kanamori, H., 1979. A moment magnitude scale, *J. geophys. Res.,* **84**(B5), 2348–2350.

Ide, S. & Beroza, G.C., 2001. Does apparent stress vary with earthquake size? *Geophys. Res. Lett.,* **28**(17), 3349–3352.

Kanamori, H. & Rivera, L., 2004. Static and dynamic scaling relations for earthquakes and their implications for rupture speed and stress drop, *Bull. seism. Soc. Am.,* **94**(1), 314–319.

Kastrup, U., Zoback, M.L., Deichmann, N., Evans, K.F., Giardini, D. & Michael, A.J., 2004. Stress field variations in the Swiss Alps and the northern Alpine foreland derived from inversion of fault plane solutions, *J. geophys. Res.,* **109,** B01402, doi:10.1029/2003JB002550.

Konno, K. & Ohmachi, T., 1998. Ground-motion characteristics estimated from spectral ratio between horizontal and vertical components of microtremor, *Bull. seism. Soc. Am.,* **88**(1), 228–241.

Malagnini, L., Mayeda, K., Uhrhammer, R., Akinci, A. & Hermann, R.B., 2007. A regional ground-motion excitation/attenuation model for the San Fransisco region, *Bull. seism. Soc. Am.,* **97**(3), 843–862.

Mayeda, K. & Walter, W.R., 1996. Moment, energy, stress drop, and source spectra of western United States earthquakes from regional coda envelopes, *J. geophys. Res.,* **101**(B5), 11 195–11 208.

Modiano, T. & Hatzfeld, D., 1982. Experimental study of the spectral content for shallow earthquakes, *Bull. seism. Soc. Am.,* **72**(5), 1739–1758.

Nicolas, M., Massinon, B., Mechler, P. & Bouchon, M., 1982. Attenuation of regional phases in western Europe, *Bull. seism. Soc. Am.,* **72**(6), 2089–2106.

Papageorgiou, A.S. & Aki, K., 1983. A specific barrier model for the quantitative description of inhomogeneous faulting and the prediction of strong ground motion, *Bull. seism. Soc. Am.,* **73**(4), 693–722.

Parolai, S. & Bindi, D., 2004. Influence of soil-layer properties on k evaluation, *Bull. seism. Soc. Am.,* **94**(1), 349–356.

Pequegnat, C., Guéguen, P., Hatzfeld, D. & Langlais, M., 2008. The French Accelerometric Network (RAP) and National Data Center (RAP-NDC), *Seismol. Res. Lett.,* **79**(1), 79–89.

Purvance, M.D. & Anderson, J.G., 2003. A comprehensive study of the observed spectral decay in strong-ground accelerations recorded in Guerrero, Mexico, *Bull. seism. Soc. Am.,* **93**(2), 600–611.

Rigo, A., Souriau, A., Dubos, N., Sylvander, M. & Ponsolles, C., 2005. Analysis of the seismicity in the central part of the Pyrenees (France), and tectonic implications, *J. Seismol*, **9**(2), 41–50.

Scherbaum, F., Cotton, F. & Smit, P., 2004. On the use of response spectral-reference data for the selection and ranking of ground-motion models for seismic-hazard analysis in regions of moderate seismicity: the case of rock motion, *Bull. seism. Soc. Am.,* **94**(6), 2164–2185.

Silva, W., Darragh, R., Gregor, N., Martin, G., Abrahamson, N. & Kircher, C., 1998. Reassessment of site coefficients and near-fault factors for building code provisions, Technical Report Program Element II: 98-HQ-GR-1010, Pacific Engineering and Analysis, El Cerrito, USA.

Stafford, P.J., Strasser, F.O. & Bommer, J.J., 2008. An evaluation of the applicability of the NGA models to ground-motion prediction in the Euro-Mediterranean region, *Bull. Earthq. Eng.,* **6,** 149–177.

Sue, C., Thouvenot, F. & Fréchet, J., 1999. Widespread extension in the core of the western Alps revealed by earthquake analysis, *J. geophys. Res.,* **104**(B11), 25 611–25 622.

Tarantola, A., 2004. *Inverse Problem Theory and Methods for Model Parameters Estimation*, SIAM, Philadelphia.

Thouvenot, F., 1983. Frequency dependence of the quality factor in the upper crust: a deep seismic sounding approach, *Geophys. J. R. astr. Soc.,* **73,** 427–447.